Canadian Nuclear Safety Commission | Commission canadienne de sûreté nucléaire

CMD 18-H6.20

Replacement/Remplacement

File / dossier: 6.01.07
Date: 2018-06-06
Edocs: 5526204

Oral Presentation

Presentation and submission from Paul Sedran, RESD Inc.

In the Matter of

Ontario Power Generation Inc., Pickering Nuclear Generating Station

Request for a ten-year renewal of its Nuclear Power Reactor Operating Licence for the Pickering Nuclear Generating Station

Commission Public Hearing – Part 2

June 2018

Exposé oral

Présentation et mémoire de Paul Sedran, RESD Inc.

À l'égard de

Ontario Power Generation Inc., centrale nucléaire de Pickering

Demande de renouvellement, pour une période de dix ans, de son permis d'exploitation d'un réacteur nucléaire de puissance à la centrale nucléaire de Pickering

Audience publique de la Commission – Partie 2

Juin 2018

Canada

The Implications of Incorporating CANDU 6 Experience in the Assessment of the Pickering Fuel Channels

P.J. Sedran

RESD Inc

Contents

Introduction

- An independent review of Pickering B Fuel Channel (FC) Assessments was performed
- Review from the specific perspective of CANDU 6 OPEX, not directly shared with OPG, in part due to industry restructuring - Fragmentation

Fragmentation of FC Assessors

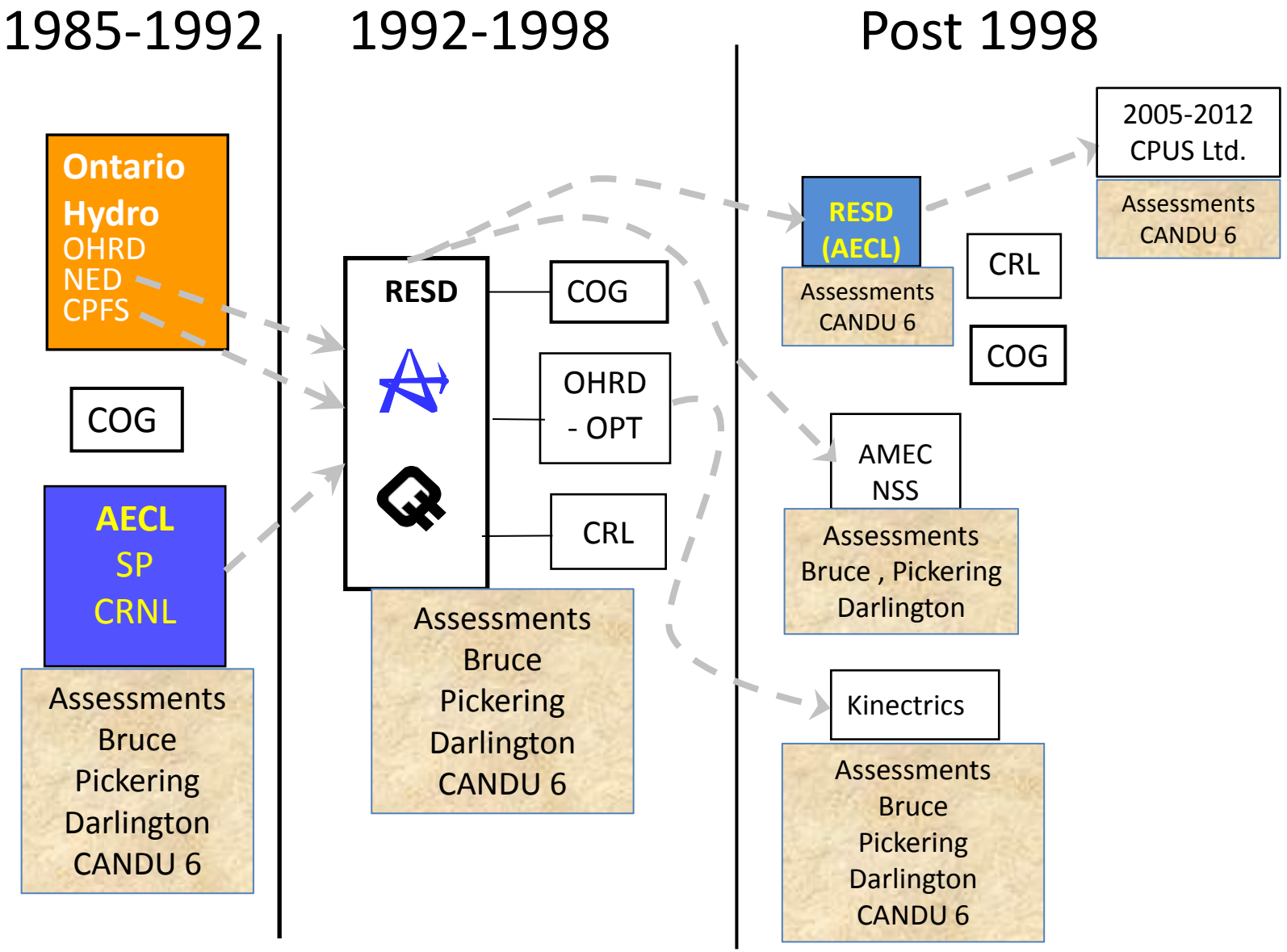

List of C6-Specific Observations

- CT Spring-Back Measurements
- Non-Linearity in PT Sag Rate
- CT Ovality Measurements
- CT-LIN Gap Measurements

CT Spring-Back Measurements

Vertical Deflection of PLF06 due to Loading/Unloading of Fuel during the 2004 Inspection

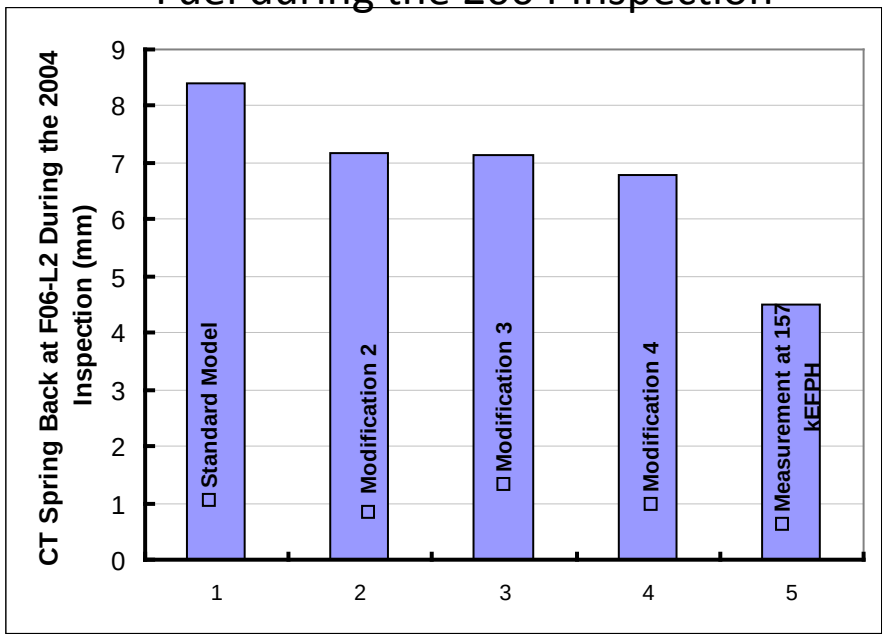

Predicted Deflection = 8.4 mm
Measured Deflection = 4.5 mm

Unit	CT-LISS Contact Time	PT - CT Contact Time (2015)
	(KEFPH)	(KEFPH)
P5	268	> 260
P6	256	> 260
P7	> 300	> 260
P8	283	> 260

Indication: FC – PT and CT are stiffer than in the current model

Implication for Pickering: Longer Predicted Times to CT-LISS Contact and CT-PT Contact

Non-Linearity in PT Sag Rate

PT Sag Measurements in PLGS and G-2

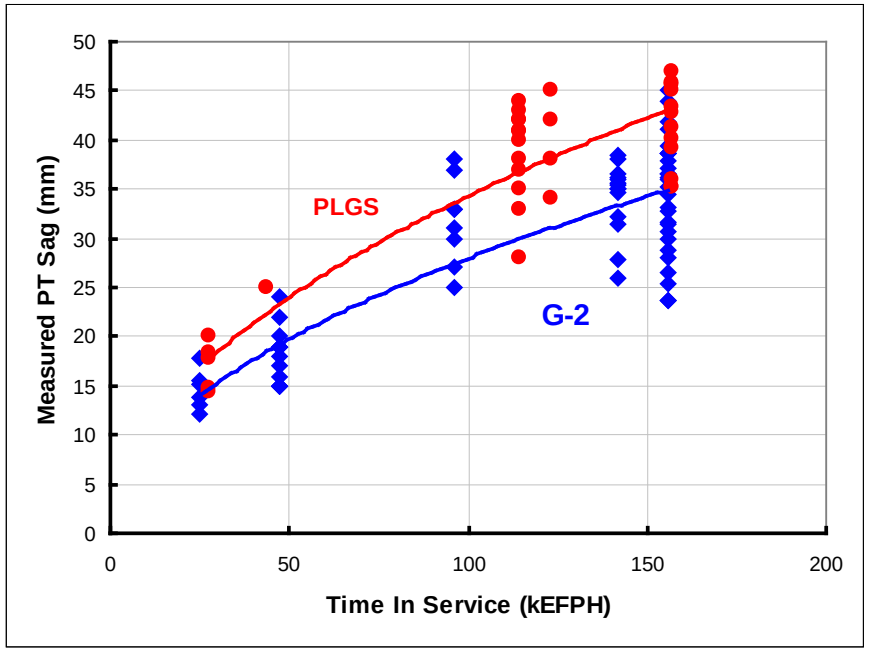

Unit	CT-LISS Contact Time (KEFPH)	PT - CT Contact Time (KEFPH)
P5	268	> 260
P6	256	> 260
P7	> 300	> 260
P8	283	> 260

Indication: PT Sag Rate is Non-Linear

May be due to reactor derating or to a geometric effect

Implication for Pickering: Longer Predicted Times to CT-LISS Contact and CT-PT Contact

CANDU 6 CT Ovality Measurements (1)

from PT UT and Gap Measurements

CT Inner Diameter Versus Angular Position from Top Dead Centre

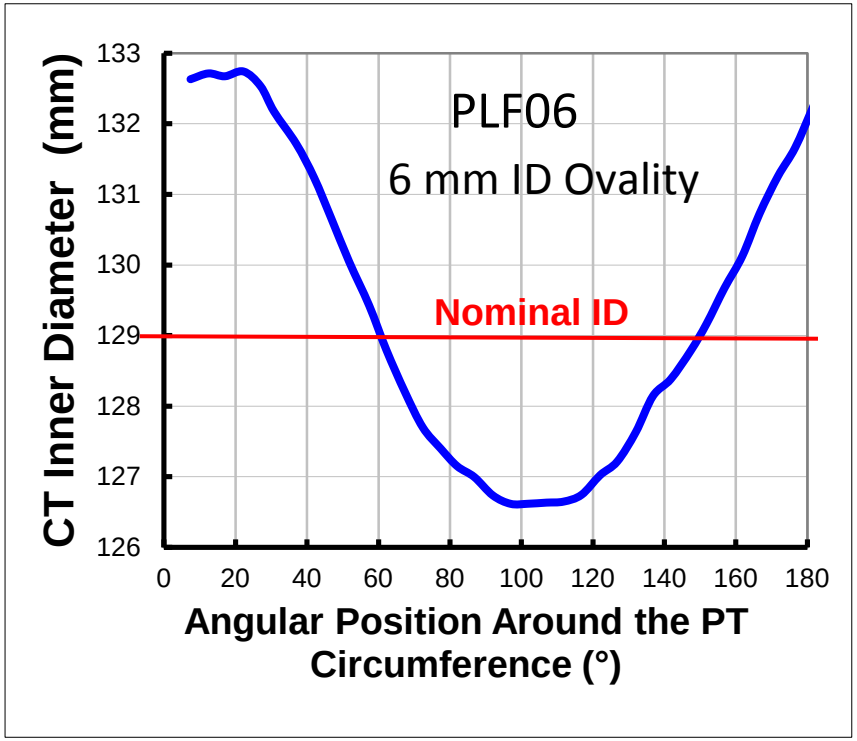

Design Condition

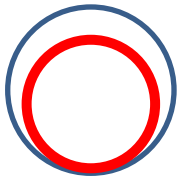

Nip-Up Condition, Circular CT

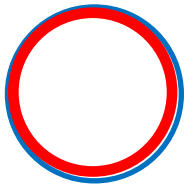

Partial Nip-Up with CT Ovality prior to Nip-Up

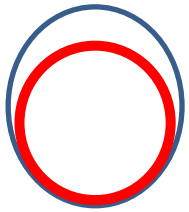

New loading Condition, Sides of Spacer pinched

Indication: CT Ovality at Spacer Locations is significant

Implication for Pickering: Spacer Nip-Up Assessments Assume Circular CT Sections but CT Ovality Results in Pinching of the spacer between the PT and CT Prior to Nip-Up – Will hinder spacer movement during SLAR

CANDU 6 CT Ovality Measurements (2)

P4M11 Gauging Measurements

Maximum, Minimum and Mean CT Inner Diameter Versus Axial Position

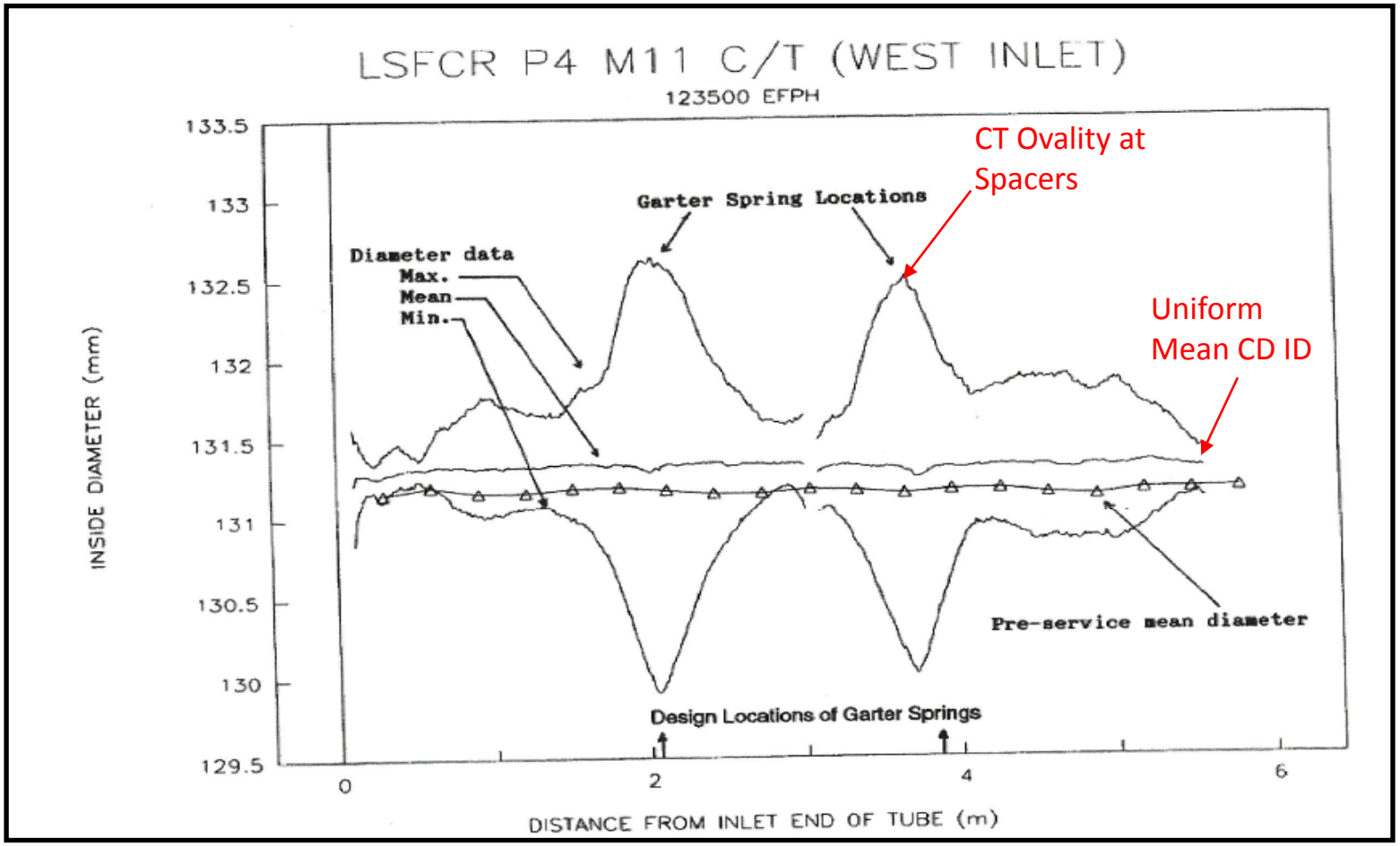

CANDU 6 CT Ovality Measurements (3)

PLF06 CT Gauging Measurements with Calibrated Gaps

$$ID_{CT\theta} = ID_{PT\theta} + w_{PT\theta} + w_{PT(\theta+180°)} + gap_{\theta} + gap_{(\theta+180°)}$$

Calibrated

Maximum, Minimum and Mean CT Inner Diameter Versus Axial Position

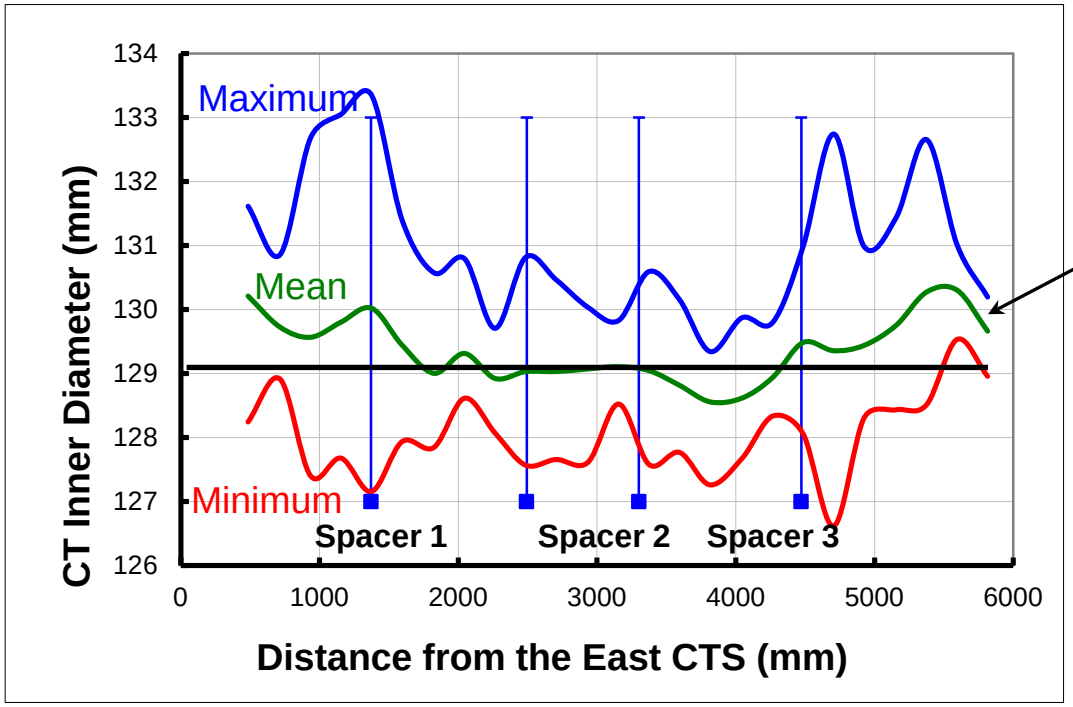

Mean CT ID is not uniform, implies diametral expansion of the CT; this was found to be due to **gap calibration**

CANDU 6 CT Ovality Measurements (4)

PT- CT Gap Calibration

Axial Distributions of Measured and Calibrated Gaps

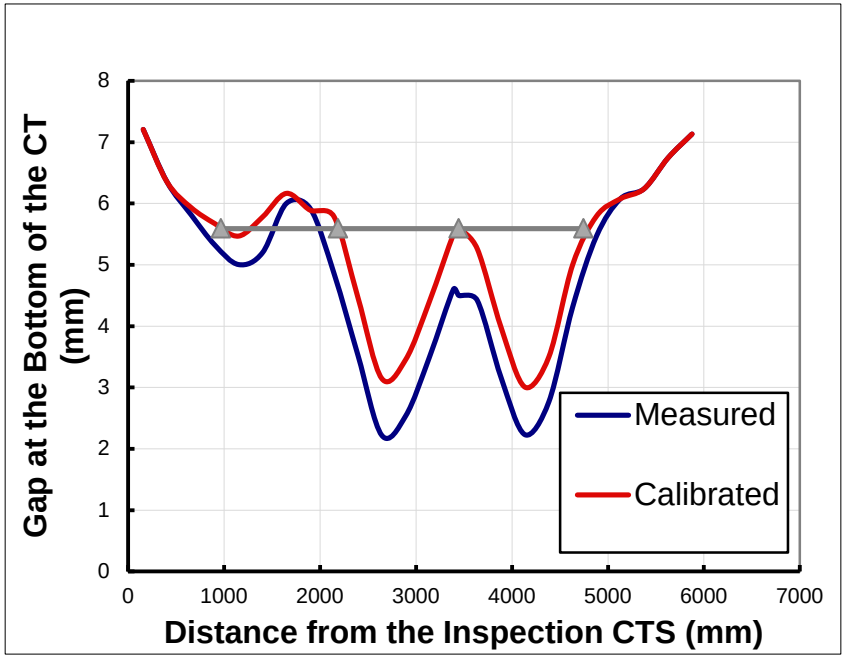

Correlation of Measured and Calibrated Gaps

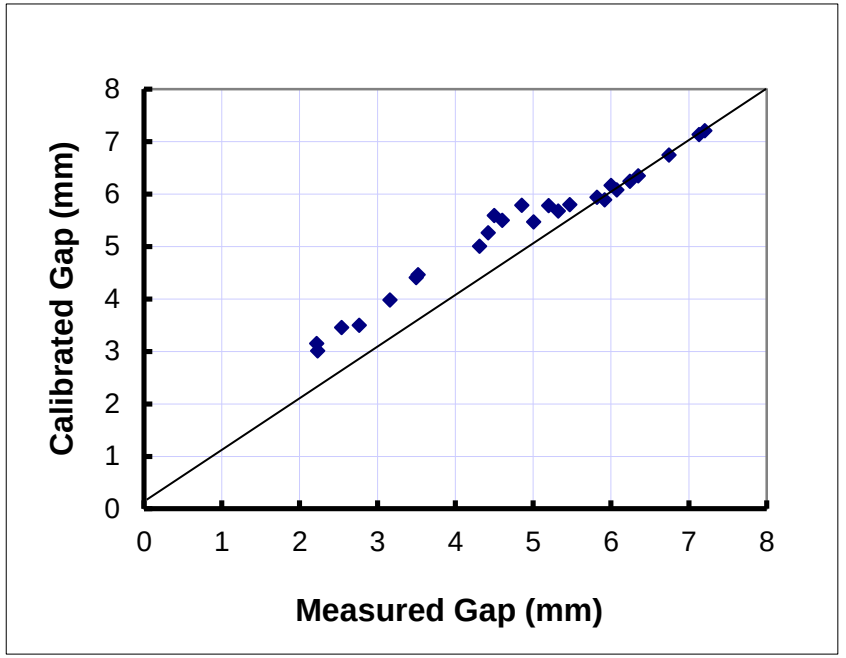

CANDU 6 CT Ovality Measurements (5)

G2H14 CT Gauging Measurements, No Gap Calibration

$$ID_{CT\theta} = ID_{PT\theta} + w_{PT\theta} + w_{PT(\theta+180°)} + gap_{\theta} + gap_{(\theta+180°)}$$

Uncalibrated

Maximum, Minimum and Mean CT ID Versus Axial Position for G2H14 in 2005

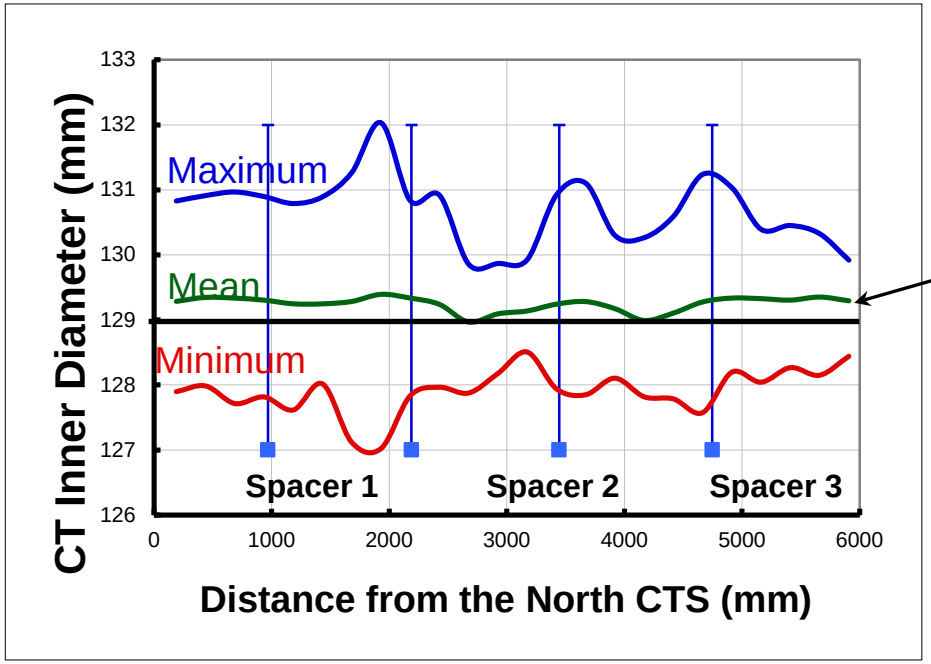

Mean CT ID is almost uniform, consistent with P4M11 measurements, implies that no gap calibration produces more realistic CT dimensions than those generated with calibrated gaps

Indication: Gap Calibration may be technically incorrect

Implication for Pickering: CT-PT contact predictions with gap calibration overestimate time to contact

CT-LISS Gap Measurements

- Measurements are used to predict CT- LISS Contact Times

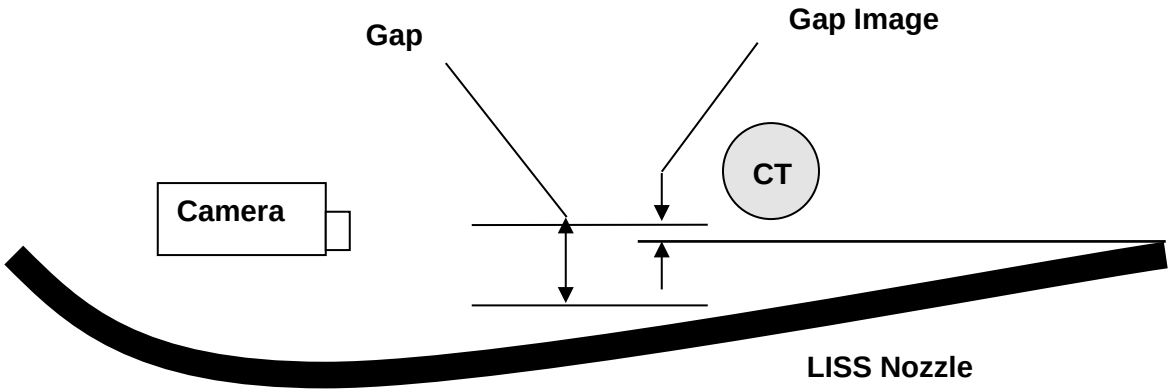

- Optical Measurement: Consistency and Repeatability Problems
- UT Measurements: Measure Gap with a Defuelled PT

Indication: Measured Gap could be understimated

Implication for Pickering: Current CT-LISS contact predictions may underpredict the time-to-contact

Suggestion for Modelling Crack Growth in PT LBB Analyses

- From P.J. Sedran, A Challenge to a Traditional Assumption in Pressure Tube (PT) Leak-Before Break Assessments, International Nuclear Components Conference November 1-4, 2015, Mississauga, Ontario, Canada

Traditional Method
Crack Growth Starts at FPH

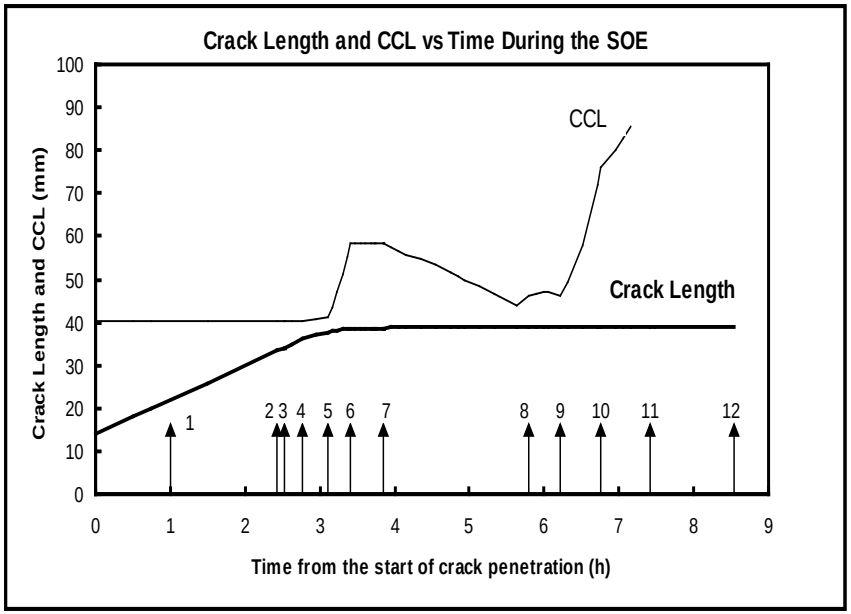

Proposed Method
Crack Growth Starts when TSSP Reached on Cooling

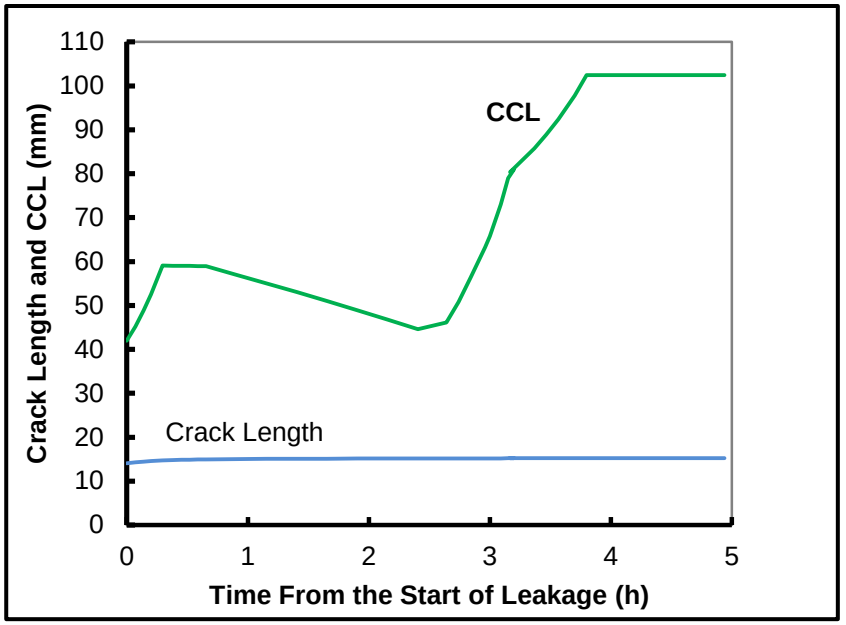

Conclusions

1. CT Spring Back Measurements imply lower PT and CT sag
2. PT Sag Measurements indicate Non-Linear PT and CT sag
3. 1 and 2 indicate increased time to PT-CT and CT-LISS contact for Pickering B compared with current assessments
4. CT Ovality Measurements show partial Nip-Up before full Nip-Up, which may interfere with spacer movement during SLAR, gap calibration should be questioned and may lead to reassessment of PT-CT contact times
5. CT-LISS Optical Gap and UT Measurements may underestimate the actual gap, giving underestimates of CT-LISS contact time
6. The assumption of crack growth at FPH conditions in the current deterministic and probabilistic LBB analyses may be excessively conservative. Should the need arise for Pickering, OPG could make a case in the LBB analysis that the crack would start to grow during the reactor shutdown/cooldown instead of at FPH conditions.

RESD Inc.
Reactor **E**ngineering **S**ervices **D**evelopment

4052 Perivale Road
Mississauga, ON
L5C 3Z8

May 31st, 2018

Mr. Marc Leblanc
Commission Secretary, CNSC
280 Slater Street, P.O. Box 1046,
Station B Ottawa, ON K1P 5S9

Re: Submission on Fuel Channel Integrity for the June, 2018 CNSC Public Hearing on the Pickering Operating License Extension

Dear Mr. Leblanc,

I am pleased about the opportunity to participate in the Pickering license extension public hearing by providing a presentation on the review of the fitness-for-service assessments for the Pickering B Fuel Channels (FC) found in OPG correspondence with the CNSC in P-CORR-00531-04953 and in P-CORR-00531-04293.

Because of the time limit on the presentation, it will be difficult for the commissionaires to gain a reasonable understanding of the topics presented in the PowerPoint slides from viewing the slides alone. Therefore, this letter was written as part of the submission to the CNSC in order to provide historical and technical background information as an aid to the comprehension of the PowerPoint slides by the CNSC.

My review of the Pickering FC fitness-for service-assessment was performed largely from the perspective of experience that was gained from working on FC fitness-for-service assessments starting in 1990, including some independent assessments in 2005 – 2010 for Point Lepreau and Gentilly-2. The work during that period of time was funded directly by the utilities without the involvement of COG and the work was not disseminated within the industry. From that work, a number of phenomena related to FC behavior were observed. These are listed in the second bullet of Slide 2 of the presentation. The implications of these observations for the Pickering FCs are discussed in the presentation and are elaborated upon in this letter.

1. Historical Background Information

The opportunity for this presentation was made possible through a series of developments within the community of FC assessment organisations from approximately 1985 to 2010, which may be of interest to the CNSC. A brief history of these developments and their influence on the material for this presentation is presented in Section 1.1.

1.1 Historical Developments in the Organization of FC Assessors.

Historically, FC fitness-for service methods development work was always performed within COG, involving specialists from AECL Sheridan Park, Chalk River Laboratories, and the utilities. As a result, the FC mechanical/materials models were developed through industry-wide

collaboration between the utilities' engineers, the consultant's engineers, and researchers. Over the years, industry reorganization has had an impact on the various groups that are involved in the fitness-for-service assessment for the Pickering FCs. The resulting organizational changes are depicted in Slide 4 of the presentation. In Slide 4, the text boxes with solid colours represent the various organisations involved and how they were grouped together over 3 different historical time periods. The marbled text boxes labelled "Assessments" indicate the stations that had their fuel channels assessed by the various assessors. In the first time period, labelled 1985 – 1992, all CANDU reactors (Bruce, Pickering, Darlington, CANDU 6) were assessed by the same organisations (AECL Sheridan Park (SP), supported by AECL CRNL and OHRD). Industry wide communication on FC issues was ensured by COG. In 1992, Ontario Hydro's Nuclear Engineering Department and Central Production Field Services merged with the FC group at AECL SP to form the joint Ontario Hydro – AECL organization, the Reactor Engineering Services Department, (RESD) as indicated by the arrows on the left side of the slide. During this time period, RESD was responsible for FC assessments for all the CANDU stations and COG continued to provide for communication among different groups.

However, after 1998, RESD was dissolved. The AECL Sheridan Park group retained the RESD name and started to work exclusively on CANDU 6 reactors, while Nuclear Safety Solutions (NSS) took over the Ontario Hydro reactors, exclusively. With different clients for their work, ongoing communication was no longer required between the two groups.

As shown in the slide, in the Post-1998 time period, another reorganization took place. Starting in 2005, CPUS Limited performed a number of FC assessments for Point Lepreau and Gentilly-2 that were outside of COG and were not shared with the industry. In fact, CPUS Limited, AECL Sheridan Park, and AMEC NSS eventually became competitors for FC-related work. As a result, information regarding FC assessments was no longer readily shared among the different groups that performed FC fitness-for-service assessments.

1.2 Information Sharing

Although some of the findings from the independent work for Point Lepreau and Gentilly-2 were issued in a number of CNS papers, it is believed that there were no investigations by OPG into the possible use of the information for the assessment of the Pickering FCs.

Despite this, It is expected that the findings that from the independent work CANDU 6 work would be directly applicable to the Pickering B which led to this presentation.

It should be noted that the Calandria Tube (CT) inner diameter profiles of Slide 8 were first generated in 2005. Various attempts were made to inform COG, NB Power Nuclear, Hydro-Quebec, and Bruce Power of the use of FC inspection results to generate in-service CT ovality profiles, but no investigations were undertaken, largely because of the fragmentation of the FC assessment specialists into several competing groups, as depicted in Slide 4. On order to disseminate the results, 2 CNS papers [1] [2] were written on the topic, but no use of the information in the papers was made until 2014, when AMEC NSS produced in-service CT inner diameter profiles for Bruce Unit 5. It is not known the extent to which the industry was informed about the CT inner diameter data generated for Bruce Unit 5 or the papers of References [1] and [2].

References [1] and [2] can be found in Attachments 1 and 2, respectively, to this letter.

The information provided in the presentation, such as the generation of CT in-service dimensions, described in Slide 8, because of its definite effect on the mechanical behavior of the Pickering FCs, should be of interest to OPG and to the regulator. In light of the difficulties encountered in presenting this information to the industry, the public hearing on the Pickering license renewal was identified as a good opportunity to present information believed to be previously unknown to OPG.

2. Review of the Pickering B FC Fitness-for-Service Assessments

As an intervenor in the public hearing on the 10 year extension of the Pickering operating license, the author of this letter was mandated by the CNSC to perform a review of licensing documentation provided by OPG. As part of that documentation, a summary of the FC aging mechanisms for the Pickering B reactors was provided by OPG to the CNSC in the technical letter of Reference [3]. In Attachment 1 to Reference [3] it is stated that the Pickering FCs were found to be fit-for-service for operation to the end of the evaluation periods given in Table 1, below.

Table 1: Equivalent Full Power Hours at End of Evaluation Period

Pickering Unit	EFPH Target Evaluated
Unit 1	182 kEFPH
Unit 4	159 kEFPH
Unit 5	276 kEFPH
Unit 6	286 kEFPH
Unit 7	279 kEFPH
Unit 8	263 kEFPH

For the public hearing, the content of Reference [3] was reviewed by the author, drawing upon his experience with FC integrity assessments. Details of the individual analyses were not made available for a full technical review of the numerical results. However, based on a knowledge of the modelling of degradation in the Pickering B FCs and fitness-for-service assessments for the Candu 6 reactors, as well as the various Candu 6-specific observations described in the presentation, the overall conclusion is that the Pickering FCs are fit-for-service within the end of the evaluation periods in Table 1. The presentation will show that the FC mechanical/materials models have a number of sources of inherent conservatism built into them. The implication in this presentation is that certain refinements to the modelling would yield significant increases in the predicted safe operating lives of the Pickering FCs beyond the EFPH targets presented in Table 1.

At this point, it should be noted that I strongly support the continued operation of the Pickering reactors, despite some of the criticisms of the details of the FC fitness for service assessements that will be offered in the presentation. My support for Pickering is based on a strong conviction that the Pickering FCs are significantly more robust than the industry is currently taking credit for.

3. Candu 6-Specific Observations of FC Behaviour that Should Apply to Pickering

Slide 2 lists a set of four observations ((1) CT Spring Back, (2) PT Sag Rate, (3) CT Ovality Measurements (4) CT LISS Nozzle Gap Measurements) related to FC behavior that were made in Candu 6 reactors, which should also apply to the Pickering FCs. It is believed that this information was not made available to OPG for use in the modelling of the Pickering FCs.

Background information for the four topics listed above is provided in the notes of Sections 3.1 to 3.4, that follow.

3.1 CT Spring Back

Spring back is defined as the vertical elastic deflection of the CT as the entire fuel string is loaded or unloaded into the PT. Spring back measurements were performed during the 2004 inspection of the FCs in Point Lepreau. Slide 6 presents a bar graph of various spring back values for PLF06, taken from Reference [4].

Reference [4] is found in Attachment 3 to this letter.

The bar on the left-hand side of the graph represents the spring back value for PLF06, predicted by executing the CDEPTH Code with the standard FC model for PLF06. The bar on the right side of the graph represents the measured spring back value for PLF06, which is substantially smaller than the predicted value. The three intermediate bars in the graph are not relevant to the presentation but represent several CDEPTH Code predictions that use modified FC models in an attempt to replicate the measured spring back results. The figure indicates that the fuel channel is stiffer than predicted with the standard model, which means that the predicted elastic curve of the FC will have a greater downward deflection than the actual elastic curve. This implies that the initial CT-LISS gap would be greater than the predicted gap, leading to longer times to CT-LISS contact than would be predicted with the standard FC model.

The table in Slide 6 presents CT-LISS contact times for Pickering 5 – 8 from Reference [3] and PT – CT contact times from the previous assessments submitted in 2015 in Reference [3], which are believed to still be valid. As a result of the possibility that the standard FC model underestimates the lateral stiffness of the FC, it is expected that the predicted CT-LISS and PT-CT contact times reproduced in Slide 6 will be exceeded by the Pickering B FCs.

3.2 Non-Linearity in PT Sag Rate

The CDEPTH Code is the industry standard computer program for the prediction of FC sag deformation . In CDEPTH analyses to predict CT-LISS contact times, CT sag is linear with time in-service. The linear CT sag model plays a significant role in the prediction of CT-LISS contact times.

As a comparison, Slide 7 presents a plot of measured PT sag versus EFPH for Point Lepreau and Gentilly-2 from Reference [5].

Reference [5] is presented in Attachment 4 to this letter.

The individual sag data points are depicted as points on the plot and the two curves represent mean fits to the data points. Some non-linearity is evident in the mean fit curves to the sag data

in that the rate of PT sag appears to be decreasing with time in service for Point Lepreau and Gentilly-2.

There are two possible explanations for the observed non-linearity in CT sag. The first is a purely geometric argument that would apply to all fuel channels including those in Pickering, advanced in Reference [5].

The second possible explanation for the apparent decrease in sag rate with time is that both Point Lepreau and Gentilly-2 underwent power derating. Early in the operating life of the fuel channels, the PT outlets operated at higher power levels and higher temperatures than those experienced during operation at derated power levels. The operating history of the Pickering reactors is also believed to have involved derating. Therefore, some non-linearity in the sag of the Pickering FCs is expected. Should a non-linear PT and CT sag model be developed for the Pickering B reactors, predicted CT to LISS contact times should exceed the current predictions presented in Slide 7.

3.3 CT Ovality Measurements

The information provided in Slides 8 to 12 was based on References [1] and [2].
In an attempt to understand the PT sag behavior shown in Slide 7, the author studied FC inspection data for Point Lepreau in 2005. With input from the FC inspectors at Chalk River Laboratories, It was discovered that the PT dimensional data could be combined with PT – CT gap measurement data to generate CT inner diameter profiles for channels that had been inspected. The formula for the calculation of the CT inner diameter at an angle θ round the circumference of the CT is given in Slide 10, explained more fully in Reference [2]. This was a significant development. Previously, CT inner diameter measurements could only be obtained for CTs that had been removed from service. Details of the method for producing the profiles are found in Reference [2]. Each profile consists of CT inner diameter values versus angular position around the circumference of the CT.

Slide 8 presents a typical plot of CT inner diameter vs angular position, possibly the first published CT inner diameter profile to be generated from PT in-service inspection data. The CT diametral ovality measured for PLF06 was determined to be 6 mm. CT ovality is not included in the existing FC models.

For the Pickering FCs, CT ovality will introduce a new loading condition on the PT, CT, and spacer, explained as follows. In the design condition, the PT rests on the spacer, which in turn sits at the bottom of the CT. The spacer contacts the CT over a short arc length at the bottom of the CT. In Slide 8, the design condition is depicted in the sketch to the right of the figure. The blue circle represents the CT and the thick red circle represents the spacer, combined with the PT. In the nip-up condition, depicted in the sketch beside the design condition,the diametral expansion of the PT forces the spacer into full circumferential contact with the CT. Nip-up therefore is a new, off-design loading condition which requires a stress analysis to ensure FC integrity. It should be noted that for the nip-up condition to develop, the CT must have a circular cross section.

However, when CT ovality develops, eventually, the CT inner diameter will interfere with the spacer outer diameter before nip-up can take place. The initial PT-CT contact would be limited to an area at the bottom of the CT and there would not be full contact around the circumference of the PT as in the case of nip-up. Essentially, with increasing ovality and increasing PT inner

diameters, the spacer will be pinched between the PT and the CT at various points. This condition, named partial nip-up in Slide 8, is illustrated in the slide.

3.3.1 The Validity of Gap Calibration Based on CT Inner Diameter Distributions

The CT ID profile data can be used to produce plots of the axial distribution for CT inner diameter, as shown in Slides 9, 10 and 12. The slides are from Reference [2], provided as Atttachment 2 to this letter. The main theme in Slide 9 to Slide 12 is that gap calibration, outlined in Slide 11, produces an axial distribution for the mean CT inner diameter that is unrealistic since it does not match the distribution seen in removed CTs, as exemplified in Slide 9.

Slide 9 presents CT inner diameter measurements versus axial positions for the CT removed from M11 in Pickering Unit 4. It can be seen that while there is ovality at the two spacer locations, the mean inner diameter is uniform over the length of the CT.

Slide 10 presents the same CT inner diameter axial distributions as in Slide 9 for PLF06, derived using gap calibration, which is defined in Slide 11. As shown in Slide 11, gap calibration consists shifting the axial gap profile upwards so that the magnitude of the gaps at spacer locations match the spacer coil diameter. The key point in Slide 10 is that with gap calibration, an unrealistic mean axial distribution of CT inner diameter results for PLF06 since the mean CT inner diameter is not uniform. Therefore, it is postulated that gap calibration is technically incorrect. Slide 12 supports the contention that gap calibration is not technically justifiable, as follows. In Slide 12, axial CT inner diameter distributions are plotted using PT-CT gaps that were not calibrated, for G2H14. It can be seen that the mean inner diameter distribution with no gap calibration in Slide 12 is much more uniform than the distribution for PLF06 in Slide 10. which features gap calibration.

Slides 9 – 12 suggest that gap calibration for Pickering should be studied. If necessary, PT-CT time-to-contact predictions that use gap calibration should be revised, as stated in the conclusions of Slide 15.

3.4 CT – LISS Gap Measurements

There are two methods used for the measurement of the gap between the CT and the LISS nozzle below it: (1) the optical camera method, and (2) the UT inspection method. The CT-LISS gap measurements in the Pickering B reactors were performed using the optical camera method.

An illustration of optical CT-LISS gap measurement is provided in Slide 13. In the optical method, an image of the gap is captured with the camera. There are two different techniques for measuring the gap: (1) a curser on the screen is lined up with the bottom of the image of the gap, the camera is raised until the curser is aligned with the top the image of the gap, and then the movement of the camera is determined, (2) the image of the gap is compared with the image of the CT and the size of the gap is determined by scaling the two images.

There are inherent difficulties with the optical gap measurement, which are outlined in 3.4.1

3.4.1 The Accuracy of Optical CT - LISS Gap Measurements

3.4.1.1 Introduction

Starting in 2003, optical measurements of CT – LISS gaps have been performed

in various reactors and the gap data has been used in predictions of the time at which the CTs would sag into contact with the LISS Nozzle.

Optical CT-LISS Nozzle measurements in Point Lepreau in 2004 did not display any problems. However, the optical gap measurements taken in Gentilly-2 in 2006 were found to be inconsistent with those taken in 2003. A study of the gap data was undertaken, from which it was concluded that some error or significant inaccuracy had occurred in the 2003 or 2006 gap measurements. The raw measurement data was reviewed by AECL and Hydro Quebec staff and consultants but the source of the inaccuracy was not found.

Therefore, it was stated in Reference [6] that the optical CT – LISS gap measurement method can produce questionable results. Reference [6] is presented as Attachment 5 to this letter. For future CT – LISS time-to-contact predictions, alternative gap measurement methods were recommended.

Section 3.4.1 presents the gap measurement data that was used determine that optical gap measurement method can produce significantly inaccurate results.

In the second part of Section 3.4.1, a physical rationale will be provided to explain why, in many cases, the size of the image of the gap between the CT and the LISS underestimates the size of the actual CT-LISS Nozzle gap.

3.4.1.2 Development of the Optical CT-LISS Gap Measurement

In 2000, CT-LISS gaps in Point Lepreau were measured using a contact finger system which used a camera to allow the operator to see that the tool was properly positioned prior to making the measurements. The resultant gap measurements were found to be erratic and Point Lepreau started searching for an alternative method for measuring the CT-LISS gap. In the inspection of Point Lepreau in 2000, high quality images of the CT and LISS were produced that displayed clear images of the CT-LISS gap. Encouraged by image quality of the camera, AECL proposed that the camera alone should be used to capture images of the CT-LISS gaps and subsequently size the images.

Two methods were devised for measuring the CT-LISS gap: (1) proximity measurement, and (2) image scaling.

In the proximity measurement, a reference line on the camera is positioned to line up with the top of the LISS at the perceived intersection point of the CT with the LISS and the camera elevation at this first position is recorded. The camera is then raised so that the reference line intersects with the bottom of the CT at the intersection point. As before, the camera elevation is recorded at this second position. The difference in the elevation of the camera from the second to the first position represents a measurement of the CT-LISS gap.

The scaling method involves the direct use of images of the CT, gap, and LISS obtained by the camera. In the scaling method, the size of image of the gap is compared to the size of the image of the LISS or CT to obtain a ratio of gap size to CT or LISS nozzle diameter. Knowing the CT or LISS nozzle diameter, a numerical value can be assigned to the CT-LISS gap.

3.4.1.3 Examples of Reasonable and Questionable Optical CT-LIN Gap Measurements

Section 3.4.1.4 presents an example of gap measurements which show consistency and, at the very least, appear to be valid. Section 3.4.1.5 presents examples of gap measurements which are inconsistent, and therefore, are questionable. Section 3.4.1.6 illustrates how the use of specific questionable gap measurements produces questionable values of LISS Nozzle sag.

3.4.1.4 Examples of Reasonable Optical CT-LIN Gap Measurements

Figure 1 presents CT-LISS gap measurements for LISS 2 in Point Lepreau and Gentilly 2, plotted versus EFPH. For G-2, the gap measurements were from 2003 and 2006. The observed rates of gap closure are quite constant in G-2 and the rates of closure for specific gaps are consistent with those observed in PLGS, which are expected results.

Figure 1 – CT – LISS Nozzle Gap Measurements for LISS 2 in PLGS and G-2

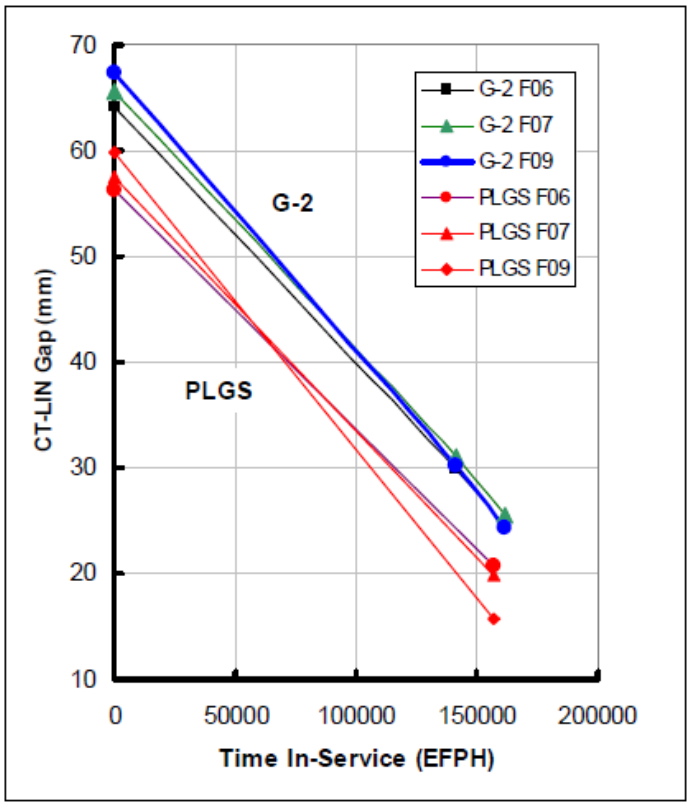

3.4.1.5 Examples of Inconsistent Gap Measurements

The same information given in Figure 1 is plotted for LISS 5 in PLGS and G-2 in Figure 2. it can be seen that there is a significant non-linearity in the plot of gap versus EFPH for G-2, which was unexpected. Therefore, the gap measurements from 2003 for LISS 5 in G-2 are inconsistent with those measured in 2006.

Figure 2 – CT – LISS Nozzle Gap Measurements for LISS 5 in PLGS and G-2

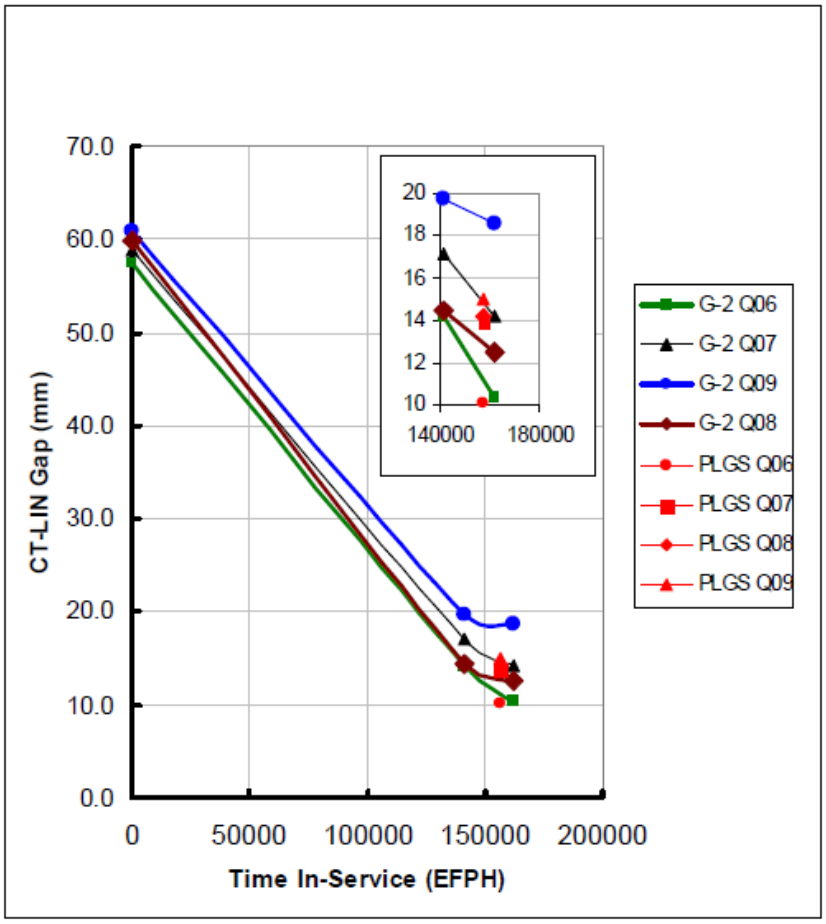

3.4.1.6 An example of the Application of Questionable Gap Measurement Data

In the design of the CT-LISS gap measurements, the gap data was to be combined with CT sag measurements or predictions to deduce the elevations of the contact points on the LISS Nozzle. In this way, the in-service deformed shape of the LISS Nozzle could be obtained. Figure 3 presents a plot of elevation versus axial position along the length of the LISS Nozzle for the nominal elastic curve of LISS 5 in G-2, depicted in blue. Note that elevation is defined as the distance below the centerline of the fuel channel and so the elastic curve in Figure 3 appears to be upside down. The two points plotted in red represent the elevations of LISS Nozzle 5 at the intersection points with the CTs of Q06 and Q08, based on the gap data obtained in 2003. The figure indicates that the in-service elevation of points along LISS Nozzle 5 is less than the elevation of the support points for the LISS Nozzle. Physically, this means that using the 2003 gap measurements, there would be points on LISS Nozzle 5 in G-2 that are located above the support points of the LISS, which does not make sense. The results in Figure 3 indicate that the 2003 gap measurements in G-2 significantly underestimate the actual gaps.

Figure 3 – Elevation of the Nominal Initial Elastic Curve and at 2 Discrete Points from the 2003 Gap Measurements for LISS Nozzle 5 in G-2.

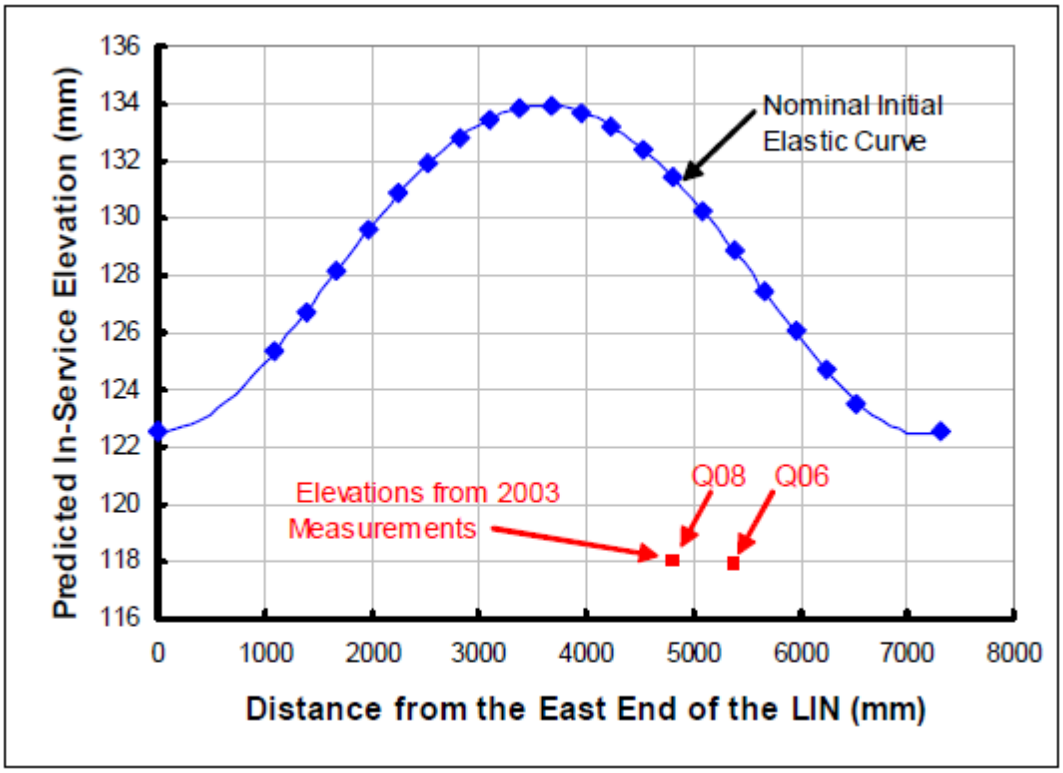

Overall, the optical CT-LISS gap measurements for Pickering will tend to underestimate the size of the gap.

In summary, it is expected that the gaps have been underestimated for the Pickering B reactors, so that the actual CT-LISS contact times would be later than those given in Slide 6, as concluded in Slide 15.

3.4.1.7 Physical Explanation for the Underestimation of Gap Size

Two factors have been identified as causes for the underestimation of gap sizes using the optical method of gap measurement: (1) Sag of the LISS Nozzle, and (2) elevation of the camera relative to gap being imaged.

Figure 4 illustrates how the image of the CT- LISS captured by the camera can underestimate the size of the actual gap as a result of LISS Nozzle sag. The image of the gap is formed by light passing between the CT and the LISS Nozzle. In this case, the camera is at the same elevation as the space between the CT and the LISS Nozzle that forms the gap image. The height of the beam of light passing between the CT and the LISS Nozzle is determined by the vertical distance between the bottom of the CT and the highest point at the top of the LISS Nozzle along its length. As shown in the figure, the bottom of the CT and the highest point at the top of the LISS Nozzle are not equidistant to the camera because of the sag of the LISS Nozzle. Because of the sag of the LISS Nozzle, as depicted in the figure, the actual gap is larger than the image of the gap, captured by the camera.

To avoid the effect of LISS Nozzle sag on gap image, gap imaging must be performed with the camera perpendicular to the LISS Nozzle. With the arrangement of view ports in the calandria, only a few of the gap images can be generated with the camera perpendicular to the LISS Nozzle.

Figure 4 – Underestimation of Gap Size due to Sag of the LISS Nozzle

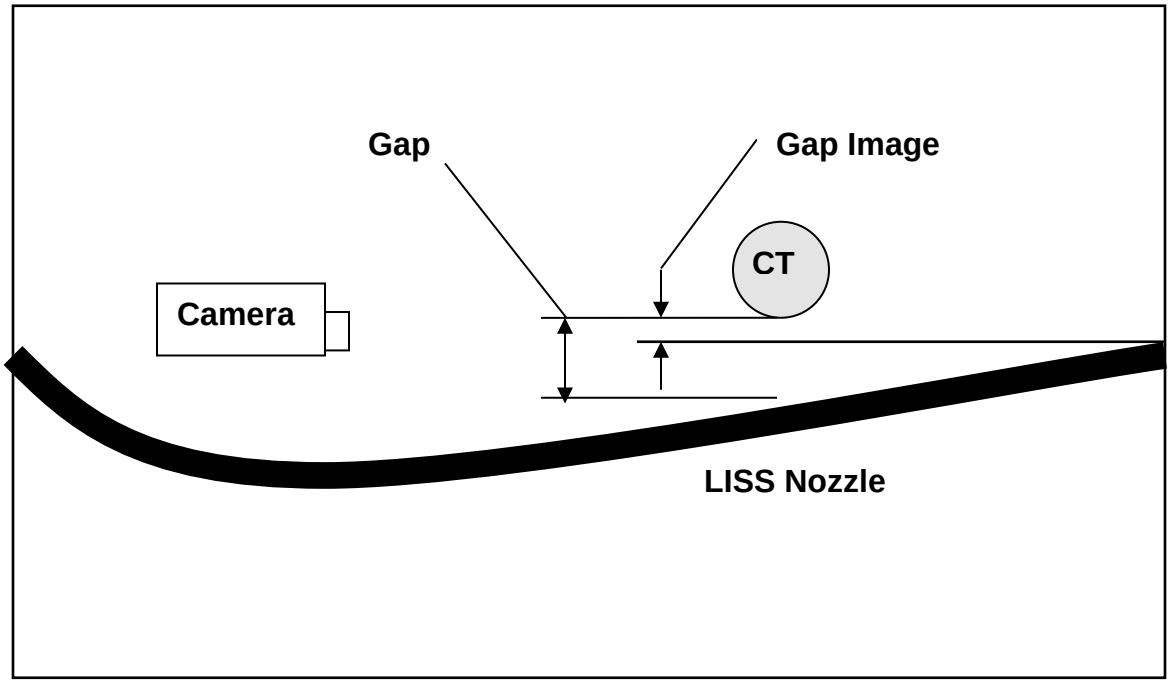

Figure 5 illustrates how elevation of the camera relative to the gap reduces the size of the gap image that is captured by the camera. In this example, the LISS Nozzle is assumed to be straight and the camera is inclined at an angle θ relative to the LISS Nozzle. At θ = 0º, the camera would be at the same height as the top of the LISS Nozzle and the gap image would be a good representation of the actual gap size. However, with increases in θ, as depicted in Figure 5, the apparent space between the CT and LISS Nozzle would decrease, reducing the size of the gap image.

It is expected that the inclination of the camera is not strictly controlled during the gap measurements.

Figure 5 – Underestimation of Gap Size due to Elevation of the Camera Relative to the CT

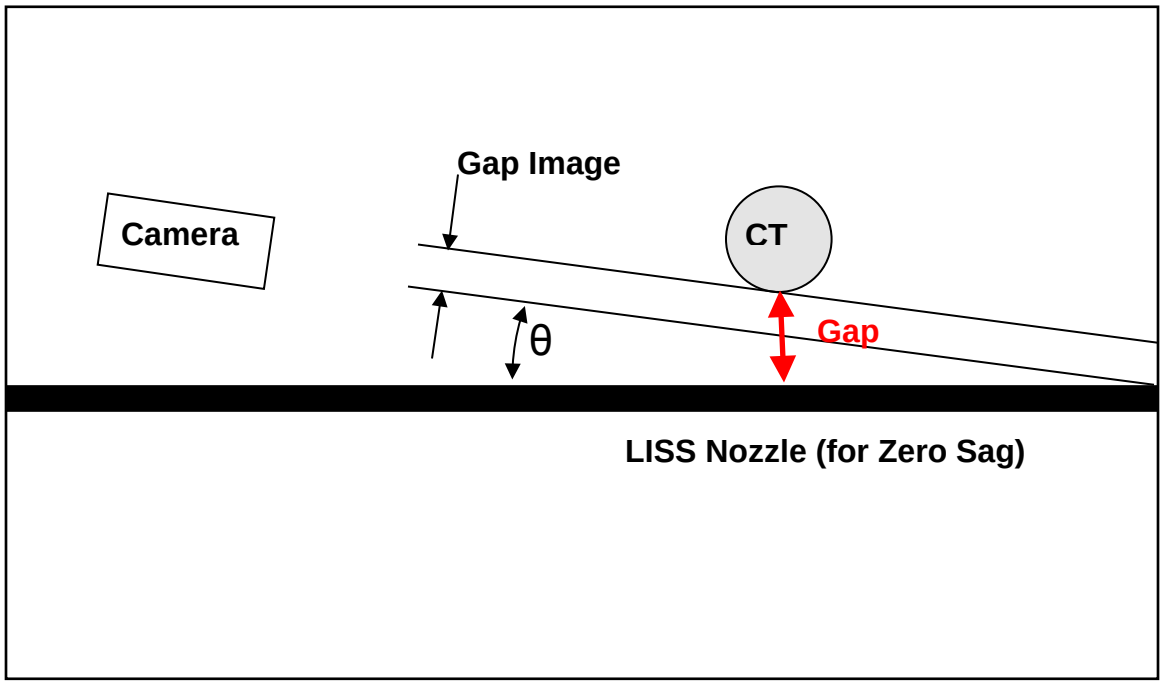

3.5 A Suggestion for a Refinement in the LBB Analysis of Pressure Tubes

The material for this topic is presented in Slide 14. The methodology used to simulate a growing crack in an LBB analysis was developed for COG in 1990. In the development process, various scenarios for the start of a leaking pressure tube event, which initiates with the penetration of a crack through the PT wall, were studied. The different scenarios were defined by the occurrence of crack penetration at different points in the operating cycle of the reactor, such as the full power hot condition, the zero power hot condition, and during reactor shutdown, cooldown, and heatup. Of all the scenarios, It was found that crack penetration at full power hot conditions presented the greatest risk to LBB. Consequently, that crack penetration would occur with the reactor at full power hot conditions was made a standard assumption in the deterministic and probabilistic LBB analyses of pressure tubes. However, there was no consideration of the validity of the assumption that crack penetration would occur at full power hot conditions. As outlined in Reference [7], included as Attachment [6] to this letter, a case can be made for stating that crack penetration is much more likely during a reactor cooldown than during operation at power. Reference [7] shows that margins against PT rupture would be significantly greater for an LBB scenario with crack penetration during a cooldown than for the standard scenario with crack penetration at full power hot conditions.

The implication for Pickering B is that the stated margins against PT rupture can be improved significantly, if required, by modifying the LBB analysis to allow for crack penetration during a reactor cooldown, as stated in Slide 15.

4. Conclusions

1. Based on the Point Lepreau CT spring back measurements, the CANDU FC, including the Pickering FC, may have greater lateral stiffness than that of the existing FC models. If this indication were confirmed for Pickering, the time-to-contact predictions in Reference [3], (both for PT-CT and CT-LISS contact), could be improved.

2. PT sag measurements in the CANDU 6 reactors have indicated a non-linear trend for sag versus time in-service. There are reasons to believe that the Pickering PT and FC should also be subject to non-linear sag with time in-service. Should this be confirmed for Pickering, the time-to-contact predictions in Reference [3], (both for PT-CT and CT-LISS contact) could be improved.

3. CANDU 6 inspection results have shown significant CT ovality, not included in the existing FC models, which is expected in the Pickering CTs as well. Based on the CANDU 6 CT ovality measurements, partial nip-up will occur before actual full nip-up in the Pickering Reactors. The partial nip-up might interfere with spacer movement during SLAR. A stress analysis of the partial nip-up condition should be added to the Pickering FC stress report to go along with the nip-up stress analysis.

4. PT-CT gap calibration appears to produce CT inner diameter profiles that are not consistent with known results from CT inner diameter gauging. The validity of gap calibration should be investigated and may lead to reassessment of PT-CT contact times for Pickering.

5. CT-LISS optical Gap and UT Measurements may underestimate the actual gap, giving underestimates of CT-LISS contact time.

6. The assumption of crack growth at FPH conditions in the current deterministic and probabilistic LBB analyses may be excessively conservative. Should the need arise for Pickering, OPG could make a case in the LBB analysis that the crack would start to grow during the reactor shutdown/cooldown instead of at FPH conditions.

The points in conclusions 1-3 and 5-6, should they be confirmed or acted upon, would generate significant improvements in the predicted behavior of the Pickering FCs, should the need arise. The issue of gap calibration is not expected to have a significant effect on time-to-contact predictions.

In summary, the above provide a good rationale for confidence in the continuing fitness-for-service of the Pickering FCs, independent of the solid work done through COG in the industry.

5. References

1. The Use of OPEX (In the Form of Inspection Data) to Obtain Unanticipated Calandria Tube (CT) Ovality Measurements, P.J. Sedran, 9th International Conference on CANDU Maintenance, Toronto, Ontario, December, 2011.

2. The Generation of Calandria Tube (CT) Inner Diameter Profiles from Fuel Channel (FC) Inspection Data, P.J. Sedran, 35th Annual Conference of the Canadian Nuclear Society, Saint John, NB, May, 2015.

3. OPG Letter, R. Lockwood to A. Viktorov, "Assurance of Fuel Channel Fitness-for-Service for the Assumed Target Service Life of the Pickering Units", CD# P-CORR-00531-04953, April 4, 2017.

4. Refinements to Calandria Tube – Liquid Injection Nozzle (CT-LIN) Contact Assessments, P.J. Sedran, 27th CNS Steam Generator to Controls Conference, Toronto, Ontario, December, 2011.

5. A Rationale for the Observed Non-Linearity in Pressure Tube Creep Sag with Time in Service, P.J. Sedran, 34th Annual Conference of the Canadian Nuclear Society, Toronto, Ontario, June, 2013.

6. P. Sedran and B. Rankin, NB Power, *A Method for Predicting CT-LIN Contact Using CANDU 6 Inspection Results*, 8th International Conference on CANDU Maintenance, November 18, 2008.

7. A Challenge to a Traditional Assumption in Pressure Tube (PT) Leak-Before- Break Assessments, P.J. Sedran, International Nuclear Components Conference, Mississauga, Ontario, November, 2015.

Regards,

Paul Sedran, P.Eng., M.Eng.

Attachment 1

SUBMITTED FOR SESSION A3:

THE USE OF OPEX (IN THE FORM OF INSPECTION DATA) TO OBTAIN UNANTICIPATED CALANDRIA TUBE (CT) OVALITY MEASUREMENTS

P.J. Sedran[1]
B. Rankin[2]
1 Canadian Power Utility Services Limited
2 NB Power Nuclear Incorporated

ABSTRACT

For fuel channel deformation studies, inspections are an essential source of OPEX and are used to generate specific data, such as pressure tube dimensions. However, additional unintended information can be extracted from raw inspection data. This paper presents examples of the generation of CT inner diameter profiles using data from the inspections of L1F06 and G2F14 to illustrate how inspection/OPEX data can contain significant hidden information.

In the CT diameter profiles for L1F06 and G2F14, it was found that spacer loading produced significant local ovality in the CT and that the resultant gap reduction is consistent with the predictions of the existing deformation models [1].

The finding of significant local CT ovality is corroborated by CT gauging measurements reported by S.A. Donahue in 2008 [2].

1. Introduction

It was observed in 2005 that PT creep sag appeared to be non-linearly decreasing with time in-service in both Gentilly-2 and in Point Lepreau. To test the hypothesis that this observation could be attributed to in-service generated CT ovality,. CT gauging measurements were needed. After discussions with AECL inspectors, it was found that, in principle, the PT gauging and circumferential CT-PT gap scan data from the 2004 PT inspection of Point Lepreau [3] could be used to determine in-service CT inner diameter profiles. When the inspection was carried out, there was no thought of using the PT inspection data to gauge the CT until the need arose several years later. The CT inner diameter profiles were subsequently generated for Fuel Channel F06 in Point Lepreau and later for Fuel Channel H14 in Gentilly-2, using dimensional data obtained during the 2005 SLAR campaign, issued in [4].

This paper presents the CT inner diameter profiles generated for Fuel Channels F06 and H14 in Point Lepreau and Gentilly-2, respectively, provides a comparison with CT gauging measurements at CRL, and discusses the implications for fuel channel integrity,

2. Calandria Tube In-Service Loading, Stress and Deformation

As a result of PT in-service creep sag, the PT is not fully self supporting and a portion of the weight of the PT is carried by the spacers, which constitutes spacer loading. The loading of the spacer consists of a downwards contact force at the inner diameter of the spacer along a line of contact with the PT and an upwards contact force at the outer diameter of the spacer along a region of CT-spacer contact.

Spacer loading has significant implications for fuel channel integrity. It drives in-service creep sag of the CT as well as local deformation at the bottom of the CT at the CT-spacer contact region, termed “gap reduction”, depicted in Figure 1a.

Figure 1a. Gap Reduction Deformation of the CT Under Spacer Loading

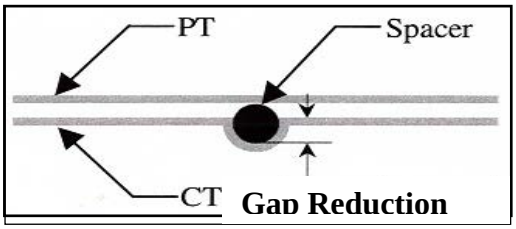

Figure 1b presents the distribution of vertical stresses in the CT due to spacer loading, from an analysis of spacer nip-up performed for Point Lepreau [5].

Figure 1b. Spacer Loading and Resultant Vertical Stresses in the CT

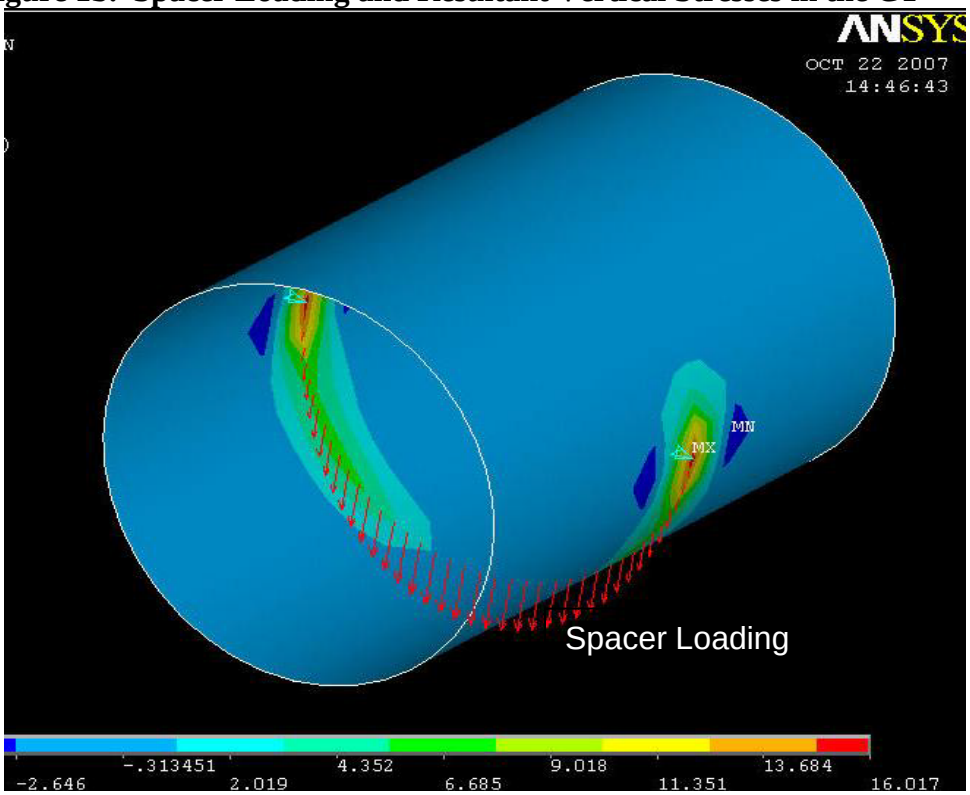

The red arrows in the figure depict the load applied by the spacer to the inside surface of the CT. As seen in the figure it is predicted that the CT cross-section at the spacer is subject to a tangential stress, due to in-service spacer loading. Under this loading, the CT should develop localised regions with expanded vertical diameters at spacer locations. The expected diametral expansion of the CT would be in addition to the gap reduction deformation of the CT along the contact line at the bottom of the CT. Both types of deformation would increase the vertical diameter of the CT by forcing the bottom of the CT in a downwards direction.

3. Inspection Data

For this paper, three sets of inspection data were used to characterise the in-service deformation of the CT: (1) PT gauging measurements and CT-PT gap measurements from the 2004 inspection of Point Lepreau (2) PT gauging measurements and CT-PT gap measurements from the 2005 SLAR operation in Gentilly-2, and (3) post-removal CT gauging measurements that were performed in CRL.

The 2004 Point Lepreau inspections were performed at 157 kEFPH. The 2005 SLAR operation at G-2 was performed at 151.7 kEFPH. The post-removal inspections were performed on three CTs: G12 from Bruce Unit 6 and two others from Pickering Unit 4. B6-G12 For this paper, B6-G12, which had accumulated 118.7 kEFPH was selected for further examination.

3.1 Fuel Channel Dimensional Data from the 2004 inspection of Point Lepreau

A summary of the 2004 inspection of the Point Lepreau Fuel Channels is provided in Reference [3]. In the inspection, the AFCIS (Advanced Fuel Channel Inspection System) tool was used produce PT inner diameter and wall thickness ultrasonic scans. CT-PT gap scans were also producing using an eddy current gap probe.

Figures 2, 3, and 4 present PT inner diameter, wall thickness, and CT-PT gap for Fuel Channel F06 in Point Lepreau.

Figure 2. Plot of PT Inner Diameter vs Distance from the Reactor A Face for Fuel Channel F06 in Point Lepreau

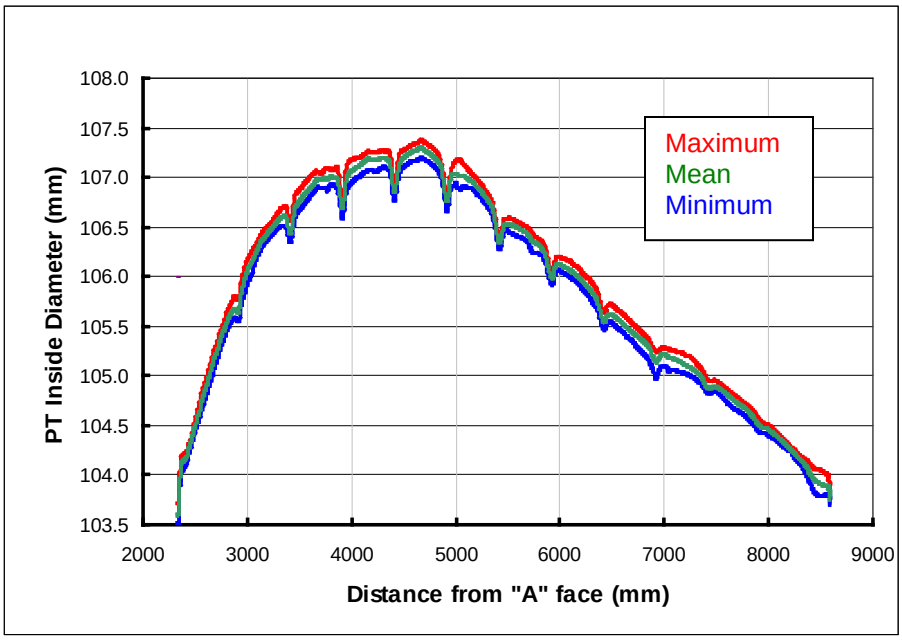

Figure 3. Plot of PT Wall Thickness vs Distance from the Reactor A Face for Fuel Channel F06 in Point Lepreau

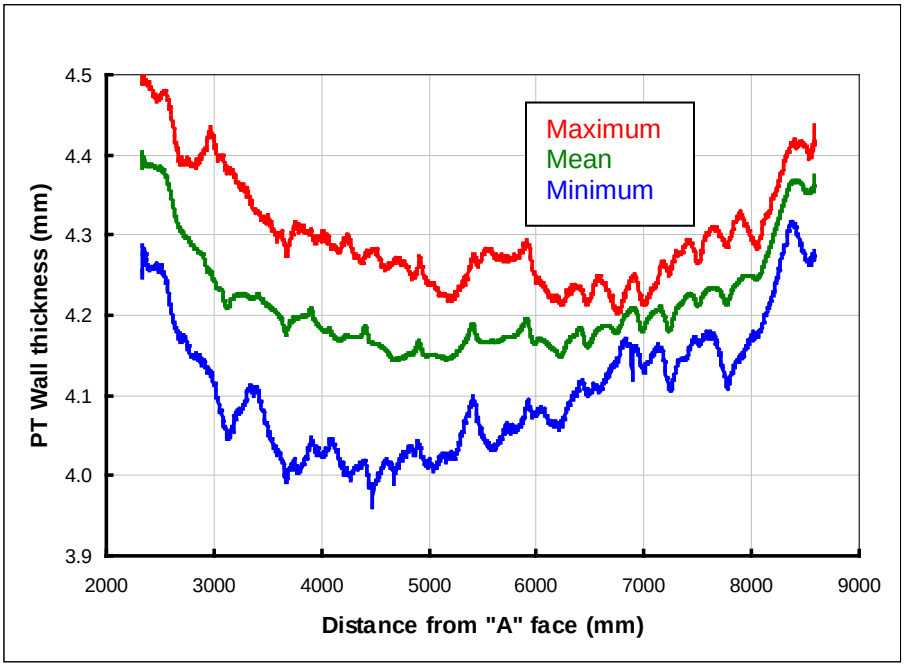

Figure 4. - Plot of CT- PT Gap versus Angular Position for Fuel Channel F06 in Point Lepreau

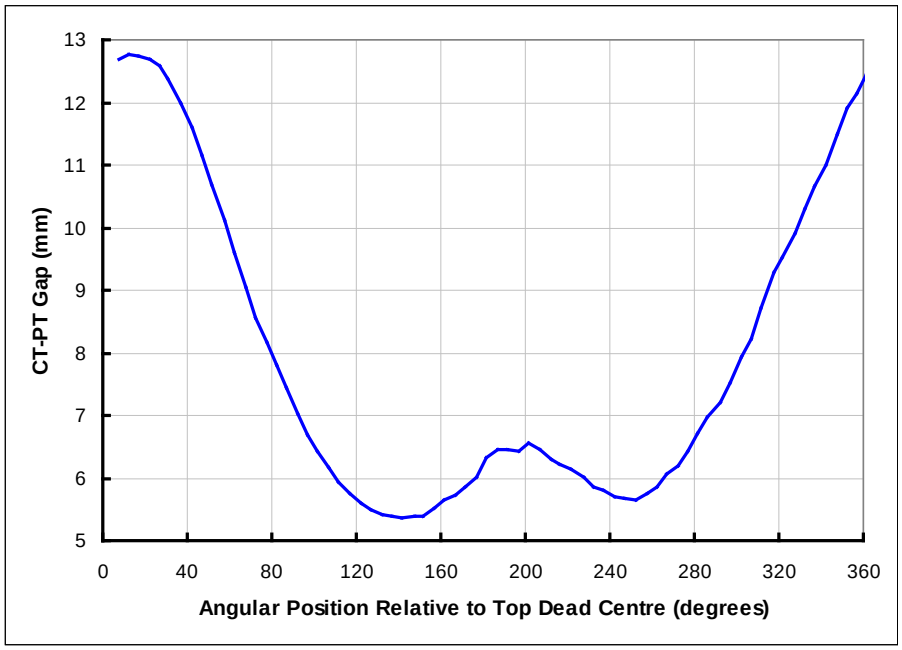

The circumferential scan for Figure 4 was for an axial location 4705 mm from the Inspection CTS.

For Figure 4, it was expected that the CT-PT gap would decrease monotonically from 0º and reach a minimum value near the bottom of the CT, as in Figure 7. Instead, the gap reaches a minimum value at 140° and rises to a peak value at 200º, which is unexpected. The anomaly in the plot of CT-PT gap could be attributable to inaccuracies in the gap measurements, discussed in Section 5 or irregularities in the shape of the CT or PT. In any case, it is expected that general shape of the plot in Figure 4 is representative of the actual CT-PT gap at the cross-section in question.

Figure 4 might indicate a possible problem with the 2004 gap data from Point Lepreau which derives from the use of a non-surface riding gap measurement probe. Although the industry has switched to a surface riding probe for gap measurements, which was used in the SyDef module in the 2005 SLAR of Gentilly-2, potential errors in the gap measurements in F06 due to probe lift-off have not been quantified.

3.2 Fuel Channel Dimensional Data from the 2005 SLAR Campaign in Gentilly-2

The dimensional data presented in this section were generated during the 2005 SLAR operation, using the SyDEF module, developed by Hydro Québec, mounted on the SLAR tool. Figures 5, 6, and 7 present PT average inner diameter, average wall thickness, and CT-PT gap for Fuel Channel H14 Gentilly 2.

Figure 5. Plot of PT Average Inner Diameter vs Distance from the End of the Fuel String for Fuel Channel H14 in Gentilly-2

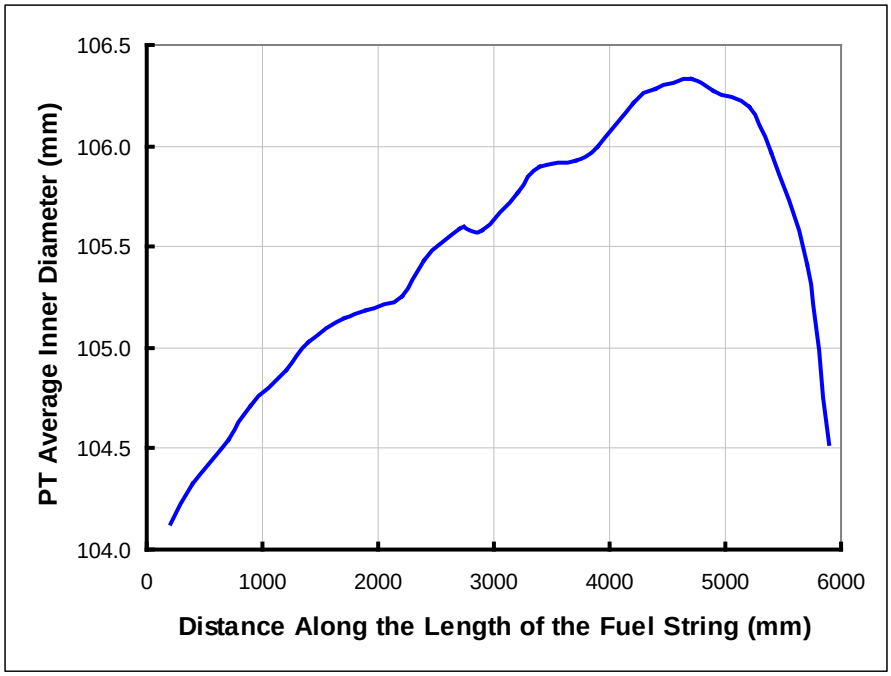

The dimensional data for Figures 5 and 6 were provided by L. Pednault of Gentilly-2 (ret) for use in Reference [6]. The data for Figure 7 is found in Reference [4].

Figure 6. Plot of PT Average Wall Thickness vs Distance from the End of the Fuel String for Fuel Channel H14 in Gentilly-2

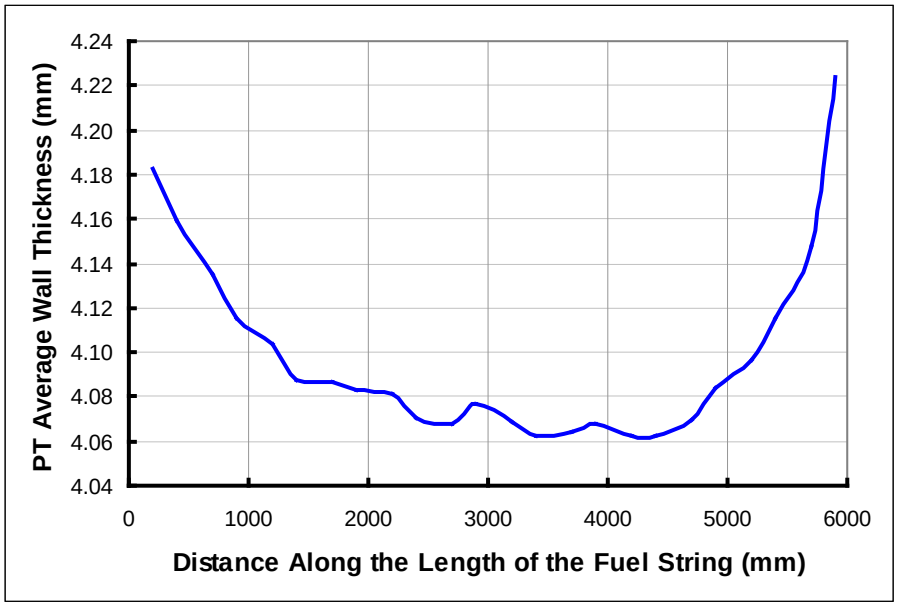

Figure 7. Plot of CT- PT Gap versus Angular Position for Fuel Channel H14 in Gentilly-2

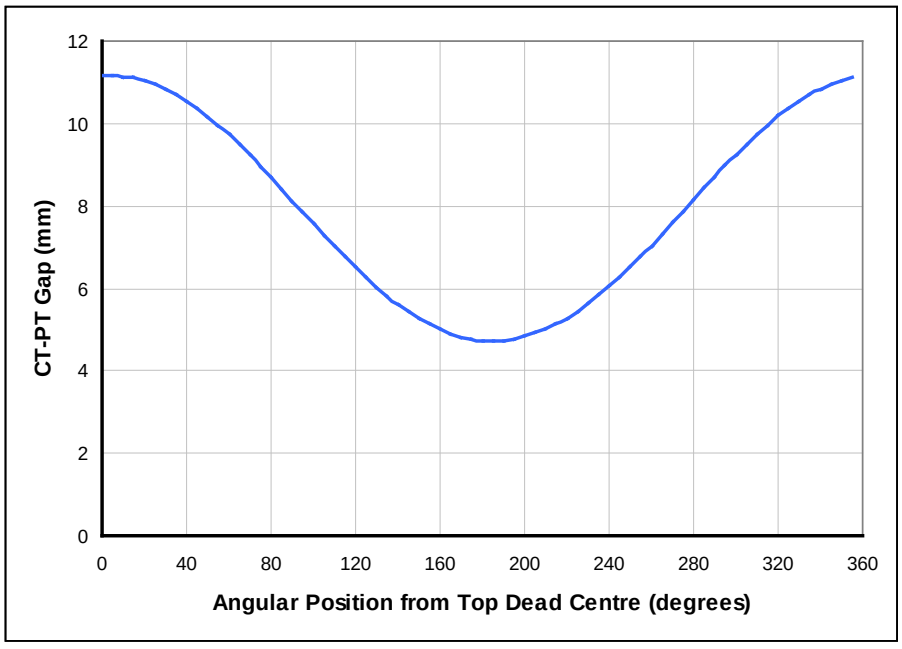

The circumferential scan for Figure 7 was for an axial location 1930 mm from the Inspection CTS.

It can be seen in Figure 7 that the distribution of CT-PT gap with angular position around the circumference of the CT is smoother than the same plot for F06, discussed later in Section 5.

4. Generation of CT Inner Diameter Profiles

As outlined previously, in the 2004 inspection of Point Lepreau and in the 2005 SLAR campaign in Gentilly-2, the following data were obtained: (1) Inner diameter profiles along the length of the PT, (2) Wall thickness profiles along the length of the PT, and (3) CT-PT gap profiles along the length of the PT,

The PT inner diameter, wall thickness, and gap profiles consist of values obtained through scans at discrete circumferential and axial locations along the length of the PT. The profiles define the variation in PT inner diameter, wall thickness, and in CT-PT gap with circumferential and axial position along the length of the PT.

To generate the inner diameter profiles for the CT, inner diameter values at different angular positions were obtained at given axial locations along the length of the CT. Each individual CT inner diameter value at an angular position from Top Dead Centre, θ, $ID_{CT\theta}$ was calculated as the sum of the PT outer diameter plus the CT-PT gap at an angle θ and at an angle (θ+180°):

$$ID_{CT\theta} = ID_{PT} + 2w_{PT} + gap_{\theta} + gap_{(\theta+180°)} \quad \ldots\ldots\ldots 1$$

where ID_{PT} is the average PT inner radius at the given axial position along the CT, gap_{θ} is the CT-PT gap at an angle θ from Top Dead Centre, $gap_{(\theta+180°)}$ is the gap that is diametrically opposite to the gap at an angle θ, and w_{PT} is the average PT wall thickness at the given axial position along the CT.

For Equation 1, the following simplifications were used: (1) each cross-section of the PT was assumed to be circular with an inner diameter equal to the average inner diameter for the cross-section, (2) the PT wall thickness at each cross-section was assumed to be uniform and equal to the average wall thickness over the cross-section. Also, polynomial expressions were fitted to the average PT inner diameter and wall thickness versus axial position data of Figures 2, 3, 5, and 6, and were used to generate PT dimensions that were subject to some smoothing from the polynomials used. The impact of these two assumptions and the polynomial approximation on the magnitude of $ID_{CT\theta}$ values is covered separately in Section 5.

In Section 5, features in the F06 and H14 CT inner diameter profiles are related to as-found spacer positions. Spacer location data are presented in Table 1.

Table 1. As-Found Spacer Location Data for the 2004 Inspection of Point Lepreau and the 2005 SLAR of Gentilly-2

Station	FC	Spacer 1	Spacer 2	Spacer 3	Spacer 4
		(mm) from the Inspection CTS			
Pt. Lepreau	F06	1371	2494	3302	4472
Gentilly-2	H14	969	2189	3445	4746

5. Results from the Generation of CT Inner Diameter Values

Using Equation 1, CT inner diameter profiles were generated for F06 in Point Lepreau and for H14 in Gentilly-2. The profiles consisted of sets of inner radius values at discrete points around the circumference of the CT, at a given axial locations, termed "circumferential scans" by the inspectors. For each set of inner radius values in a circumferential scan, which defines a particular CT Cross-section, the angular position ranged from 0° to 358°, noting that 0° is at the Top Dead Centre position. Each circumferential scan consisted to 72 data points. In F06, the circumferential CT-PT gap scans were 220 mm apart and were 248 mm apart in H14..

5.1 Properties of Individual CT Cross-Sections

Figure 8 presents a plot of CT inner diameter at various angular orientations around the circumference of the CT for F06 in Point Lepreau. The same plot for H14 in Gentilly-2 is provided in Figure 9. The CT cross-sections corresponding to the two plots are typical of those located near spacer positions, as outlined in Section 4.2. As seen in the two figures, the vertical inner diameter of the CT (at 0°) is larger than the horizontal inner diameter (at 90°). For a nominal as-installed CT inner diameter of 129 mm for F06 and H14, it can be seen that the deformation of the CT cross-section has involved both an expansion of the vertical diameter and a reduction of the horizontal diameter of the CT.

Figure 8 – Plot of CT Inner Diameter vs Angular Position for Fuel Channel F06 in Point Lepreau

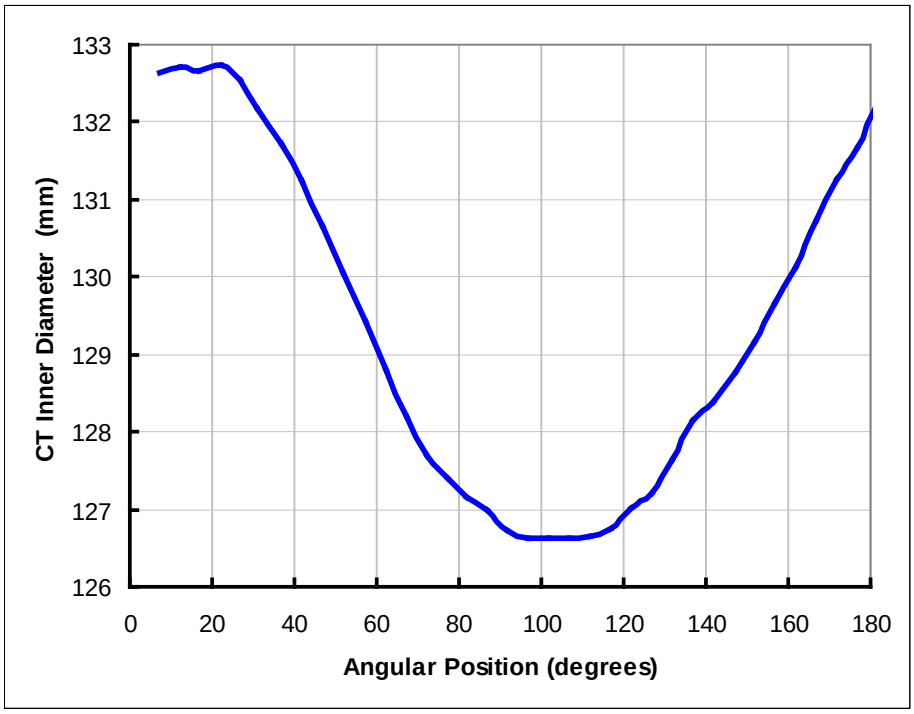

The circumferential scan for Figure 8 was for an axial location 4705 mm from the Inspection CTS.

Figure 9 – Plot of CT Inner Diameter vs Angular Position for Fuel Channel H14 in Gentilly-2

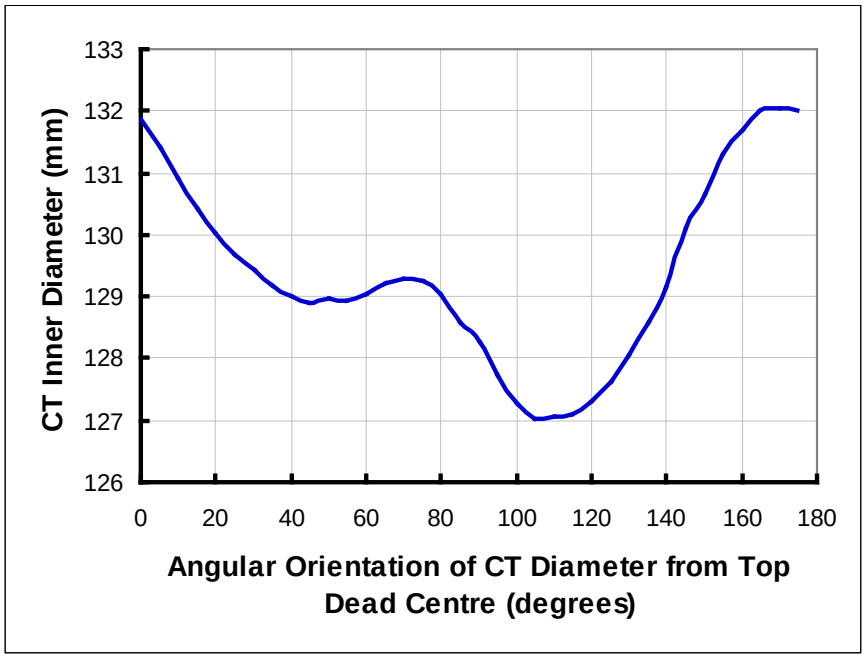

The circumferential scan for Figure 9 was for an axial location 4705 mm from the Inspection CTS.

5.2 Axial Distribution of CT Ovality

Figures 10 and 11 present the distribution of CT ovality along the length of the CT for F06 and H14, respectively. Ovality is defined on diameter, as the difference between the maximum inner diameter and the minimum inner diameter for the given circumferential scan. As-found spacer locations are indicated in the figures.

As seen in the figures, there are multiple local ovality peaks in the axial profiles for F06 and H14. Ideally, it was hoped that the spacer locations in Figures 10 and 11 would line up exactly with the local peaks in the CT ovality profiles. In this case, actual maximum ovality values would be captured in the CT ovality profiles. Unfortunately, the axial spacing for the circumferential CT-PT gap scans, illustrated in the figures, was too wide to capture the local ovality peaks at the spacer locations. By coincidence, a number of spacer positions in Figures 10 and 11 are aligned with local peaks in the CT ovality profiles. Overall, the figures support the association of CT ovality peaks with spacer positions, although not as exactly as was hoped.

Figure 10. Plot of CT Ovality on Inner Diameter vs Axial Position Along the Length of the CT for Fuel Channel F06 in Point Lepreau

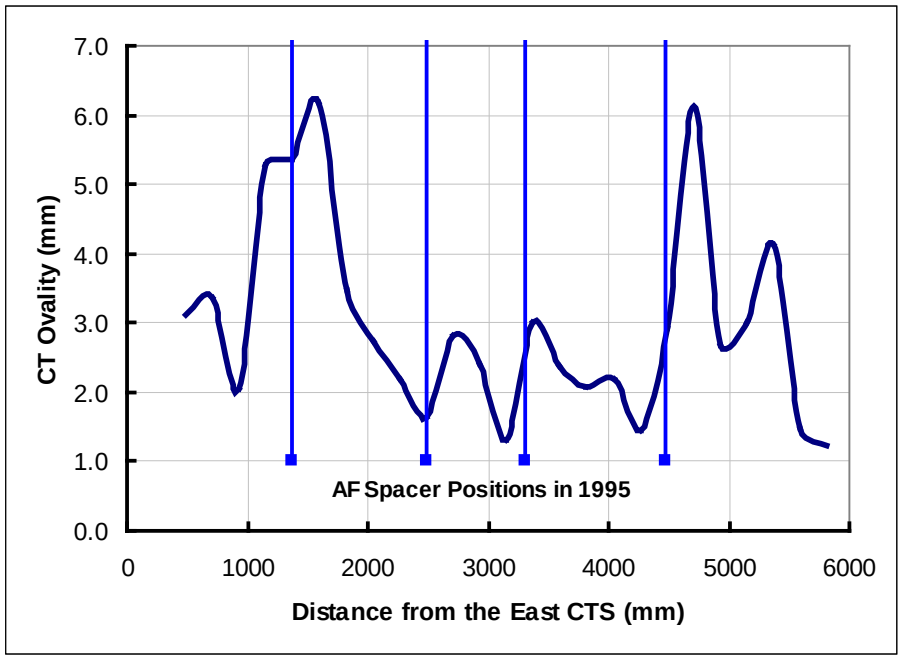

Figure 11. Plot of CT Ovality on Inner Diameter vs Axial Position Along the Length of the CT for Fuel Channel H14 in Gentilly-2

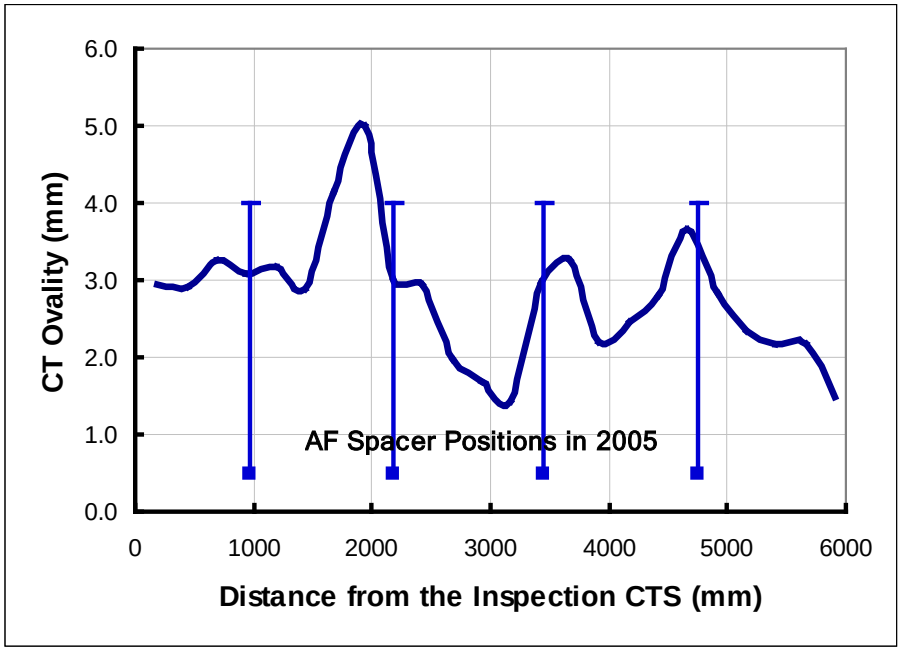

5.3 CT Axial Inner Diameter Profiles

Figures 12 and 13 for F06 and H14 provide a more complete description of the distribution of CT inner diameter than the previous figures. In Figures 12 and 13, maximum, mean, and minimum inner diameter values are plotted at discrete axial positions along the length of the CT. The general trends are that local maxima in the maximum inner diameter plot coincide with local minima in the minimum inner diameter plots and local minima in the maximum inner diameter plots coincide with local maxima in the minimum inner diameter plots.

It is interesting to note that a small general diametral expansion of the CT is indicated at the spacer locations for F06 and H14 in Figures 12 and 13.

Figure 12. Plot of CT Inner Diameter vs Axial Position Along the Length of the CT for Fuel Channel F06 in Point Lepreau

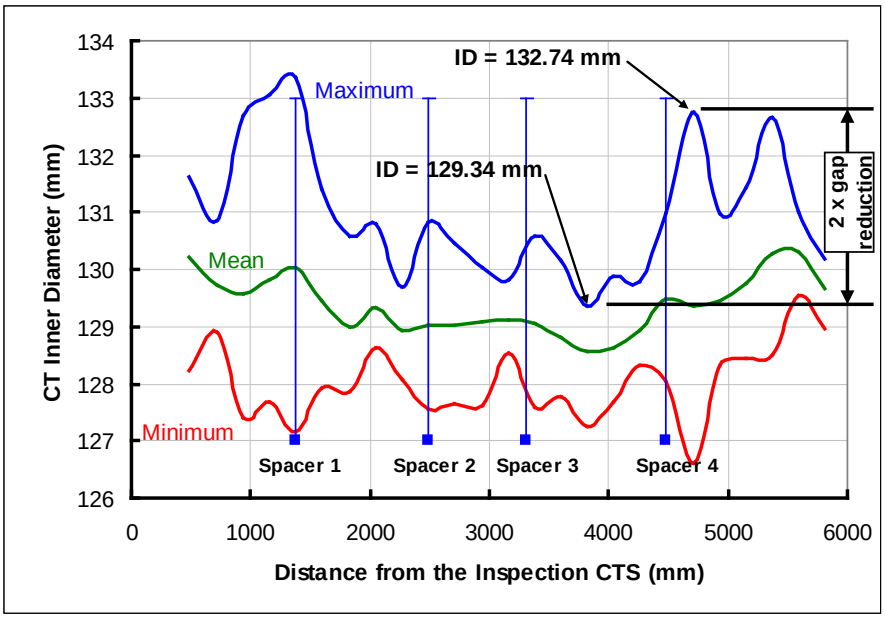

Figure 13. Plot of CT Inner Diameter vs Axial Position Along the Length of the CT for Fuel Channel H14 in Gentilly-2

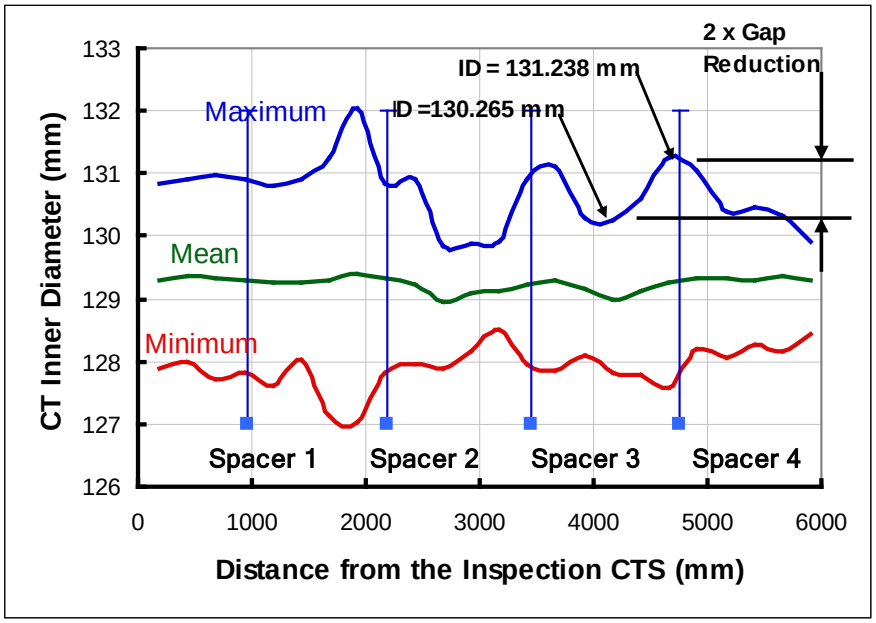

6. Discussion of Results

6.1 Accuracy of the CT Inner Diameter Profiles

Table 2 presents a summary of an error analysis for the CT inner diameter values in this paper.

Table 2. Accuracy of CT Inner Diameter Values

Parameter (mm)	Accuracy (± mm)
PT Inner Diameter Measurement	0.1
PT Wall Thickness Measurement	0.1
CT-PT Gap Measurement	0.1
Polynomial Approximation of PT Inner Diameter	0.025
Polynomial Approximation of PT Wall Thickness	0.0
CT Inner Diameter Value	0.425

It is estimated that the accuracy of the CT inner diameters is ± 0.425 mm. With this magnitude of inaccuracy in the CT inner diameter values in this paper, the observation of ovality at the spacer locations would not be invalidated. However, the observation of a general increase in CT inner diameter (increased inner circumference) for H14 could be invalidated by the consideration of inaccuracy in the CT inner diameter values.

6.2 Comparison with the Gauging of Removed CTs at CRL

In 2008, inner diameter measurements were performed on three removed CTs at CRL [2]. Figure 14 presents a summary of the CT gauging measurements that were performed on the CT from Fuel Channel B6-G12.

Figure 14. Plot of Maximum, Mean, and Minimum CT Inner Diameter Values for B6-G12

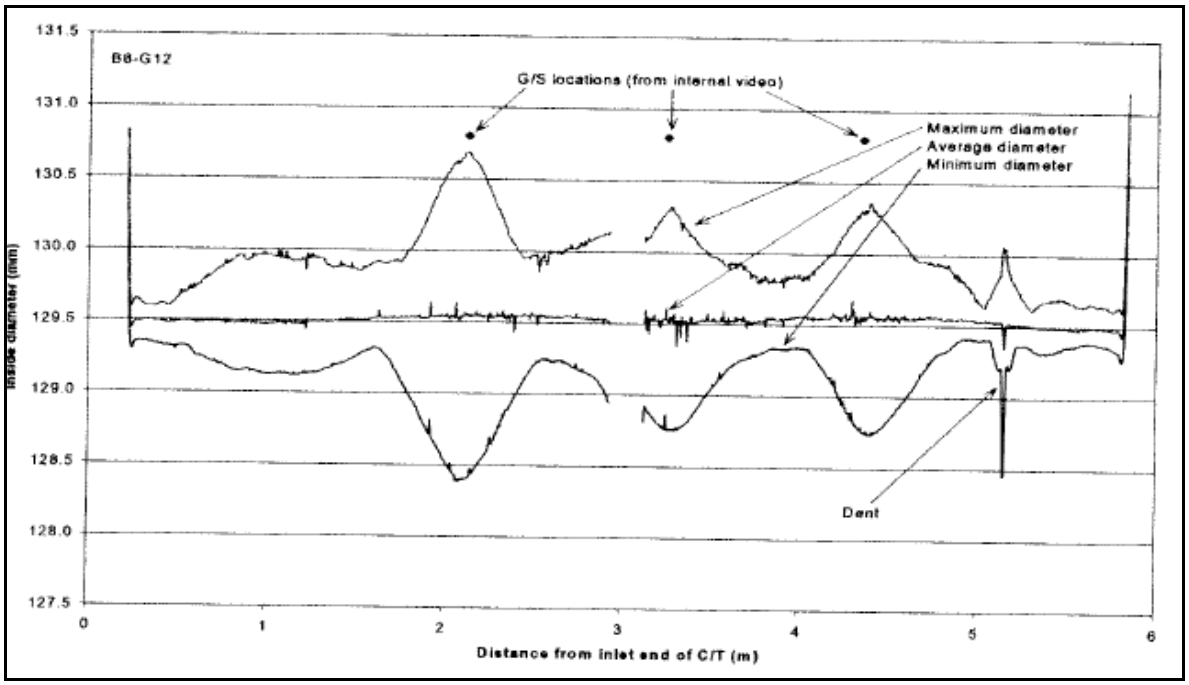

The figure presents plots of maximum, mean, and minimum CT inner diameter, as in Figures 12 and 13.

The main point from Figure 14 is that spacer positions were found to coincide with the locations of peak ovality, indicated as local maxima and minima in the CT maximum and minimum inner diameter plots. As outlined previously, this must be the case in order for spacer loading to be responsible for the CT deformation observed.

Figure 14 indicates very little if any increase in the mean inner diameter of the CT as compared with the increases in mean diameter displayed in Figures Z and C for F06 and H14. The difference in mean inner diameter seen in F06 and H14 compared with B6-G12 may be attributable to a difference in the inspection technique. For F06 and H14, 72 data points were collected around the circumference of the CT compared to 18 for B6-G12. With a much coarser circumferential spacing of data points, peaks in the circumferential distribution of CT inner radius could have been missed, resulting in lower mean inner diameter values for B6-G16.

Another contributing factor to the lower mean inner diameter of B6-G12 compared with F06 and H14 is that F06 and H14 were in service for a longer time than B6-G12 when the gauging measurements were taken. Creep deformation of CTs F06 and H14 at the spacer positions under spacer loading for 157,000 hours and XXXXXX hours respectively, should be greater than that under 123,000 hours for B6-G12.

6.3 Comparison of Results for F06 with the Predictions of Existing Models

From Figure 12, the vertical diameter of CT F06 increased by of 4.5 mm from the nominal 129 mm value under the loading imposed by Spacer 4, over a period of 156 kEFPH. However, the gap reduction between Spacer 3 and 4 is seen to be about 3.4/2 mm = 1.7 mm as a result of the deformation at Spacer 4.

From the Point Lepreau SLAR records, the spacer was not moved from the previous SLAR in 1995 when it was left with a spacer load of 154 lbf . Assuming that the as-left spacer load for Spacer 1 had been constant at 154 lbf from 0 to 156 kEFPH, the gap reduction deformation was predicted to be 0.8 mm, for the formulation in Reference [1], which apparently, is not in agreement with Figure 12.

However, the comparison presented above may be misleading because of inaccuracies in the F06 CT-PT gap measurements. Accounting for an inaccuracy of ± 0.425 mm in the inner diameter values at Spacer 4 and between Spacers 3 and 4, the gap reduction in Figure 12 would be distributed as shown in the Table below:

Table 3. Upper Bound, Mean, and Lower Bound Gap Reduction Values for F06

Case	ID at S4 (mm)	ID between S3 & S4 (mm)	Gap Reduction (mm)
Nominal	Nominal	Nominal	1.7
Lower Bound (Best) Case	Nominal – 0.425	Nominal + 0.425	0.85
Upper Bound (Worst) Case	Nominal + 0.425	Nominal – 0.425	2.55

For the best case scenario, the 0.85 mm gap reduction agrees well with the predicted 0.8 mm value, but there are significant.differences for the nominal and upper bound scenarions.

Therefore, given the inaccuracies in the CT inner diameter values for F06, it is possible that the existing model predicts actual gap reduction values adequately but Table 3 shows that this is not likely as the nominal and upper bound values for measured gap reduction a significantly higher than the predicted 0.8 mm value.

Important factors to be considered in the review of the results for F06 are that: (1) the axial spacing between circumferential scans (220 mm) likely causes locations of peak ovality to be missed, and (2) the use of a non-surface riding gap probe suggests that the F06 CT-PT gap data could have been affected by probe lift-off errors. The later could explain the higher gap reduction values for F06.

6.4 Comparison of Results for H14 with the Predictions of Existing Models

From Figure 13, the gap reduction in CT H14 due to the deformation at Spacer 4 was determined to be 0.49 mm. In this case, a prediction of the deformation at Spacer 4 in H14 was not performed. However, some idea of the validity of the deformation model [1] was obtained by examining CT gap reduction predictions performed for Point Lepreau for one spacer in 196 different channels. For the analyses it was found that the average gap reduction deformation was 0.67 mm. It is expected that the prediction for H14 would not be far from 0.67 mm. This provides a rough indication that the 0.49 measured gap reduction would be in agreement with gap reduction predictions from the current model.

Comparing Figures 13 and 12, it is seen that the gap reduction for F06 is significantly greater than that for H14. It is possible that the non-surface-riding gap probe used in F06 overestimated the PT-CT gap compared with the surface-riding probe used in H14.

6.5 Shape of the CT Cross-Section Near Spacer 4 for F06

Figure 15 was generated to illustrate the shape of the cross-section of CT F06 at an axial position 4705 mm from the Inspection CTS, the same location for Figures 4 and 8. The deformed PT outer surface, assuming a circular shape for the PT, is depicted with a red line. The thick and thin blue line represent the deformed and undeformed CT. The undeformed CT was assumed to be circular with a nominal inner diameter of 129 mm.

In Figure 15 it is seen that there is roughly a 4 mm diametral expansion of the CT along a diameter inclined at about 30° to the vertical direction, indicated with a dashed line. In the direction perpendicular to that line, also depicted as a dashed line in Figure 15, it is seen that the deformed CT has a smaller inner diameter than the nominal CT. This suggests that the spacer loading has induced in-plane bending of the bottom of the CT, forcing the top and bottom of the CT apart but bringing the sides together.

Figure 15. Comparison of a Nominal and Deformed Cross-Section for CT F06 with the Deformed PT also Illustrated

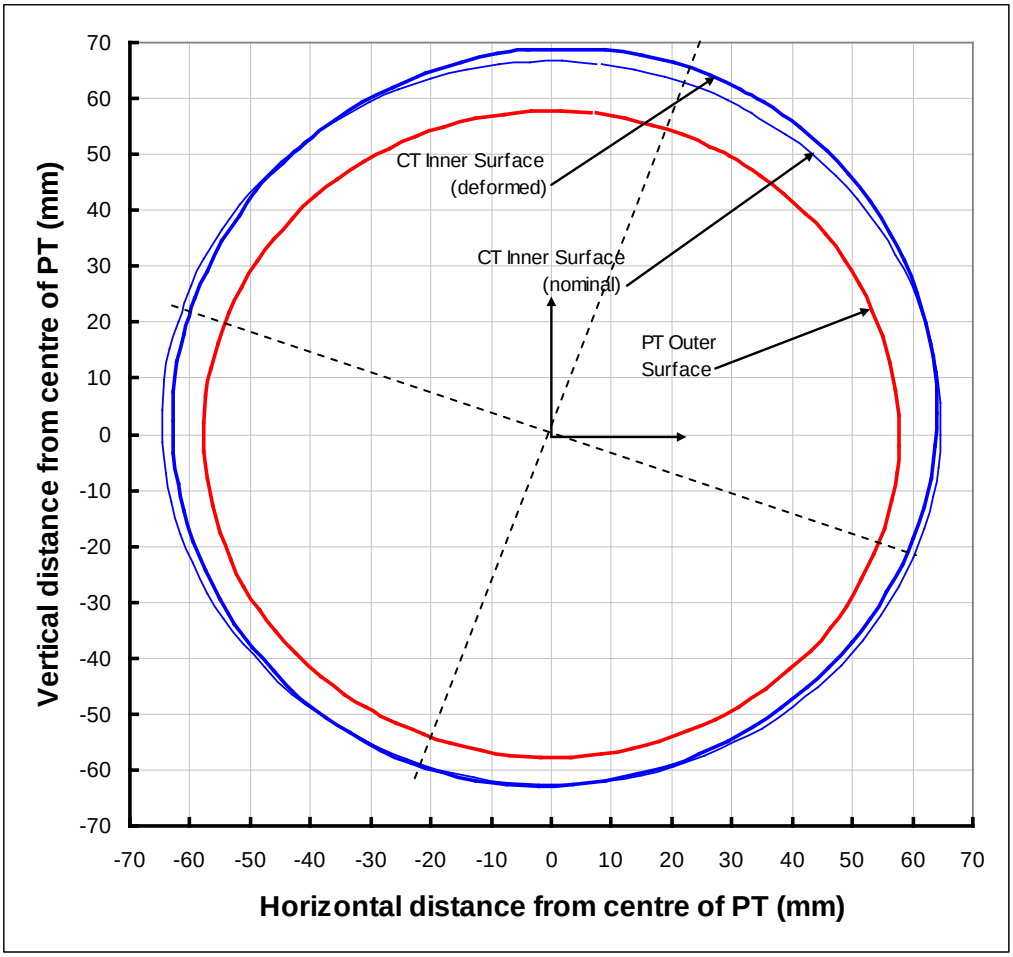

6.7 Recommendations for Future Work

In order to capture CT ovality peaks in future inspections, the spacing between circumferential gap spans should be decreased.

To characterize CT deformation, CT inner diameter profiles should be generated for the CT of every fuel channel with PT gauging and CT-PT gap measurements. The CT deformation in the profiles can then be correlated to spacer loads for comparison with the current CT deformation model [1].

7.0 Use of CT Inner Diameter Profiles

For the analysis of PT deformation and stress, very accurate inner diameter and wall thickness distributions are provided by UT inspections. For the CT, only semi-empirical sag profiles are available. Deformation of the CT cross-section is not accounted for in fuel channel or fuel channel safety analyses. Using the technique outlined in this paper, CT inner diameter profiles can be generated for use in various applications: (1) to refine

the modelling of CT stiffness and gap reduction in CDEPTH, (2) to refine safety analyses involving the CT, and to refine spacer Nip-Up predictions for the fuel channels.

8. Conclusions

1. PT dimensional inspection data (that includes CT-PT gap measurements) can be used to generate inner diameter profiles for in-service CTs. This represents an unexpected benefit from PT gauging inspections.

2. In the CT inner diameter profiles, regions of significant local ovality, consisting of an expansion of the vertical diameter and a reduction in the horizontal diameter, were detected in the circumferential scans nearest the spacers. In between spacers, CT ovality and maximum inner diameter were significantly smaller than near the spacer locations.

3. The CT axial inner diameter profiles for H14 resulting from spacer loading feature gap reduction deformations that are in reasonable agreement with the predictions of current fuel channel deformation models. For F06, good agreement between predicted and measured gap reduction values is only possible if lower bound measurements for CT inner diameter are realised. In F06, higher gap reduction measurements may result from the use of a non-surface-riding gap probe.

.

4. There are indications that spacer loading can induce a general diametral expansion of the CT which may contribute to a delay in the onset of spacer nip-up.

9. References

1. Khajehpour, S., Sauvé, R.G., "Effect of Calandria Tube Creep Ovality on Contact Gap Reduction", Kinectrics Report 8745-001-TM-0001-R00, September 14, 2001.

2. Donahue, S.A., "Out-of-Reactor Diameter and Sag Measurements of the Calandria Tubes B6-G12, P4-N01, and P4-N22 at Chalk River Laboratories, COG COG Technical Note TN-07-1059, April, 2008.

3. Mayo, W., "Fuel Channel Periodic Inspection: 2004, May, Final Report", AECL Report, 87- 31100-PIP-003, 2005 01.

4. Craig, S.T., Olfert, J., Smit, R., "Pressure-Tube to Calandria-Tube Gap-Analysis Blind Tests", COG Technical Note TN-08-1023, March 2009.

5. Sedran, P.J., "Assessment of Fuel Channel Spacer Nip-Up Prior to Retube", REPT 0065 0004 00, Feb 21 2008.

6. Sedran, P.J., "Prediction of Onset Times for CT-LIN Contact in Gentilly-2, CPUS Technical Report 0078 REPT ENG 0001 00, October 15, 2007.

Attachment 2

The Generation of Calandria Tube (CT) Inner Diameter Profiles from Fuel Channel (FC) Inspection Data

P.J.Sedran[1], B. Rankin[2], and C. Lemire[3]

[1] Fuel Channels Consultant, AMEC NSS
(paul.sedran@amec.com)
[2] NB Power
(brankin@nbpower.com)
[3] Hydro-Québec
(Lemire.Christian@hydro.qc.ca)

Abstract

Studies of CT deformation at spacer locations, key to the development of FC deformation modelling, have been limited by the availability of gauging measurements from removed CTs. In [1], it was proposed that CT dimensional profiles could be generated using FC inspection data. Since then, the concept was investigated further by assessing: (1) the normalisation of gap measurements to the diameter of the spacer coil, (2) the validity of gap measurements from inspections of Point Lepreau and Gentilly-2, and the CT dimensional profiles generated from the inspection data. It was concluded, from the work presented in this paper, that the CT-PT gap data and the CT dimensional profiles generated using the data from the two subject inspections are reasonable.

1. Introduction

The modelling of CT local creep deformation at spacer locations has been an active topic since 2001, when the first CT local ovality model was coded into CDEPTH 8.2. With the recent gauging of a small number of removed CTs, researchers have identified a need for additional CT inner diameter (ID) measurements [2] to be used to calibrate the modelling of local CT creep deformation at the spacers. Independent of that work, the generation of CT ID profiles from FC inspection data was demonstrated in [1], but, the proposed methodology was not implemented because the accuracy of the CT-PT gap data used at the time was challenged. Since that time, the following work has been performed to further research the use of FC inspection data to generate CT ID profiles:

1. An examination of CT-PT gap measurements from 2004 and 2005 from Point Lepreau, (PLGS) and Gentilly-2, (G-2)
2. An assessment of normalising the CT-PT gap measurements to the diameter of the spacer coil
3. The generation and assessment of CT ID profiles for PLGS and G-2.

2. Fuel Channel Inspection Data

Details of the FC inspection data examined for this paper are presented in Table 1.

The inspection data used here are the PT ID, PT wall thickness, and CT-PT gap. Gap measurements are discussed in some detail but the others are not addressed, since the PT measurements have been standardised and are now routine, whereas the gap measurements are more recent developments.

Table 1 – Details of CT-PT Gap Inspections

FC	Inspection		FCs Inspected	Inspection Equipment	Measurement Spacing		Calibration	Gap Fitting Routine
	Date	EFPH			Axial (mm)	Angular (°)		
PLF06	May 2004	156,511	12	AFCIS	220	4.6	Gap at Spacer	Point Fit
G2H14	May 2005	161,000	15	SyDef Module	249.2	5	None	Point Fit & Circle Fit

Note: AFCIS is the AECL Advanced Fuel Channel Inspection System and SyDef is the inspection module developed by Hydro-Quebec for the SLAR Tool.

From Table 1, for the PLGS inspections, only point fit gap data were provided. For the G-2 inspections, both point and circle fit gap measurements were provided.

2.1 Processing of CT-PT Gap Measurement Data

The gap measurements obtained during FC inspections are subject to (1) circle and point fitting, and (2) calibration to the spacer coil outer diameter, covered in Sections 2.1.1 and 2.1.2.

2.1.1 Circle and Point Fitting of Gap Data

CT-PT gap measurements are based on the detection of eddy current signal variations with gap, as the gap probe scans the FC. To measure the gap, the gap probe response requires calibration to known gap values. The calibration of the PLGS and G-2 gap measurements was based on a two stage process: (1) circle-fit routine - the gap around the circumference of the PT, to be correlated to the gap probe signal, was determined assuming that the PT and CT were circular. The gap measurements were then correlated to the known CT-PT gap, calculated from the measured PT dimensions and the CT as-installed ID. The use of as-installed CT dimensions ignores CT deformation, but the average gap is not affected significantly. The gap measurement to the known gap correlation was used to derive a relationship between the gap measurement and the known gap. (2) point-fit routine - the above gap measurement to gap relationship is used directly to obtain the gap, not assuming circular geometries, allowing for more accurate gap measurements that capture the local deformation of the CT.

2.1.2 Calibration of CT-PT Gap Measurements Based on the Spacer Coil Outer Diameter

In many channels, the measured gaps at the spacers were smaller than the nominal outer diameter of the spacer coil, (5.588 mm), and were thought to need correction. The calibration depicted in Figure 1was typically used to adjust the measurements. The figure shows gap measurements at the bottom of the CT versus axial position along the length of the CT for G2H14. The lower blue line and the upper red line represent the measured and calibrated gaps. The grey triangles, plotted at a gap value of 5.588 mm, represent the spacers. Figure 2, which presents the calibrated gap versus the measured gap, details the numerical scheme that was used in the gap calibrations. The implications of this gap calibration are discussed later.

3. Examination of Historical CT-PT Gap Data from CANDU 6 Inspections

Figure 3 depicts the theoretical distribution of CT-PT gap vs angular position (θ) around the PT circumference, assuming perfectly circular tubes with nominal dimensions. Throughout this paper, the origin for angular position is at the top dead centre of the PT. The horizontal red line in Figure 3 represents the gap for a concentric PT and CT.

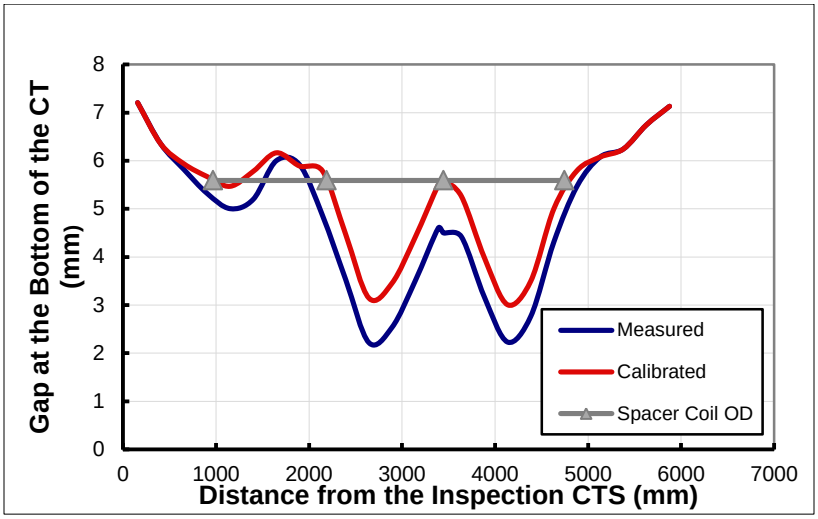

Figure 1. Measured and Calibrated Gap at the Bottom of FC G2H14

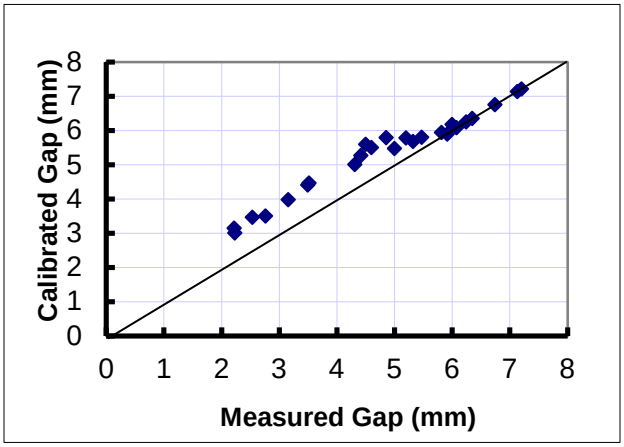

Figure 2. Calibration Scheme for the Gap Measurements from the Inspection of G2H14

The blue sinusoidal curve represents the gap at a spacer location, assuming no CT deformation at the point of contact with the spacer. Figure 3 is useful as a general guide for roughly judging the validity of gap measurements at a given axial location in the fuel channel.

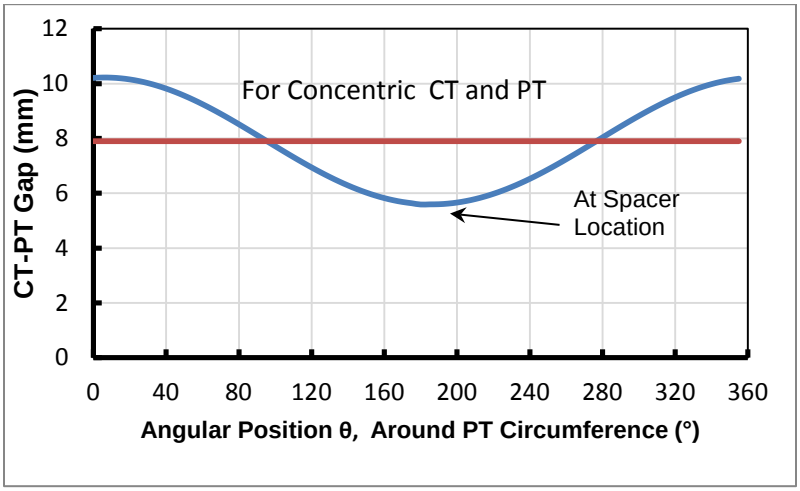

Figure 3. Idealized CT-PT Circumferential Gap Distribution

3.1 Gap Distribution Near the End of the PT

A verification of gap measurements was attempted by examining the circumferential gap distribution near the end of the PT, where CT and PT cross-sections are expected be close to circular, presented in Figures 4 and 5, for PLF06 and G2H14, respectively. The gap profile of Figure 4 is located 139 mm inboard of the West Calandria Tube Sheet (CTS) and 268 mm inboard of the West end fitting taper. The measured gap is depicted as the blue line and the red line represents the expected gap, which was calculated based on PT sag measurements, assuming the following:

1. The PT and CT cross-sections remain circular and have design dimensions
2. During the gap measurement , the centreline of the deformed PT remained in a vertical plane

The PT sag at the axial location of the gap measurements of Figure 4 was found to be 1.42 mm. The measured gap in Figure 4 is in reasonable agreement with the expected gap, but is larger in the region from 280 to 80 degrees, at the top of the CT. The gap data in Figure 4 were calibrated by adjusting the gap to the spacer coil outer diameter. Since the gap calibration tends to increase the gap measurements, an explanation for Figure 4 is that the calibration resulted in an overestimation of the actual gap.

Figure 5 presents 3 gap distributions for G2H14 at 189.4 mm inboard of the North Calandria Tube Sheet (CTS) and 164.4 mm inboard of the North end fitting taper. The red undulating line is the point-fit gap and the blue line is the circle fit gap.

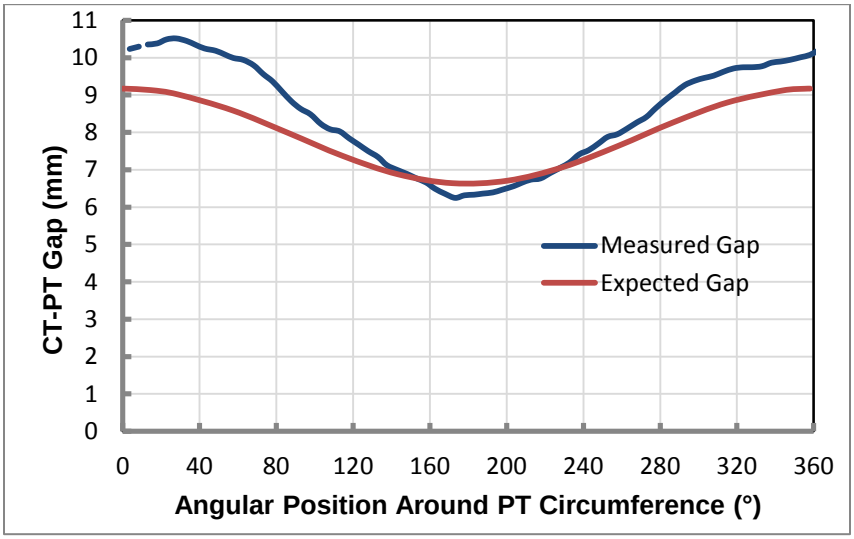

Figure 4. Circumferential Gap Distribution for PLF06 139 mm Inboard of the West CTS

The black curve represents the calculated gap for a measured PT sag of 4.94 mm at 189.4 mm inboard of the North CTS, for the same assumptions used for PLF06. The overall match of the circle-fit and point-fit gaps to the expected gap is reasonable. At various θ values, the point-fit gap is closer to the expected gap than the circle-fit gap, indicating that the former is the better fit to the actual gap. However, the 1 mm undulations observed in the point-fit gap are not explicable by PT ID and wall thickness variations (0.2 mm). Regardless, Figures 4 and 5 indicate that the point-fit routine with no calibration of gap measurements produces the most accurate gap distribution near the ends of the CT.

3.2 Gap Distribution Between Spacers

The circumferential CT-PT gap distribution at the minimum gap location in G2H14, critical for CT-PT contact, is presented in Figure 6. The blue and red lines represent circle and point fits to the gap measurements, respectively. At the minimum gap location, the circle-fit and point-fit gaps are in close agreement, so either can be used to determine the minimum gap values. However, point-fitting provides a more detailed distribution for the gap around the circumference of the PT.

Considering Figures 4 – 6, it is recommended that the un-calibrated point-fit method be used to establish CT-PT gap distributions. However, point-fitting versus circle-fitting will not influence the minimum gap values at the bottom of the CT.

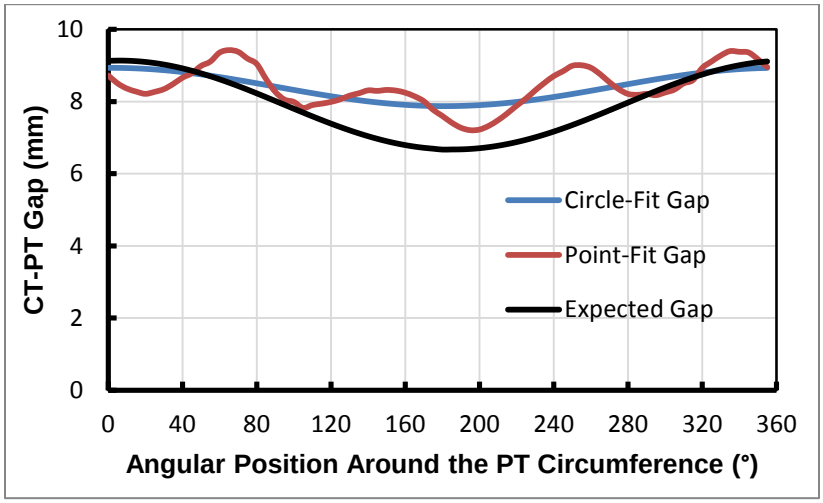

Figure 5. Circumferential Distribution of the Gap in G2H14 189 mm Inboard of the North CTS

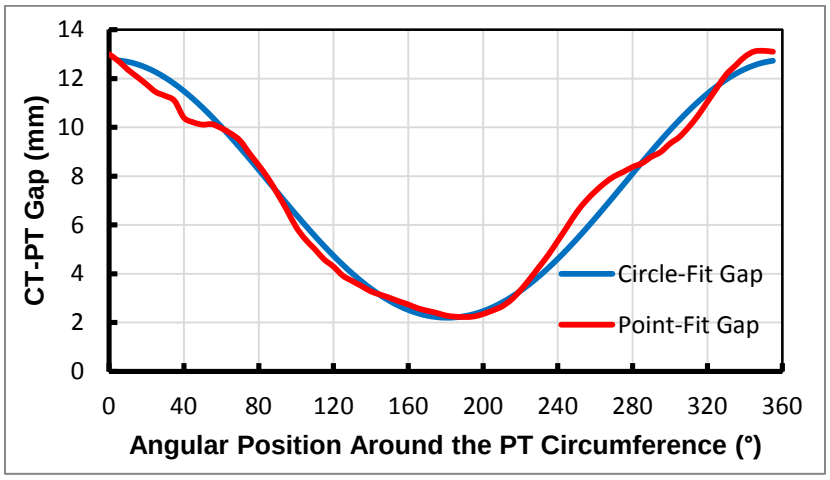

Figure 6. Circumferential Gap Distribution in G2H14 at the Location of the Minimum Gap

3.3 Gap Distribution at Spacer Locations

Figure 7 presents plots of the calibrated gap versus θ at three spacer locations for PLF06. At the spacers, there are conspicuous unexplained irregularities in the gap distribution from 80 to 300°, the sector over which the spacer would be in contact with the CT.

3.4 Axial Distribution of CT-PT Gap

For this assessment, the gap measurements at 180 ° (at the bottom of the CT) were combined with PT sag and wall thickness measurements to generate a series of elevation points for the CT inner surface along the length of the CT. Here, elevation is defined as the vertical distance of a point below the reference plane, which is a horizontal plane tangent to the inside surface at the bottom of the PT, for a straight and horizontal PT.

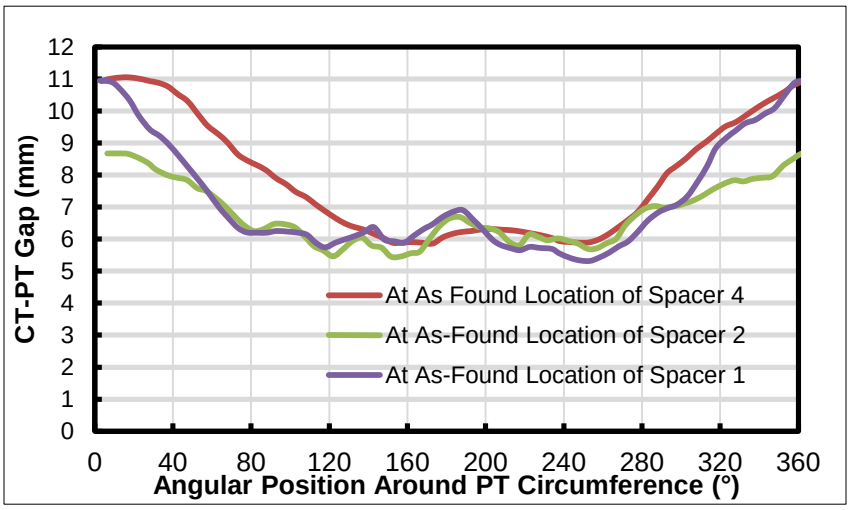

Figure 7. Circumferential Gap Distribution in PLF06 at Spacer Locations

The elevation of the CT bottom inner surface was determined using:

$$Y_{CT} = Y_{PT} - w_{PT} - Gap_{CT\text{-}PT}$$

Where Y_{CT} and Y_{PT} are the elevations of the CT and PT bottom inner surfaces; w is the wall thickness.

The resultant CT elevation profile and the elevations of the PT inner and outer surfaces for PLF06 are given in Figure 8.

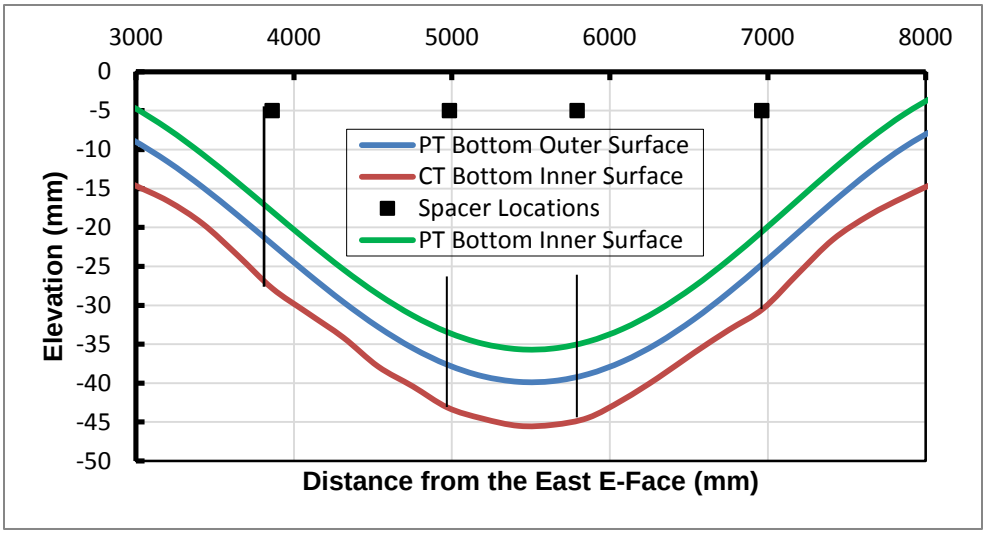

Figure 8. Elevation Profiles for the Inner and Outer Surfaces of the PT and CT in PLF06

The curves in the figure represent the intersection of the PT inner and outer surfaces and the CT inner surface with a vertical plane. The black square points in the figure indicate as-found spacer locations from the 1995 SLAR campaign. The elevation of the PT inner surface curve, depicted as the green line, was determined from the PT sag profile for PLF06, from the 2004 inspection. Although a quantitative evaluation of the results in Figure 8 is not possible, the following qualitative evaluation can be made. The

CT bottom inner surface elevation and that of the PT appear to be of similar form, as expected. In Figure 8, there are shallow depressions in the CT bottom inside surface at spacer locations 1, 2, and 4. The locations and extents of these depressions are consistent with those observed in removed CTs [2]. Although the assessment is not quantitative, there are no indications any of problems with the results in Figure 8.

4. Generation of CT Inner Diameter (ID) Profiles

Originally, FC inspections were limited to PT gauging and sag measurements, but, the addition of a gap probe module allowed for the determination of the radial distance from the centre of the PT to the inside surface of the CT ($R_{CT}(\theta,x)$) at various angles (θ), where x is the axial position along the CT. $R_{CT}(\theta,x)$ is the sum of PT inner radius plus the wall thickness and the PT-CT gap:

$$R_{CT}(\theta, x) = IR_{PT}(\theta, x) + w_{PT}(\theta, x) + gap(\theta, x) \quad (1)$$

where IR_{PT} and w_{PT} are the PT inner radius and wall thickness. For given values of x and θ, the CT inner diameter is the sum of $R_{CT}(\theta, x)$ and the radial distance diametrically opposite to it:

$$ID_{CT}(\theta, x) = R_{CT}(\theta, x) + R_{CT}(\theta+180°, x) \quad (2)$$

Using Equations (1) and (2), CT ID values at angular orientations ranging from 0 to 180° were generated for various cross-sections along the length of the CT for PLF06 and G2H14. The CT ID values were used to produce axial distributions of minimum, average, and maximum CT ID, and circumferential profiles of CT ID at spacer locations, presented in Sections 4.1 and 4.2.

4.1 CT ID Profiles for PLF06

Figure 9 presents axial CT ID profiles (maximum, mean and minimum ID values along the length of the CT) for PLF06, using calibrated gap measurements. Also plotted in the figure are the four as-found spacer locations from the 1995 inspection of the channel, which were close to the as-found locations in the 2004 inspection. The circumferential CT ID profile for the CT, at 4700 mm from the East CTS, close to spacer 4, is presented in Figure 10.

4.2 CT ID Profiles for G2H14

Figure 11 presents axial CT ID profiles for G2H14, using uncalibrated gap measurements, along with the four as-found spacer locations from the 2005 inspection. A circumferential CT ID profile for the CT cross-section located at 1930 mm from the North CTS, close to Spacer 2, is presented in Figure 12.

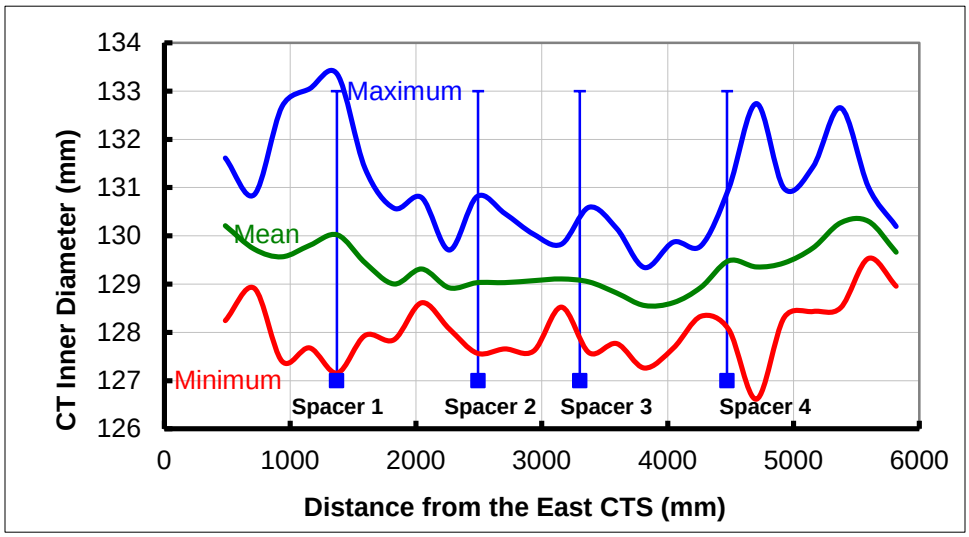

Figure 9. Axial CT ID Profiles for PLF06

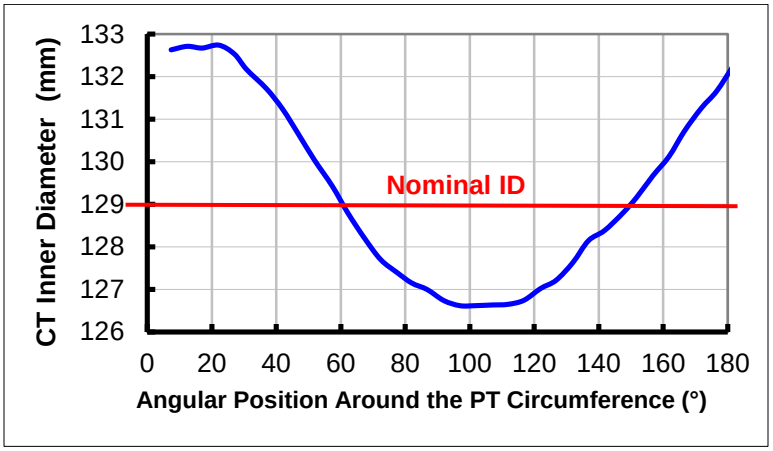

Figure 10. Circumferential CT ID Profile for PLF06 at 4700 mm from the East CTS

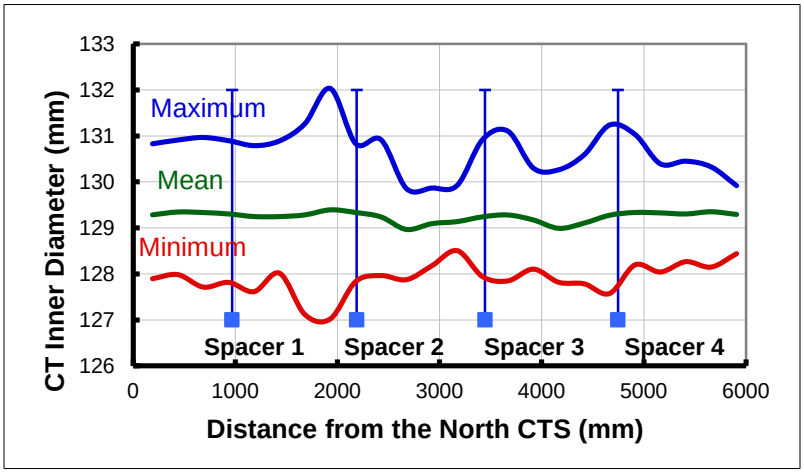

Figure 11. Axial CT ID Profiles for G2H14

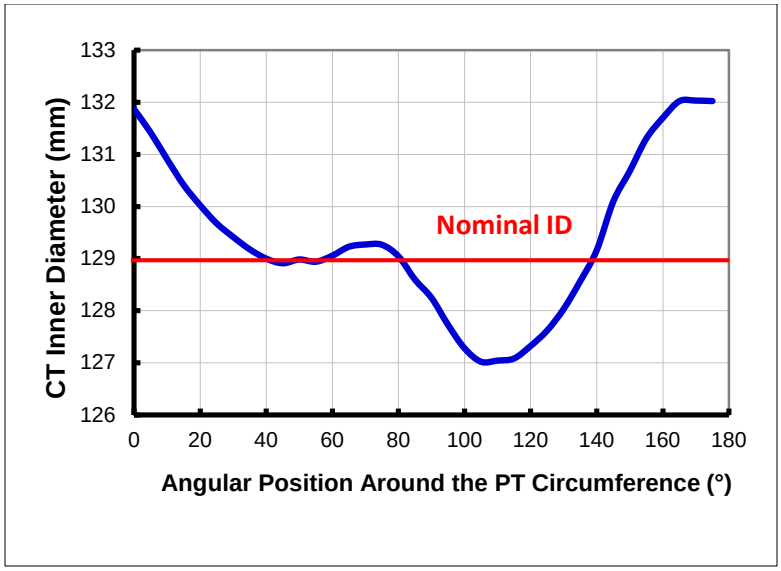

Figure 12. Circumferential CT ID Profile for G2H14 at 1930 mm from the North CTS

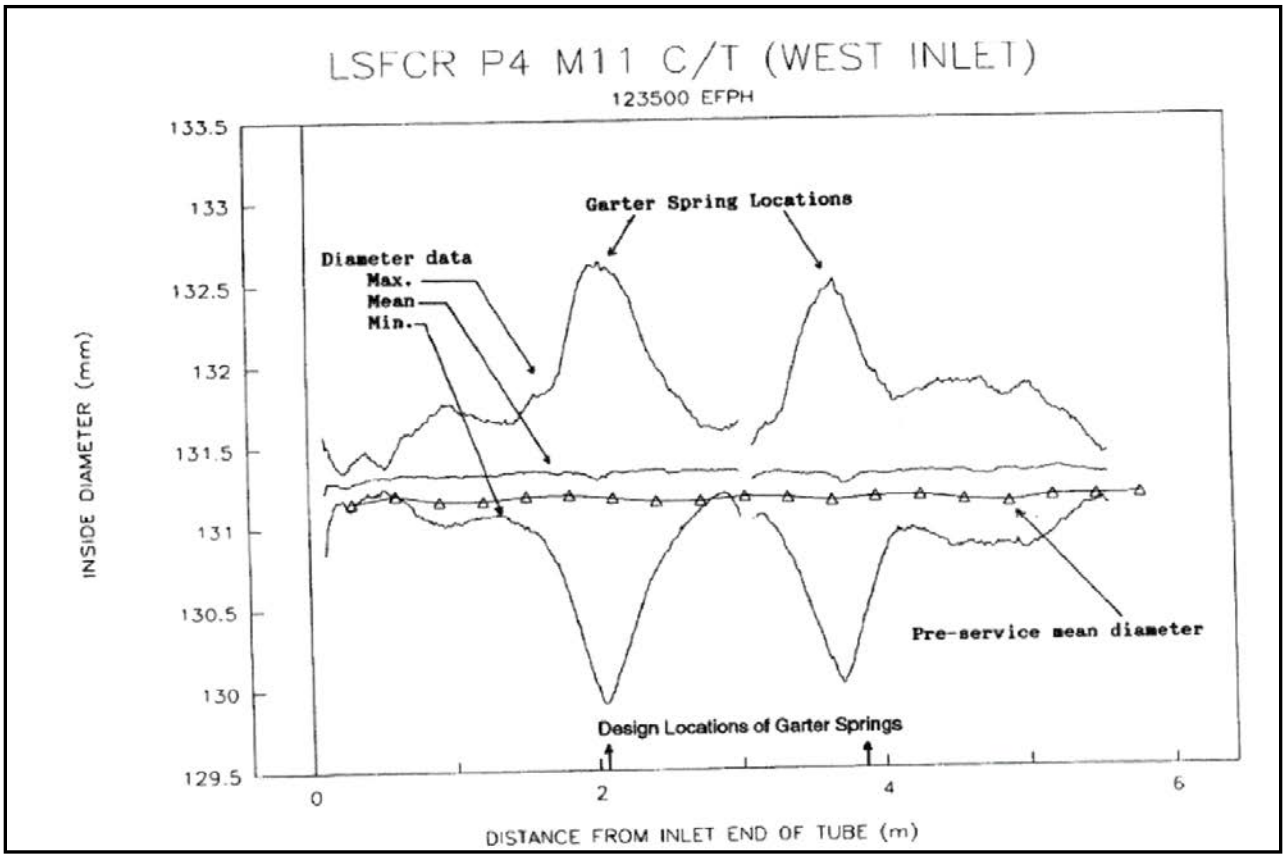

Figure 13. CT Gauging Measurements for P4M11 [2]

5.0 Discussion of Results

Figure 13, reproduced from Reference [2], presents axial ID profiles obtained from the post-removal gauging of the CT from P4M11 (Pickering Unit 4). The main features of the CT ID profiles of Figure 13 are deformation peaks that are centred at spacer locations , with uniform average ID values, close to pre-service values, which can serve as benchmarks for a comparison with other CT ID Profiles. Comparing Figures 9 and 11 with Figure 13, it can be seen that the CT ID profiles for PLF06 and G2H14 are similar to that in Figure 13. All three sets of profiles feature local ID maxima and minima at spacer locations, attributable to the local creep deformation of the CT under spacer loading. Noteworthy in Figure 9 are significant variations in the CT average ID above the nominal design value, not present in Figures 11 and 13. It is proposed that the gap calibration scheme used to produce the CT ID profiles of Figure 9 resulted in an overestimation of various gap values, manifested in Figure 9 as an overestimate of the CT average diameter at different points along the CT.

Figures 10 and 12 depict the deformed shape of the CT cross-section at a spacer location, which features increased vertical and decreased horizontal inner diameters, relative to the nominal inner diameter. As an example, in PLF06, the CT vertical diameter has increased by 3.7 mm while the horizontal diameter has decreased by 2.3 mm. Of various possible implications of this deformation, one consideration is the possibility that an ovalised CT could interfere with a spacer during spacer repositioning by contacting the spacer at the 90 and 270 degree locations.

In Figure 10, the CT ID circumferential distribution is quite smooth around the circumference of the CT, as expected. However, in Figure 12, there is an irregularity in the shape of the CT ID profile, of unknown origin, which did not appear in the PLF06 CT ID profiles. Although it is expected that the deformed shape of the CT in G2H14 should be more regular, it is conceivable that some local distortions of the CT shape could occur because of the effects of as-installed residual stresses in the CT, which should be investigated.

6.0 Conclusions

1. The un-calibrated gap data examined generally agree reasonably well with expected gap values and the gap measurement profiles have shapes that are reasonable. However, there are consistent, noticeable irregularities in the shape of the circumferential gap profiles where the PT and spacer are in contact.

2. At specific axial locations, some perturbations in the circumferential gap profile shape, of unknown origin, were detected.

3. The calibration of gap measurements, based on spacer outer coil diameter, implies greater CT diametral expansion than that observed in CT gauging measurements [2], indicating that gap calibration may not be technically justifiable.

4. Using G2H14 and PLF06 as examples, reasonable CT ID profiles can be generated using PT inspection data and un-calibrated CT-PT gap data.

5. A significant feature in the CT ID profiles generated for this paper is the development of ovality of the CT cross-section at spacer locations, consisting of an expansion of the vertical axis, and a contraction of

the horizontal axis of the CT. The latter may have implications for spacer movement during spacer repositioning in some channels.

7.0 Recommendations

1. The observed irregularity in the CT ID profile shape of Figure 12 should be investigated, starting with the hypothesis that as- installed CT residual stresses are responsible for distortion of the shape of the CT cross-section.
2. The apparent underestimation of the gap at spacer locations should be investigated to establish whether or not gap calibration can be justified.
3. Once these issues are resolved, it is recommended that CT ID profiles be generated for all inspected FCs so as to develop a database of CT gauging measurements in support of a model for local CT deformation at the spacers.

8.0 References

[1] Sedran, P.J., Rankin, B., "The Use of OPEX (In the Form of Inspection Data) to Obtain Unanticipated Calandria Tube (CT) Ovality Measurements, 9th International Conference on CANDU Maintenance, Toronto, Dec 4 – 6, 2011.

[2] Song, C., "Evaluation of Calandria Tube Ovality from CANDU Fuel Channel Gauging Data, COG-10-1048, June, 2011.

9.0 Acknowledgement

Dr. Thomas W. Krause was consulted on the topics of circle and point fitting of gap data and contributed to Section 2.1.1 of this paper.

Attachment 3

Refinements to Calandria Tube – Liquid Injection Nozzle (CT-LIN) Contact Assessments

P.J. Sedran[1]

[1]Fuel Channel Consultant – RESD Inc.

ABSTRACT

In recent years, the issue of CT-LIN contact, which first gained attention in 1989, has been addressed through CT-LIN gap measurements, followed by analytical predictions of time-to-contact. CT-LIN time-to-contact predictions have been preformed independently by CPUS Limited for Point Lepreau and Gentilly-2 and by AECL Sheridan Park (now Candu Energy Inc.) for Bruce Power and Gentilly-2. Both companies used the CDEPTH code in combination with CT-LIN gap measurements.

Subsequent to the assessments for Point Lepreau and Gentilly-2, a recommended approach for future assessments was presented at the 2008 CANDU maintenance conference. Since that time, a number of refinements to the overall strategy for predicting CT-LIN time-to-contact have been developed and are outlined in this paper. The refinements include:

1. The use of ultrasonic LIN elevation measurements to confirm LIN creep sag behaviour
2. The development of a non-linear empirical CT Creep Sag Model
3. The development of a rationale for discrepancies observed in repeated optical CT-LIN gap measurements and a discussion of alternative CT-LIN gap measurements

With these refinements, more accurate CT-LIN time-to-contact predictions can be obtained.

For stations that plan to refurbish by 210,000 EFPH, the improvement in time-to-contact predictions resulting from the fore mentioned refinements will not be of any real benefit.. However, for stations that are planning life extensions in order to operate beyond 210,000 EFPH, CT-LIN contact will be an issue. For these stations, improvements in CT-LIN contact time predictions would be beneficial.

This paper presents a summary of the proposed refinements and demonstrates how they would impact CT-LIN time-to-contact predictions.

1. INTRODUCTION

The issue of CT-LIN contact, which first gained attention in 1989, has long been recognized as a life-limiting factor for the CTs. In recent assessments, CT-LIN time–to-contact predictions indicate a significant risk of contact should the reactor operate beyond 210 kEFPH.

In reactors that have been refurbished, (Bruce Units 1 and 2, Point Lepreau, and Wolsong Unit 1), or are planning refurbishment by 210 kEFPH, CT-LIN contact will not be an issue for many years. However, for stations that are planning life extensions in order to operate beyond 210,000 EFPH, CT-LIN contact will be an issue because of potential fretting damage to the CT. For these stations, which would benefit from improvements in time-to-contact prediction accuracy, (Bruce 3 -8 and Darlington) a number of refinements to the overall strategy for predicting CT-LIN time-to-contact have been developed and are outlined in this paper. The refinements include:

1. The use of ultrasonic LIN elevation measurements to confirm LIN creep sag behaviour
2. The development of a non-linear empirical CT Creep Sag Model
3. The development of a rationale for discrepancies observed in repeated optical CT-LIN gap measurements and a discussion of alternative CT-LIN gap measurements

Section 2 contains a summary of the CT-LIN contact work performed to date.

Section 3 provides details of the proposed refinements to the CT-LIN contact analysis, listed above. A brief discussion of the results is presented in Section 4. Conclusions and Recommendations are presented in Sections 5 and 6, respectively.

2. RECAP OF PROGRESS TO DATE

Various CT-LIN contact assessments have been performed over the years, starting in the 1980s. This paper covers developments since 2005, when the CANDU 6 stations took a renewed interest in the topic.

2.1 CT-LIN Contact Analyses

There are three components to the prediction of CT-LIN contact: (1) Prediction of the LIN creep sag rate, (2) Prediction of the CT creep sag rate, and (3) The determination of the CT-LIN gap at a given time in-service.

Section 2.1.1 briefly covers the work on LIN creep sag. A summary of the work on the prediction of CT creep sag is presented in Section 2.1.2. Section 2.1.3 presents the work performed on determining the CT-LIN gap at given times in-service.

Section 2.1.4 presents examples of typical CT-LIN tine-to-contact predictions, illustrating changes that have been made from 2005 to 2008. The analyses performed in 2005 have been termed “First Estimate Predictions”. Further refinements subsequent to 2005 involved the updating and calibration of CDEPTH models to obtain less conservative CT creep sag rates, giving rise to “Updated “ and “Calibrated CT-LIN time-to-contact predictions”, which are explained later in the paper.

All the examples presented in this paper are from the Point Lepreau Generating Station (PLGS) or from Gentilly-2 (G-2),

2.1.1 LIN Creep Sag Modelling

Starting in about 2000, optical CT-LIN gap measurements were introduced into the strategy for dealing with potential CT-LIN contact. Since CT-LIN gap measurements were available in 2005 for PLGS and G-2, it was decided that the measurements would form the basis for calculating LIN sag rates, rather than using analytical methods. The CT-LIN gap measurements were performed at critical gaps in the reactor core. A main strategy was to measure the gap for a fuel channel that was inspected in the same outage. This would allow gap and PT sag measurements to be combined, as outlined below. The following method for determining the creep sag of the LIN (the in-service elastic curve) and the creep sag rate, was used:

1. Predict the initial elastic curve for the LIN using ANSYS 9.0
2. Using PT sag measurements for a channel directly above a LIN, calculate the elevation at the bottom of the CT at the intersection of the CT with the LIN – ideally for more than one CT, Note that elevation denotes distance below the centerline of a straight LIN
3. Add the CT-LIN gap measurement to the elevation points at the bottom of the CT to obtain points on the in-service elastic curve of the LIN (which includes creep sag).
4. Use the points on the in-service elastic curve of the LIN from 3. to generate an empirical in-service elastic curve for the LIN
5. Use in-service creep sag profiles of the CTs above the LIN and the empirical in-service elastic curve of the LIN to find the distribution of CT-LIN gaps over the length of the LIN
6. To determine the creep sag rate at any point of the LIN, subtract the in-service elevation in the empirical in-service elastic curve from the elevation in the initial elastic curve and divide by the time in service when the CT LIN gap and PT sag measurements were performed.

Figure 1 illustrates the use of LIN elevation measurements to derive in-service elastic curves for the LIN. Note that elastic curves for different end conditions of the LIN are depicted.

2.1.2 CT Creep Sag Modelling

For the predictions of CT creep sag, the CDEPTH fuel channel deformation code was the clear and obvious choice. The results shown in this paper were produced using CDEPTH 8.2.

For the time-to-contact predictions, the CDEPTH code was executed to generate fuel channel sag computations at discrete points in time, to the end of fuel channel life. The CDEPTH runs were performed for the Row F and the Row Q channels, which could contact LIN #2 and LIN #5, respectively. .

For each CT analysed with CDEPTH, the elevations at the intersection point of the CT with the LIN below it, were extracted from the CDEPTH output.

A typical plot of predicted CT elevation versus time in-service is presented in Figure 2. The CT elevation is specifically at the bottom of the CT at the intersection point of Fuel Channel Q07 with LIN #5 (denoted as Q07-L5) in PLGS.

Figure 1 – Determination of the In-Service Elastic Curve for Lin #5 in PLGS at 157 kEFPH

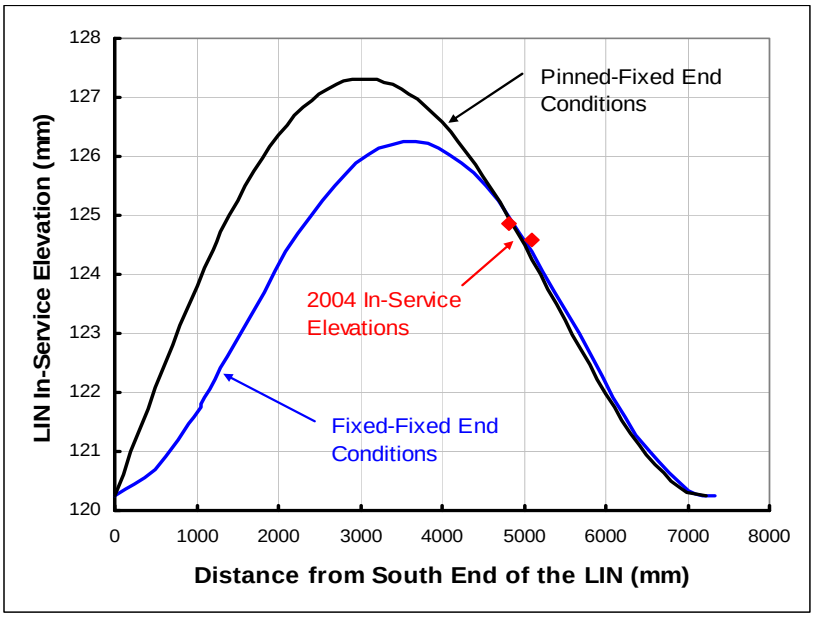

Figure 2 – Predicted Elevation of Q07-L5 Versus Time In Service With the Standard CDEPTH Fuel Channel Model

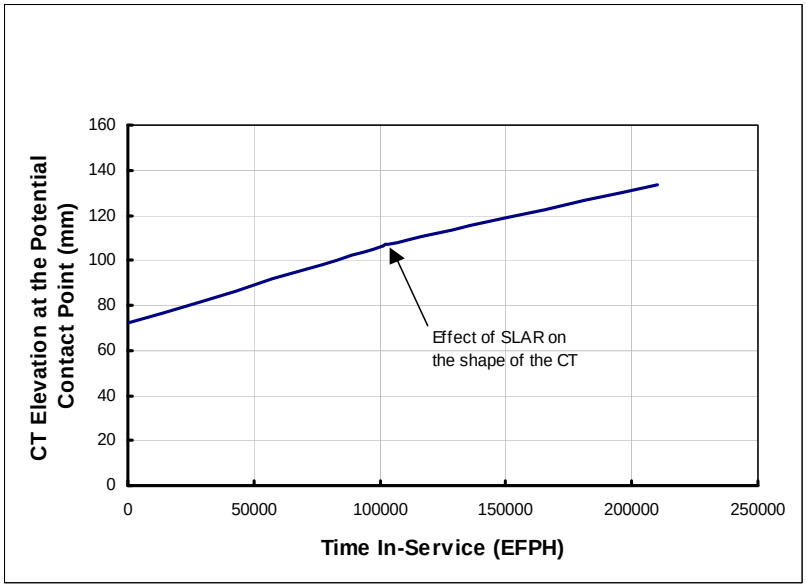

It should be noted that in the CDEPTH code, creep sag of the CT depends upon fast neutron flux, temperature, and stress. In the formulation of the input files for CDEPTH, constant lifetime average values are used for flux and temperature and stresses are calculated using initial PT and

CT dimensions. Therefore, CT creep sag rates in CDEPTH are inherently linear with time in-service.

The general feeling regarding the results in Figure 2 was that there were several sources of conservatism in the fuel channel.creep sag predictions.

Figure 3 illustrates the conservatism in the CDEPTH PT sag predictions resulting from the CDEPTH models used to generate the results in Figure 2. Figure 3 provides a comparison of measured and predicted PT sag for G-2. The data points in Figure 3 present MP ratio versus predicted sag for the inspected PTs in G-2. MP ratio denotes the ratio of Measured PT sag to the Predicted PT sag. The general trend is for MP ratio to start off around 1 early in the operating life of the reactor and then to decline with time in service. Figure 3 implies that on average, a PT with a predicted maximum creep sag of 55 mm is expected to have an actual maximum creep sag that is 18 % lower.

Figure 3 – MP Ratio for PT Sag vs Predicted PT Sag for G-2

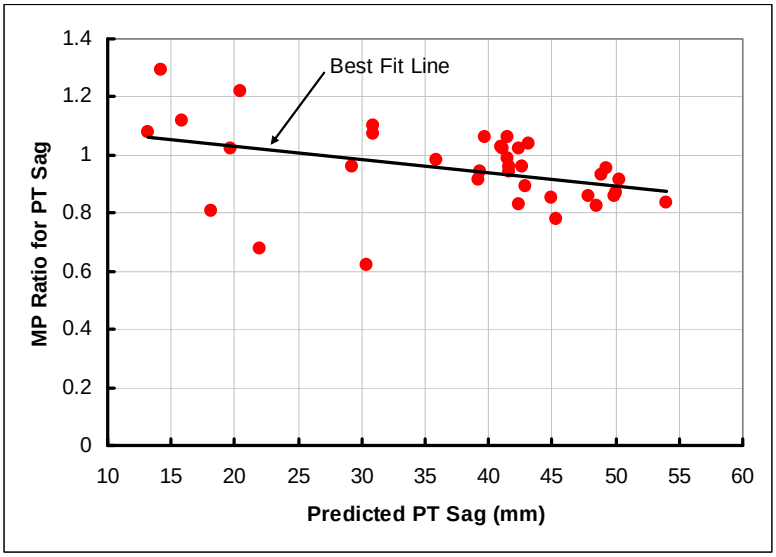

Besides the PT sag measurements, in 2004, during a fuel channel inspection in PLGS, it was found that the defueling of FC F06 resulted in a spring back of the CT of 4.5 mm, measured near the centre of the FC at the intersection point of F06 with LIN 2. The standard CDEPTH model for F06 at the time predicted a spring back of 8.4 mm due to defueling. Therefore, the overall elastic stiffness of the CDEPTH model for F06 in PLGS was found to underestimate that of the actual FC and was expected to be complicit in the over estimation of PT sag versus in-service.

2.1.2.1 Refinement to CT Creep Sag Modelling – Updated and Calibrated CDEPTH Models

Because of the findings shown in Figure 3, various modifications to the CDEPTH input models for the PT and the CT were investigated, which are outlined in Reference [1]. The purpose of the modifications was to introduce justifiable changes in the CDEPTH models to reduce conservatism in the prediction of PT sag. The modifications to the standard CCEPTH model involved:

1. PT In-Service Dimensions and CT End Bell Modelling
2. PT End Support Conditions

3. CT Ovality at Spacer Locations
4. The CT East End Support Condition

The modified CDEPTH model was termed the updated model to signify that the standard model was updated to reflect the current properties of the fuel channel.

An example of the results of updating the CDEPTH models is shown in Figure 4, in which predicted deflections of a point at the bottom of the CT in PLGS, due to elastic and creep sag, are plotted versus time in service. The standard CDEPTH model predictions are plotted in the line at the top, and the lower line represents the predictions of the updated CDEPTH model. The single data point represents the expected elevation of the CT, based on PT sag measurements

Figure 4 – Predicted CT Deflections for PLGS F06 Using Standard and Updated CDEPTH 8.2 Models

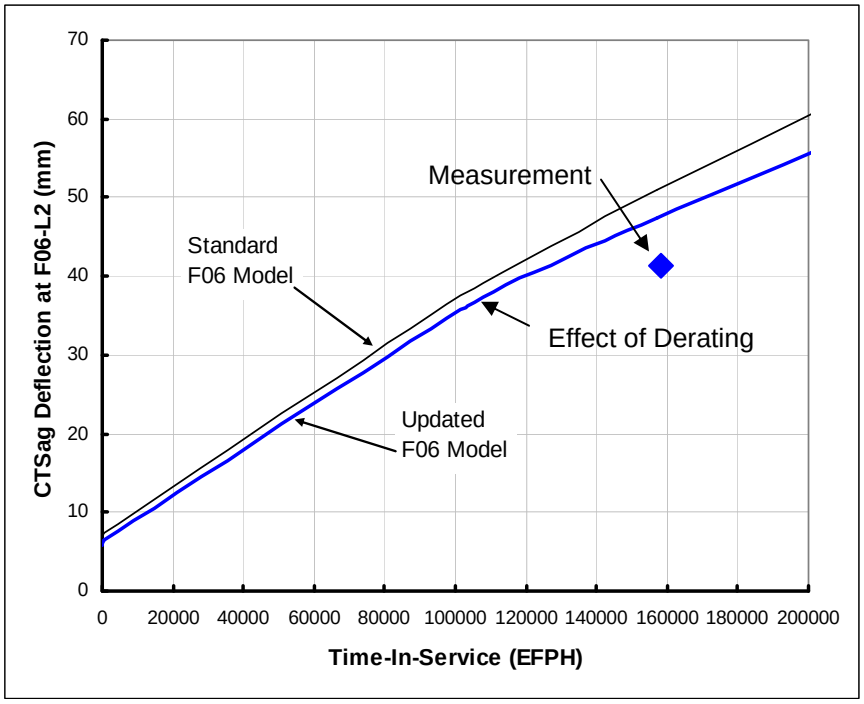

Figure 4 shows that the updated model reduces some of the conservatism in the predictions of the standard model but considerable conservatism remains, considering the position of the single measurement in the plot relative of the opdated F06 model..

A second approach involved simply calibrating the CT creep sag predictions based on MP ratio, the results of which are shown in Figure 5. In the figure, predicted elevations at Q06-L5 for G-2 from the standard and the calibrated CDEPTH models are plotted versus time in service. Also plotted as the single data point is the elevation of Q06-L5, based on PT sag measurements. Figure 5 shows that the creep sag of the CT with the calibrated model is significantly lower than that predicted with the standard model and agrees well the CT elevation expected from the PT sag measurement.

A similar approach for reducing the creep sag rates predicted with CDEPTH was used by AECL in 2010 in an analysis of Bruce Units 3 and 4. In that assessment, one of the creep constants in the CRNL 4003 deformation equation was modified to reduce the rate of creep sag for the fuel

channels. The modified predictions matched measurements fairly well, but the modified CDEPTH creep sag predictions were still linear with time in service.

2.1.3 Determination of CT-LIN Gaps.

For the assessments described so far, CT-LIN gap measurements were performed by AECL using an optical camera system, as described in Reference [2]. To measure the gap, the camera was inserted into the calandria via one of the calandria view ports and the camera was positioned to record an image of the gap to be measured. The measurements involved scaling the image of the CT-LIN gap against images of the LIN or CT, which are of known dimensions

Figure 5 – Predicted CT Elevations for G-2 Q06 With Standard and Calibrated CDEPTH Models

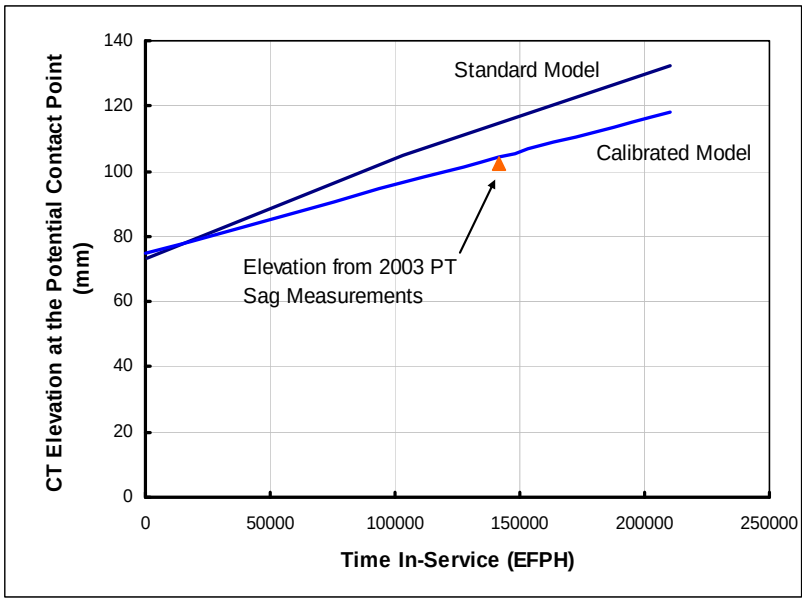

.Figure 6 displays examples of the gap measurements that were obtained in three inspections in PLGS and in G-2. The inspections in PLGS were performed in 2004 and the G-2 inspections were performed in 2003 and were repeated in 2006. The gaps plotted in Figure 6 are between the Row Q CTs and LIN #5.

Figure 6 – Example of CT-LIN Gap Measurements in PLGS AND IN G-2

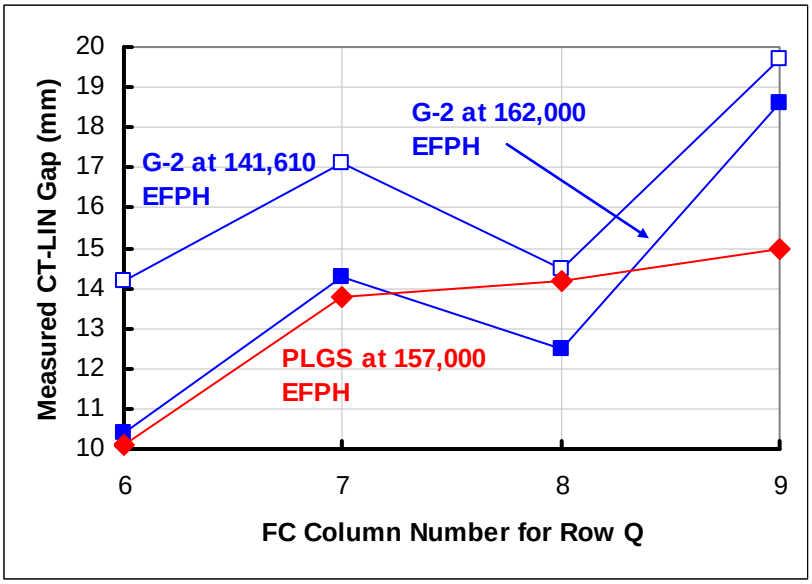

In the figure, the gap measurements are for Q06 – Q08, which could contact LIN #5.

2.1.4 CT-LIN Time-to-Contact Predictions

2.1.4.1 First Estimate Predictions of CT-LIN Time-to-Contact

These predictions were generated using CDEPTH 8.2 to model CT sag versus time in-service, while CT-LIN gap measurements were used to deduce both the rate of LIN creep sag and the initial gap between the CT and the LIN.

Time-to-contact predictions generated in this manner for Point Lepreau are presented as an example in Figure 7. The first estimate predictions indicate a number of channels with CT-LIN contact earlier than 185 kEFPH, the planned time for shutdown of the reactor for refurbishment for Q07, which was unacceptable. The earliest time-to-contact was predicted to be 181 kEFPH.

Figure 7 – Example of First Estimate CT-LIN Time-to Contact Predictions For Contact of Row Q CTs with LIN #5 in PLGS - 2005

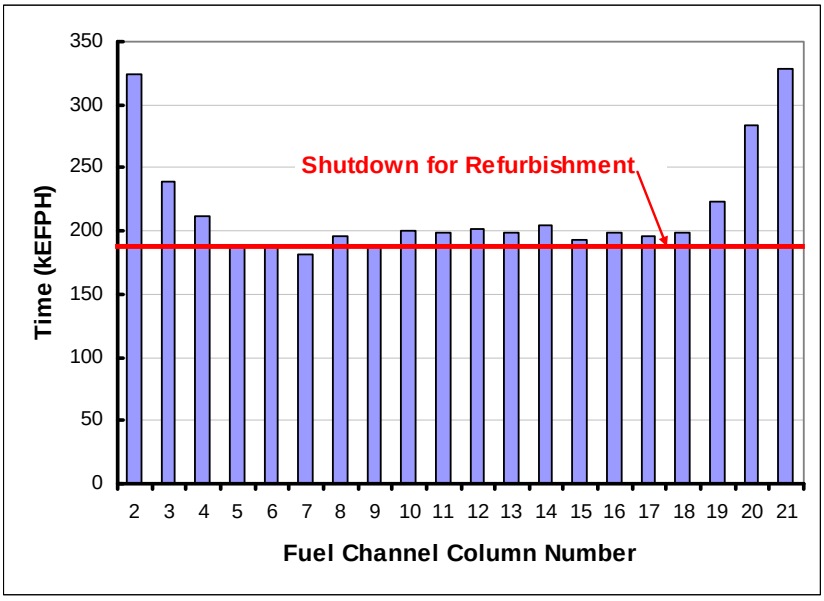

2.1.4.2 Calibrated Predictions of CT-LIN Time-to-Contact

In order to improve upon the results in Figure 7, the time-to-contact predictions were repeated using the updated and calibrated CDEPTH models. The time-to-contact predictions with the calibrated CDEPTH models are presented in Figure 8, which were considered to be acceptable. With the calibrated CDEPTH models, the earliest time-to-contact was predicted to be 210 kEFPH, an improvement of 29 kEFPH over the results in Figure 7.

Figure 8 – Time-to-Contact Predictions for the PLGS Row Q Fuel Channels Using Calibrated Fuel Channel Models With Different LIN Creep Sag Rates

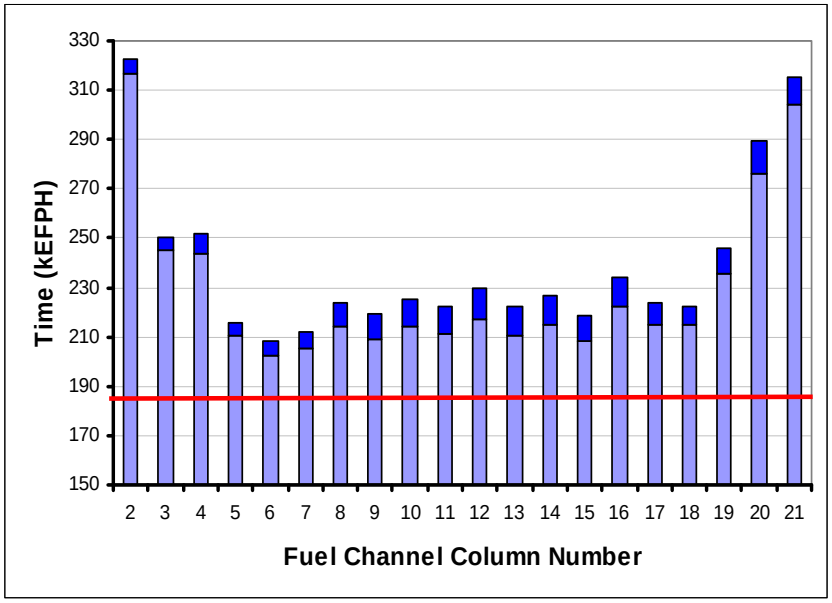

Note: the light bars represent time-to-contact for zero creep sag of the LIN beyond 157 kEFPH. The dark bars represent the increase in time-to-contact for creep sag of the LIN at the estimated rate. The total height of the light and dark bars represents the time-to-contact for creep sag of the LIN at the estimated rate. The horizontal line represents the planned time in-service for plant shutdown for retubing.

3. FURTHER REFINEMENTS TO CT-LIN CONTACT ANALYSIS

The sections that follow describe further advancements that have been made which will have an impact upon the accuracy of CT-LIN contact predictions.

3.1 APPARENT NON-LINEARITY IN PT CREEP SAG WITH TIME IN-SERVICE

From a theoretical perspective, it is expected that the creep sag rate of the fuel channel should **not** be constant but should decrease with time in service. Figure 9 presents a plot of maximum PT sag, (roughly at the centerline of the reactor) versus time in service for PLGS and for G-2.. The data covers all the PT sag measurements in the two reactors. The PLGS data are plotted in Figure 9 in red. The red line is a power function regression for PT sag versus time in-service for PLGS. Similarly, the G-2 data and power function regression a shown in blue in Figure 9.

Figure 9 – PT Maximum Sag Data with Regression Lines for PLGS and G-2.

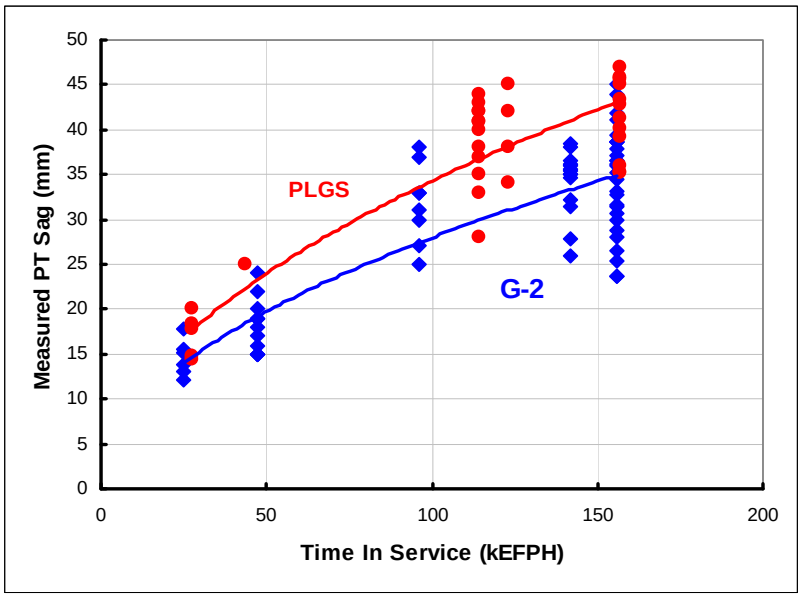

The hypothesis suggested by Figure 9 is that PT creep sag is non-linear with time in service and because of the scatter in the measurements, is multivariable. In this case, the missing variable would be fast neutron flux, based on irradiation-induced deformation theory. The measurements in Figure 9 are reminiscent of various plots that have been made of PT diametral expansion versus time in-service, which in 2005 – 2007 led to the development of multivariable regression models for PT diametral expansion for the PLGS and the G-2 PTs, issued in [3] and [4]. With the multivariable regression modeling for PT diametral expansion as a precedent, a similar analysis was tried for the PT sag data of Figure 9, the results of which are presented in Figure 10.

Figure 10 is a surface fit plot for G-2 PT sag versus time in service and FC power, noting that FC power is proportional to fast neutron flux and temperature and was chosen as a proxy for fast neutron flux

Figure 10 - Multivariable Regression Analysis for PT Sag versus Time In Service and Fuel Channel Power

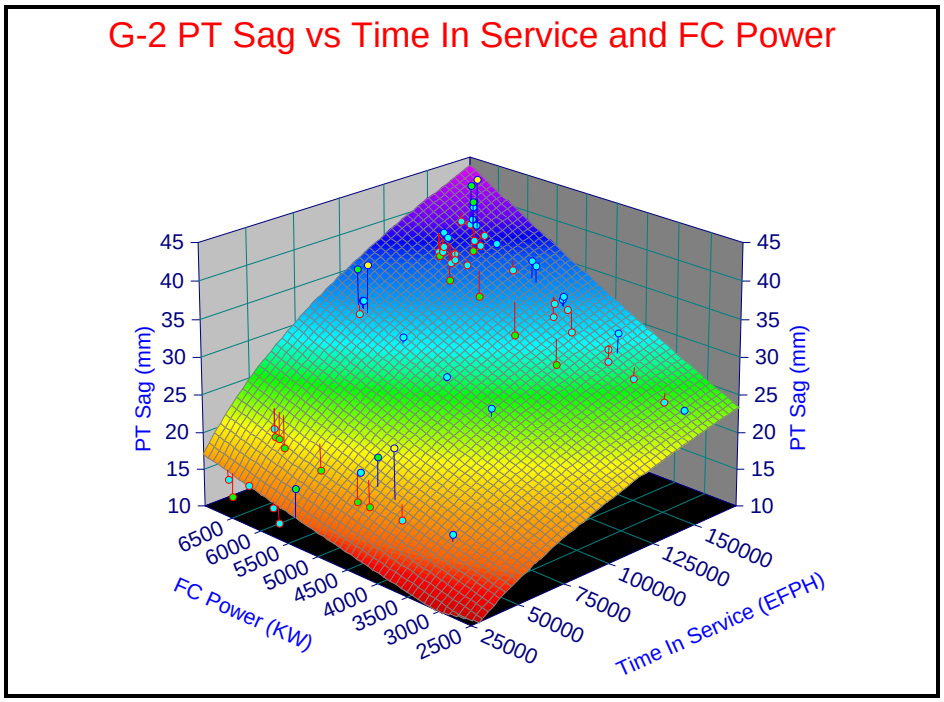

Figure 10 illustrates that the PT sag data is suitable for being fit to a non-linear multivariable model for sag versus time in-service and fuel channel power (or fast neutron flux). As an example, the surface fit depicted in Figure 10 is of the form:

$$\text{Ln (PT Sag)} = A + B/\ln(\text{Time}) + C\ (\text{FC Power})^{0.5}\ \ln(\text{FC Power})$$

Where A, B, and C are constants.

The implications of the non-linear behaviour of PT sag versus time in service for CDEPTH predictions of PT and CT sag are illustrated in Figure 3. The general trend is for MP ratio to start off around 1 early in the operating life of the reactor and then to decline with time in service. This trend is consistent with the non-linearity in PT sag observed in Figure 9. The linear sag deformation model in CDEPTH is quite representative of the PT sag measurements early in the life of the reactor, but with increasing time in service, the PT sag measurements deviate from a linear trend, causing decreases in MP ratio.

3.1.1 Rationale for the Apparent Non-Linearity in PT Creep Sag

When indications of non-linear creep sag of the PTs appeared, a physical explanation was sought for why the creep sag of the PT would decrease with time in-service, which led to the investigations summarized in this section.

In CDEPTH, the elements of the PT and CT models are modelled as straight beams, conventionally with a uniform cross-section. Intuitively, because the deformations of the PT and CT seem to be relatively small, the use of straight beam models for the PT and CT has continued in CDEPTH without any concern. However, in recent years, fairly significant PT and CT deformations have been detected. Early speculation was that the diametral deformation of the

CT and curvature of the CT would increase its stiffness and would reduce the rate of creep sag with time in-service, explaining the trend seen in Figure 9.

An investigation of the effects of PT deformation on the PT was carried out, from which it was found that seemingly small diametral expansions, combined with changes in curvature, resulting from PT sag, would influence the axial stress distribution in the PT, compared to that of a pristine PT. Similarly, small deformations of the CT would alter the stress distribution in the CT, compared to that in a pristine CT.

An example of the effect of CT curvature, due to creep sag, combined with local deformation of the CT cross-sections on the distribution of axial stress due to bending of the CT, is presented below. The example is for the CT of Fuel Channel F06 in PLGS, which was inspected in 2004 at 157 kEFPH.

From the inspection of F06, in 2004, PT sag and curvature measurements were obtained. The sag and curvature profiles aee given in Figure 11. In addition, PT gauging data were combined with PT-CT gap profiles to generate estimated CT inner diameter profiles, depicted in Figure 12. The profiles feature local diametral expansion of the CT at spacer locations. The expansions are in the vertical direction only, and induce ovality in the CT, such that at the spacer location, the vertical diameter of the CT exceeds the horizontal diameter. Both curvature due to sag and CT diametral expansion were thought to stiffen the CT.

Figure 11 – PT Sag and Curvature for PLGS F06 at 157 kEFPH

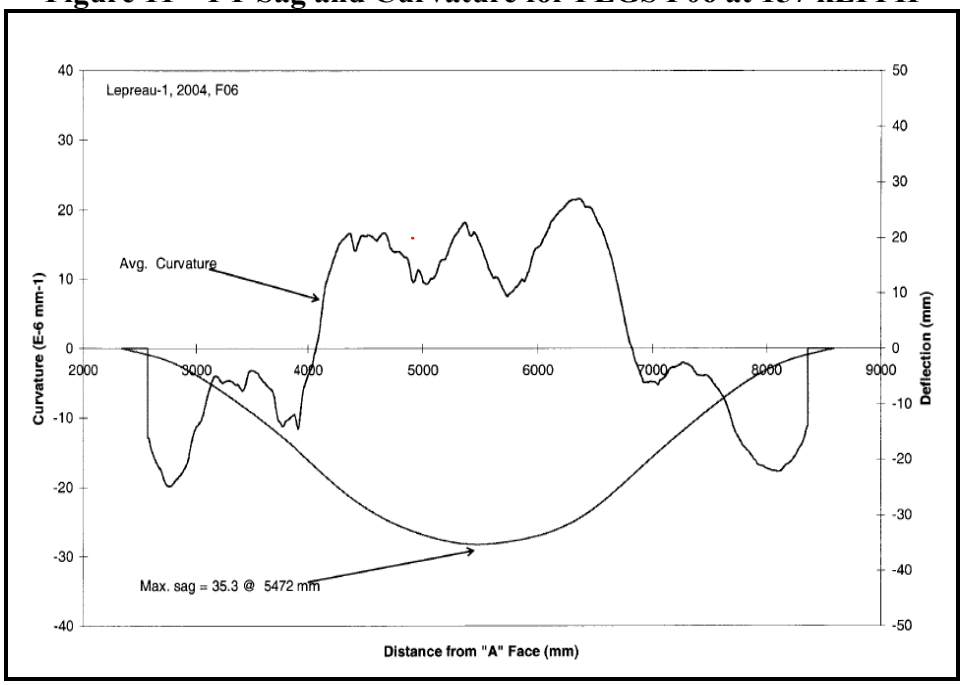

Figure from 87-31100-PIP-003, provided by T. Langlais, NB Power Nuclear

Figure 12 -Inner Diameter Profiles for the CT of F06 in PLGS at 157 kEFPH

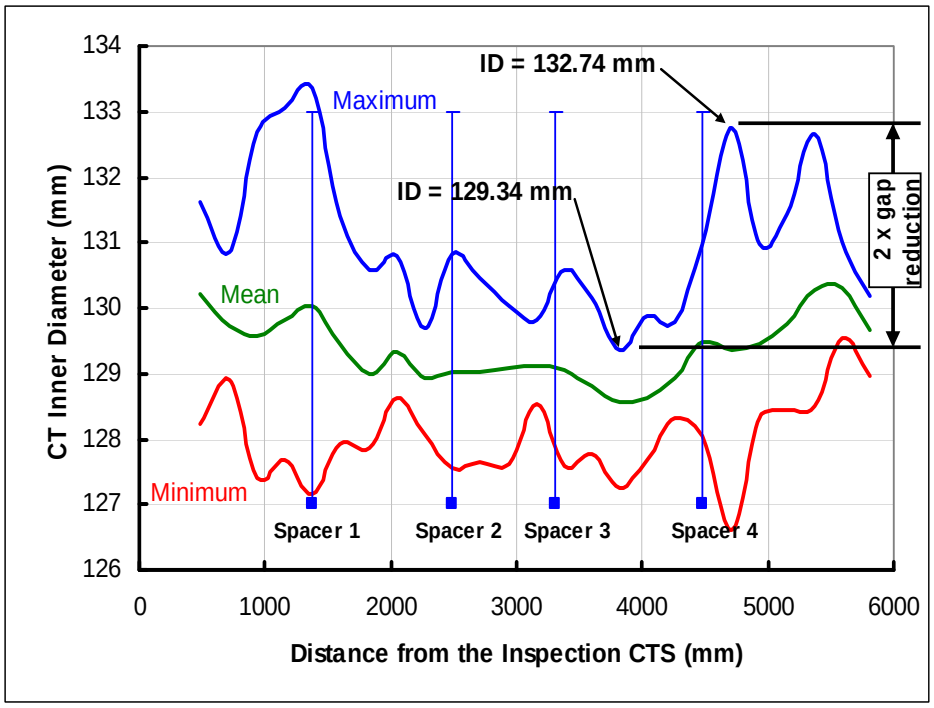

CTS stands for calandria tube sheet. The nominal inside diameter of the CT is 129 mm. At various sections of the CT, deformation has altered the section properties of the CT. The stress distribution at these sections deviates from that for a circular CT.

Following that line of thought, a comparative stress analysis was performed for the pristine CT in F06 and for the deformed CT at 157 kEFPH. . The pristine CT was assumed to be straight and cylindrical, which is how the stresses in the CT are calculated in CDEPTH. The deformed CT was assigned local curvatures due to creep sag and vertical and horizontal outer diameters based on the results of the inspection at 157 kEFPH, shown in Figures 11 and 12.

For both cases, . $\boldsymbol{\sigma}$/M was calculated for sections of the CT at discrete axial positions along the length of the CT, where $\boldsymbol{\sigma}$ is the axial stress due to bending and M.is the applied bending moment. For the pristine CT, $\boldsymbol{\sigma}$/M was calculated using the flexure formula for straight beams.

For the deformed CT, $\boldsymbol{\sigma}$/M was calculated using the following closed form solution for beams of constant curvature:

$$\sigma = \frac{My}{Ae(R - y)}$$

Where y is the distance from the neutral axis for the given section, A is the cross-sectional area of the section of the CT, e is the eccentricity of the section (the distance between the neutral axis and the geometric centroid of the section, and R is radius of curvature for the section.

The results of the comparative stress analysis are presented in Figures 13 and 14. In Figure 13, σ/M values at the top and bottom of the pristine and the deformed CT, at a section near the centre of the CT, are plotted versus distance from the neutral axis.

Based on Figure 11, the maximum axial stress in the deformed CT of Fuel Channel F06 near the central plane due to bending of the CT is 0.4 times the corresponding stress in the straight CT. Since the radius of curvature if the deformed CT is considered to be very large, the results in Figure 13 were surprising.

Figure 13 – Plot of Axial Stress due to Bending for the Pristine and the Deformed CT of F06 at 157 kEFPH at a Central Section

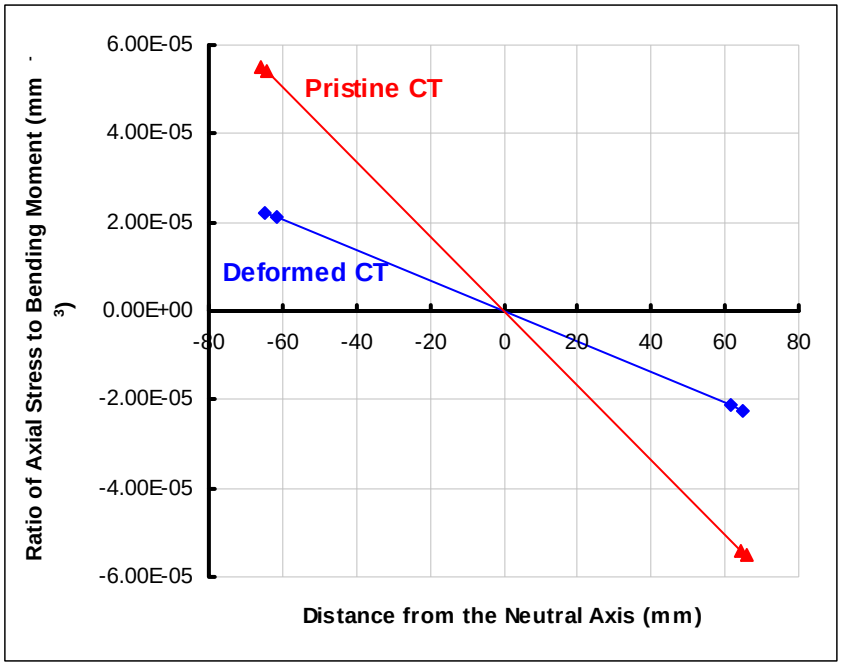

In Figure 14, the ratio of maximum σ/M value for the deformed CT to that for the pristine CT is plotted for various sections of the CT. Over most of the length of the CT, the ratio approaches 0.4, as can be seen in the Figure.

The reduction in bending stress in the deformed CT is due to a combination of the curvature of the CT and an increase on the cross-sectional area of the CT because of diametral expansion of the CT.

Figure 14 – Plot of Bending Stress Ratio for the Deformed and Pristine CT from F06 in PLGS versus Distance from the Outlet EF Taper

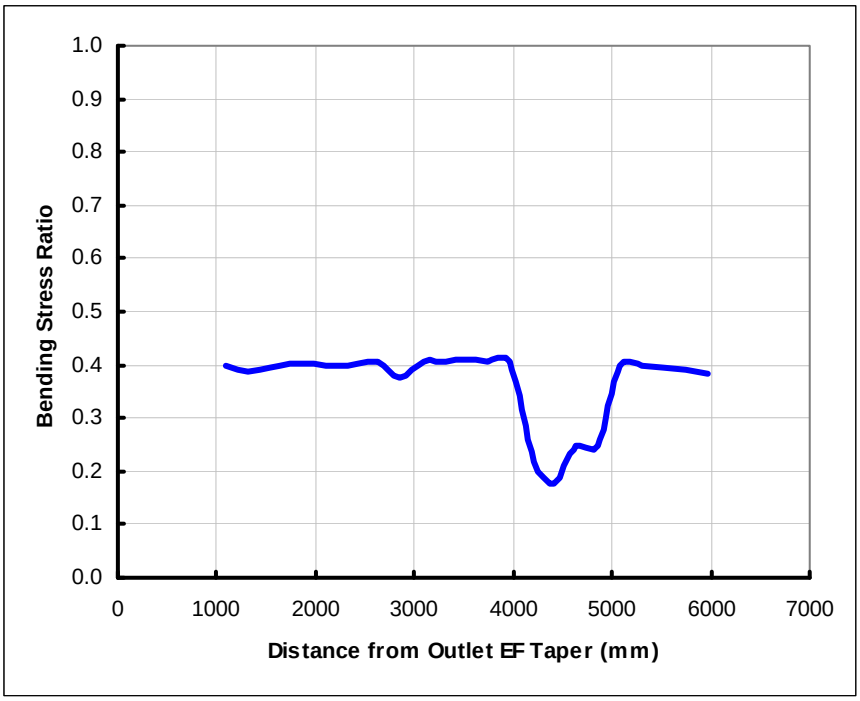

Note: EF stands for End Fitting. CT diameter data was questionable from 0 – 1000 mm and so the stress ratio was not plotted for this range. The local depression in the stress ratio from 4000 – 5000 mm coincides with a region of higher curvature and increased ovality of the CT due tospacer loading.

Since bending stress drives creep sag of the CT, for a bending stress at 157 kEFPH in the deformed CT that is 0.4 of the stress for a pristine CT, the CT creep sag rate at 157 kEFPH should be 0.4 of the initial creep sag rate, if all other parameters that affect CT sag were constant.

The possible relationship between CT creep sag rate and the reduction in bending stress in the deformed CT was investigated in Figure 15. In the figure, PT creep sag rate, determined from the PT sag data for PLGS of Figure 9, was plotted versus time in-service, together with a best-fit line and a trend line for F06, depicted in red. From Figure 15, the mean initial creep sag rate and the mean creep sag rate at 157 k EFPH were found to be 4.2 and 1.8 mm per 7 kEFPH. On average, over all inspected PTs, the creep sag rate at 157 kEFPH was found to be 0.43 of the initial sag rate, measured at 27 kEFPH.

Similarly, from the trend line for F06 drawn in Figure 13, the final PT creep sag rate at 157 kEFPH was found to be 0.39 times the initial PT creep sag rate for F06.

In summary, assuming that the CT creep sag rate for F06 is proportional to the PT creep sag rate, the predicted bending stress reduction in the CT of (100 – 40)% = 60% from 27 to 157 kEFPH was accompanied by a CT creep sag rate reduction of (100 – 39)% = 61%.

Note that the stress reduction numbers quoted above assume that there were no changes in bending moment at the central section of the CT from 27 to 157 kEFPH. In reality, complications such as SLAR and the redistribution of spacer loading could alter the bending moment distribution acting on the CT. These effects could introduce secondary changes to the bending stress in the CT. Therefore, the actual bending stress in the CT of F06 at 157 kEFPH could deviate from 0.40 of the stress for an undeformed CT.

Another point to consider in comparing the predicted stress reduction in the CT to the creep sag rate of the PT is that there will be small differences in the sag rate of the PT and CT between the spacers. Therefore, except for the spacer locations, using the PT sag rate as the CT sag rate will overestimate the sag rate of the CT

Setting aside, temporarily, the complications that could have changed the bending moments acting on the CT of F06 during operation to 157 kEFPH, the implication is that stress reductions in the CT due to CT deformation could be responsible for 60/61 = 98% of the reduction in creep sag rate for F06 from 27 to 157 kEFPH.

Figure 15 – PT Creep Sag Rates Versus Time In Service for PLGS

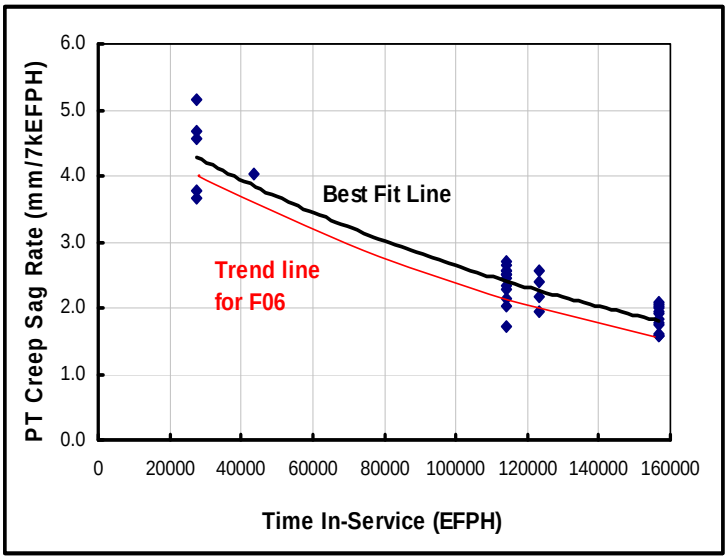

3.2 LIN CREEP SAG BEHAVIOUR

The original approach for establishing the in-service elastic curve of the LIN was to use the elevation of the deformed PT plus the PT gap to calculate the in-service elevation of the LIN at its intersection point with the fuel channel. This strategy was abandoned when discrepancies in some of the CT-LIN gap measurements came to light, as outlined in 3.3.

Later, it was found that ultrasonic measurements of LIN elevation in Wolsong, reported in Reference [5] produced in-service sag profiles that agreed very well with predictions generated with the NOZZLE code. Figure 16 provides a plot of the initial and in-service elastic curves at 1.8 and at 18 years in service for the Wolsong reactors, based on NOZZLE predictions. The data points shown in red in Figure 16 represent measurements [6}.

For CANDU 6 reactors, LIN creep sag can be calculated using the data of Figure 16. For other reactors, the NOZZLE code should give very good results.

FIGURE 16 – Comparison of Sag Measurements with Sag Profiles from the NOZZLE Code for the Wolsong Reactors

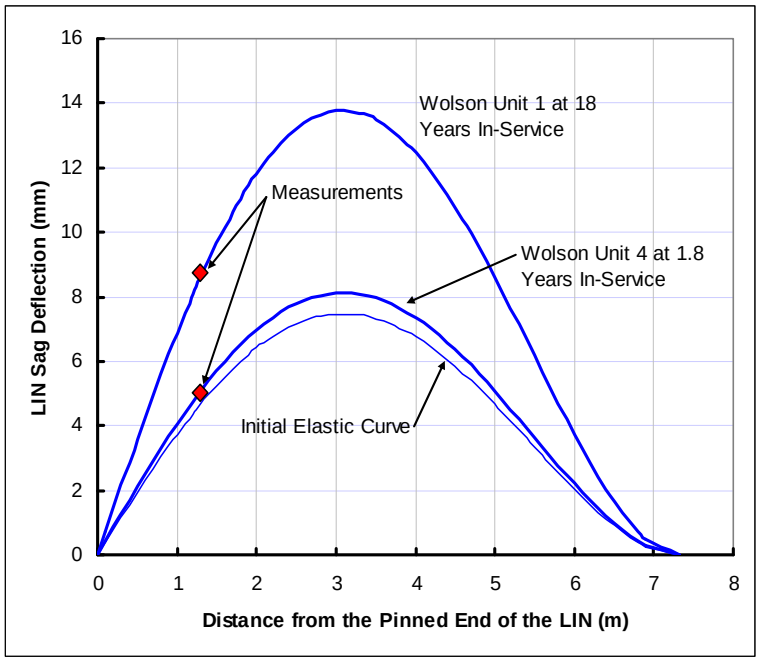

3.3 CT-LIN GAP MEASUREMENTS

Following an examination of the optical CT-LIN gap measurements for G-2, it appeared that some of the gaps were underestimated by about 10 mm, based on the known elevation of the fuel channel and as-installed elevation . The accuracy of the gap measurements was investigated at length but an explanation for the apparent discrepancies was not found.

Recently, two factors have been identified as causes for the underestimation of gap sizes using the optical method of gap measurement: (1) Sag of the LIN, and (2) elevation of the camera relative to gap being imaged.

Figure 17 illustrates how the image of the CT- LIN captured by the camera can underestimate the size of the actual gap as a result of LIN sag. The image of the gap is formed by light passing between the CT and the LIN. In this case, the camera is at the same elevation as the space between the CT and the LIN that forms the gap image. The height of the beam of light passing between the CT and the LIN is determined by the vertical distance between the bottom of the CT and the highest point at the top of the LIN along its length. As shown in the figure, the bottom of the CT and the highest point at the top of the LIN are not equidistant to the camera because of the sag of the LIN. Because of the sag of the LIN, as depicted in the figure, the actual gap is larger than the image of the gap, captured by the camera.

To avoid the effect of LIN sag on gap image, gap imaging must be performed with the camera perpendicular to the LIN. With the arrangement of view ports in the calandria, only a few of the gap images can be generated with the camera perpendicular to the LIN.

Figure 17 – Underestimation of Gap Size due to Sag of the LIN

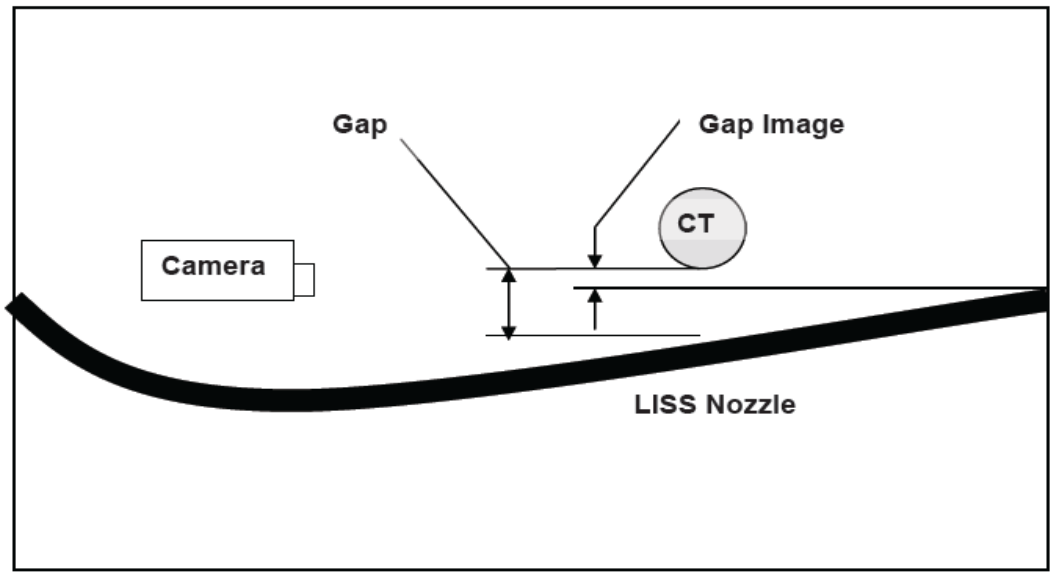

Figure 18 illustrates how elevation of the camera relative to the gap reduces the size of the gap image that is captured by the camera. In this example, the LIN is assumed to be straight and the camera is inclined at an angle θ relative to the LIN. At θ = 0º, the camera would be at the same height as the top of the LIN and the gap image would be a good representation of the actual gap size. However, with increases in θ, as depicted in Figure 5, the apparent space between the CT and LIN would decrease, reducing the size of the gap image.

It is expected that the inclination of the camera is not strictly controlled during the gap measurements.

Figure 18 – Underestimation of Gap Size due to Elevation of the Camera Relative to the CT

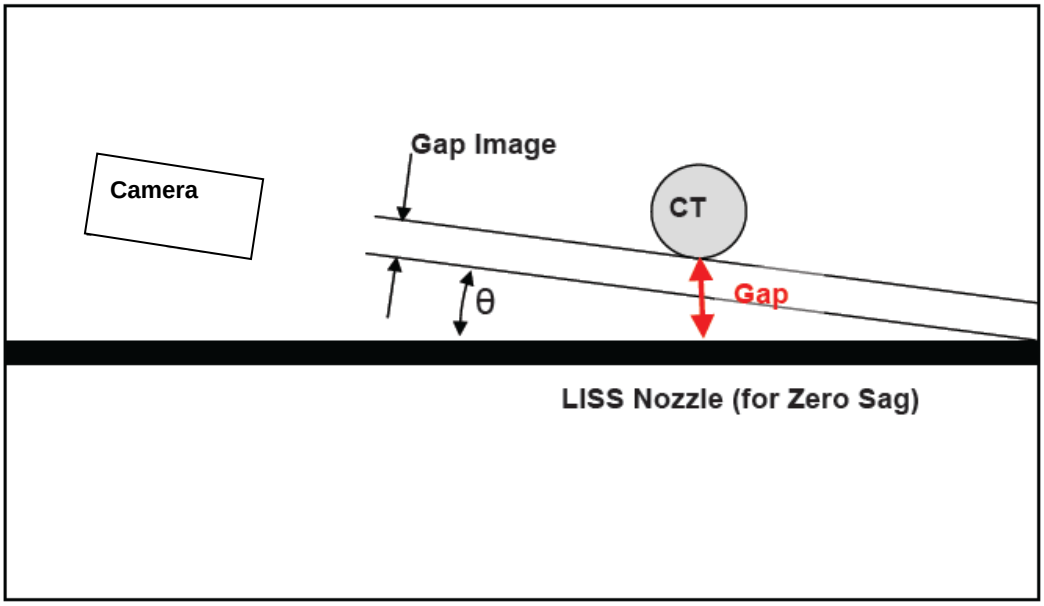

4. DISCUSSION

The comparative stress analysis of the deformed and pristine CT in F06 produced a stress ratio that was very close to the observed reduction in PT creep sag rate for F06, which was very encouraging. However, the analysis was overly simplistic. A number of variables were excluded from the stress analysis, such as changes in bending moment due to evolution in spacer load and SLAR and differences in the creep sag rate of the PT and the CT. It is expected that the stress ratio will change somewhat if a more elaborate stress analysis were performed. This means that in order to take credit for the effects of stress reductions in the CT, far more detailed finite element stress analyses of the CT should be conducted that account for the actual 3D shape of the CT, with realistic time-dependent spacer loads, including simulations of SLAR.

Regarding the creep sag behaviour of the LIN, it is noteworthy that the NOZZLE code, from 1981, generated initial elastic curves and creep sag prediction that agree well with the ultrasonic LIN sag measurements in Wolsong, issued in 2005.

5. CONCLUSIONS

1. PT sag measurements from the inspection of PLGS and G-2 indicate that PT, and therefore CT creep sag, are non-linear functions of time in service.

2. Based on a simple comparative stress analysis of a pristine and a deformed CT, deformation of the CT (creep sag and diametral expansion) will reduce bending stresses in the CT.

3. In the case of F06 in PLGS, it was found that the predicted percentage bending stress reduction due to the measured deformation of the CT at 157 kEFPH, corresponded very closely to the observed percentage reduction in PT creep sag rate from 27 to 157 kEFPH. This result implies that the reduction in bending stress associated with the deformation of the CT causes a proportionate reduction in the creep sag rate of the CT with time in service.

4. For the optical CT-LIN gap measurements, reasonable accuracy in the measurement can only be achieved if the camera is in close proximity to the gap being recorded.

5. The predictions of LIN creep sag behaviour from the NOZZLE code [5], agree closely with ultrasonic measurements of LIN elevation performed in Wolsong Units 1 and 4 [6].

6. RECOMMENDATIONS

1. In the absence of reactor-specific CT-LIN gap or LIN sag measurements, LIN creep sag predictions should be performed with the NOZZLE code or an equivalent formulation.

2. Future predictions of CT-LIN time-to-contact should take advantage of the observed non-linearity in the rate of fuel channel creep sag with time in service. To do this, CDEPTH or whichever code is used to predict PT and CT deformation, should be modified to calculate operating stresses that account for ovality and curvature of the PT and the CT, which will increase with time in service. This modification should be supported by a detailed finite element study of the in service stresses of as many inspected fuel channels as possible.

3. In future CT-LIN gap measurements, the optical camera system should only be used if the camera can be positioned at the gap to be recorded. If not, then an alternative method should be implemented.

7. REFERENCES

1. P.J. Sedran, CPUS Limited, *CT-LIN Time-to-Contact Predictions for PLGS using Updated FC Models*, CPUS Technical Report 0040 REPT ENG 0003 00, September 30, 2005
2. T. Campbell, *AECL Inspection Report Calandria Tube to LISS Nozzle Gap Measurement*, 87-31230-INR-001 Revision 1, January 2005.
3. E. Nadeau, W. Hartmann, AECL Technical Document 87-31100-220-054, *Diametral Expansion Assessment of Gentilly-2 and and Point Lepreau NGS –*

Interim Results , 2005 05.

4. P.J. Sedran, CPUS Limited, *Multi-Variable Regression Analysis of Diametral Expansion for the PLGS Pressure Tubes*, 0065-REPT-ENG-003 Rev. 00, April 27, 2007.
5. A.R. Causey and J.D. Brown, *Deflection of Liquid Poison Injection Nozzles Resulting from Irradiation-Induced Creep and Growth*, CRNL 2145, November 1981.
6. T.R. Kim, S.M. Sohn, J.S. Lee, Korea Electric Power Research Institute, *Ultrasonic Devise to Measure Gap Between Calandria Tube and LISS Nozzle*, 7th International CANDU Maintenance Conference, Toronto, November 20 – 22, 2005.

8. ACKNOWLEDGEMENTS

Thanks are due to Bill Rankin, NB Power Nuclear, PLGS and to Michel Cantin, Hydro-Québec - Centrale Gentilly-2 for permission to use data from various inspections and for their review of the paper. Ness Azer and Majid Tabatabai of AMEC NSS are acknowledged for their contributions as well.

Attachment 4

A Rationale for the Observed Non-Linearity in Pressure Tube Creep Sag with Time in Service

P.J. Sedran[1]

[1] Fuel Channel Consultant – RESD Inc.
paulsedran@sympatico.ca

Abstract

In 2012, a paper was presented at the CNS SGC Conference which included an explanation for measured non-linear trends in Pressure Tube (PT) creep sag. The section of the 2012 paper covering this topic was revised and is presented as the main subject of this paper. The practical applications for the prediction of long-term Fuel Channel (FC) creep sag include the analysis of Calandria Tube – Liquid Injection Nozzle (CT-LIN) contact, and fuel passage and PT replacement assessments.

The current practice for predicting FC creep sag in life cycle management applications is to use a linear model for creep sag versus time in service. However, PT sag measurements from the Point Lepreau Generating Station (PLGS) and Gentilly-2 (G-2) have displayed a non-linear trend with a creep sag rate that is decreasing with time in service.

As an example, for PT F06 in PLGS, a 60% reduction in the nominal creep sag rate was observed for measurements taken 18 years apart. Subsequently, it was found that a 56% reduction in the creep sag rate for F06 over 18 years could be attributed to a fundamental geometric property of the PT creep sag profile. In addition, a further 1.6% decrease in the creep sag rate of the CT over the same period could be attributed to bending stress reductions due to the deformation of the CT.

The resultant reduction in the PT creep sag rate for F06 was predicted to be 57.6%, closely matching the observed PT creep sag rate reduction of 60%. Therefore, this paper provides a rationale to explain the observed non-linear trends in PT creep sag, the use of which could benefit stations engaging in asset management as a means of FC life extension.

This paper presents a summary of the worked performed to correlate the observed reductions in PT creep sag rate to the geometrical properties of the PT creep sag profile and the predicted bending stress reductions in the CT.

1. Introduction

The issue of CT-LIN contact, which gained significant attention through a COG workshop in 1990 [1], has long been recognized as a life-limiting factor for the CTs. The measurement and prediction of FC creep sag rates have been central to the analysis of CT-LIN contact. In recent assessments, CT-LIN time–to-contact predictions for the CANDU 6 reactors indicate a significant risk of contact should the reactors operate beyond 210 kEFPH (kilo Effective Full Power Hours)

In reactors that have been refurbished, (Bruce Units 1 and 2, Point Lepreau, and Wolsong Unit 1), or are planning refurbishment by 210 kEFPH, CT-LIN contact will not be an issue for many years. However, for stations that are planning asset management strategies in order to operate beyond 210,000 EFPH, FC creep sag rates will factor into the remaining life of the FCs. For these stations, (Bruce 3 - 8 and Darlington) a number of refinements to the overall strategy for predicting CT-LIN time-to-contact have been developed. The refinements included the development of a non-linear empirical CT creep sag model. To justify the model, an explanation for the model's prediction of a decreasing creep sag rate with time in service is proposed in this paper, the contents of which are as follows:

Section 2 provides PT creep sag data for PLGS and G-2.

Section 3 provides a description of the geometric relationship between the rate of PT creep sag and the rate of creep-induced elongation of the arc length at the bottom of the PT.

Section 4 describes the acquisition of full-length CT inner diameter and curvature profiles from in-service PT inspection measurements in a selected channel in PLGS.

In Section 5, a comparative bending stress analysis for a pristine and a deformed CT is presented. The rationale for the analysis was based on the idea that possible bending stress reductions in the CT could result in decreasing FC creep sag rates with time in service.

A discussion of results is presented in Section 6.

Conclusions and Recommendations are provided in Sections 7 and 8.

References and Acknowledgements are found in Sections 9 and 10.

2. PT Creep Sag Data

Figure 1 presents a plot of maximum PT sag, (roughly at the centerline of the reactor) versus time in service for PLGS and for G-2. The data, which covers all of the PT sag measurements in the two reactors, are consistent with data used in the FC life cycle management documents for PLGS [2] and G-2 [3]. The PLGS data are plotted in Figure 1 in red. The red line is a power function regression for PT sag versus time in-service for PLGS. Similarly, the G-2 data and power function regression are shown in blue in Figure 1.

The PT sag data of Figure 1 was used to calculate nominal (not accounting for a 1 mm measurement accuracy in sag) PT creep sag rates. PT creep sag rate measurements for PLGS are presented in Figure 2. In the figure, a best fit line is plotted with the complete data set for PLGS. The red line in the figure represents a trend line for the PT in FC F06.

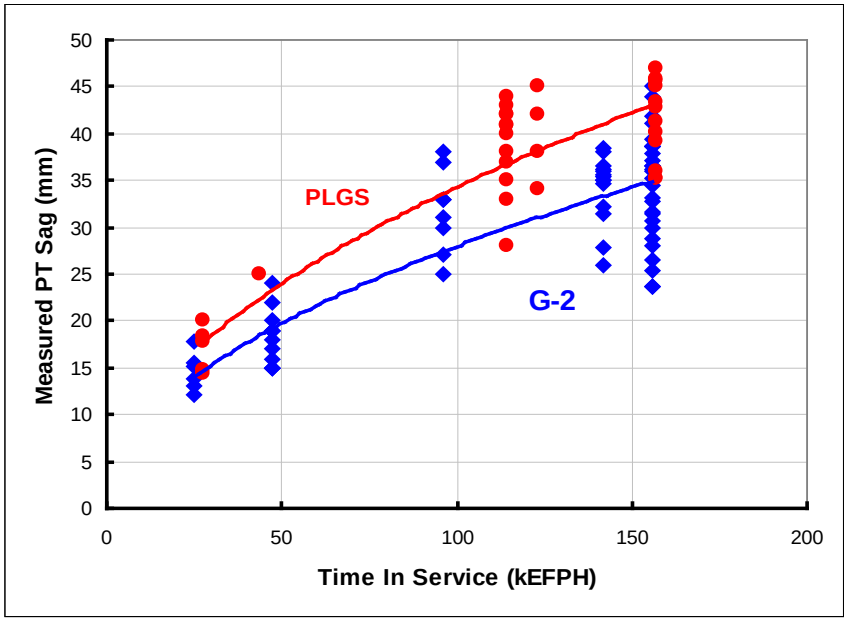

Figure 1 – PT Nominal Sag Data (at Peak Sag Locations)
with Regression Lines for PLGS and G-2

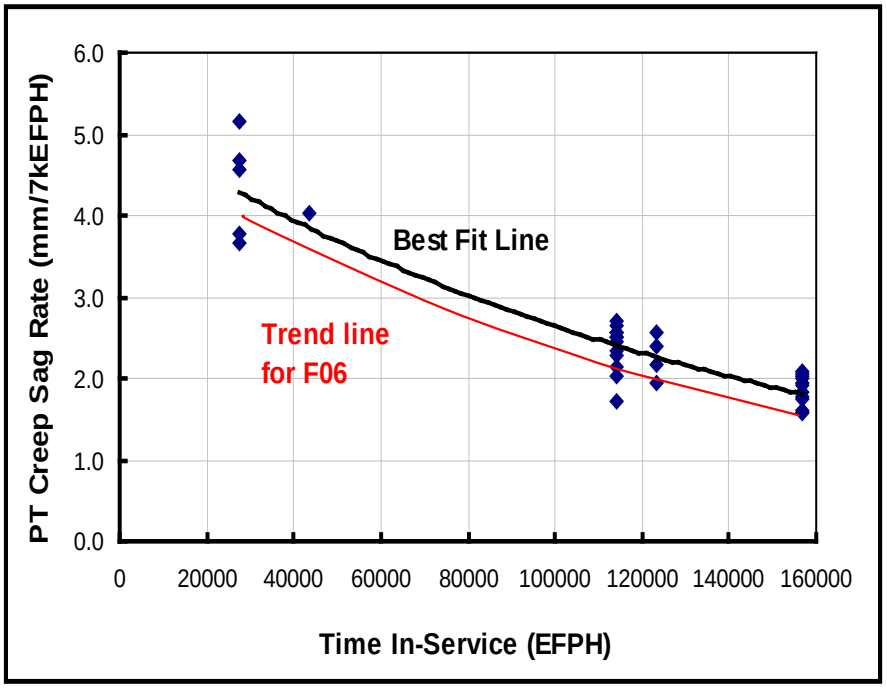

Figure 2 – PT Creep Sag Rates Versus Time In Service for PLGS

Based on Figure 2, the nominal PT sag rate for F06 has decreased from 4.0 mm/7 kEFPH at 27 kEFPH to 1.6 mm/7 kEFPH at 157, a decrease to 40% of the value at 27 kEFPH, which represents a reduction of 60% in the creep sag rate over the time period in question.

The implications of non-linear PT creep sag for the accuracy of creep sag predictions are illustrated in Figure 3. In the figure, MP (Measured to Predicted) ratio for PT sag is plotted versus time in-service. The predicted value of PT sag for each MP ratio data point in Figure 3 was generated using the CDEPTH code [4]. The trend is for MP ratio to start off around 1.0 early in the life of the reactor and then to decline with time in service. This trend is consistent with the non-linearity in PT sag observed in Figure 1. The linear sag deformation predictions are representative of the PT sag measurements early in the life of the reactor, but with increasing time in service, MP ratio decreases because the creep sag predictions of the linear model are increasingly different than the creep sag measurements, which follow a non-linear trend.

Figure 3 – Plot of MP Ratio for PT Sag in PLGS

3. Relationship between PT Creep Sag Deflection Rate and the Rate of Creep Induced Elongation of the Bottom of the PT.

In various analyses, for all CANDU stations, PT creep sag has been modelled as being linear with time in-service. The linear models do seem to fit the various data sets reasonably well and are conservative.

In previous assessments of CT-LIN contact, the CDEPTH code [4] was used to compute PT and CT creep sag, and there was no need to examine the fundamental geometry involved in the deformation of the PT. However, the examination of the fundamental geometry of PT deformation was undertaken in the attempt to explain the trends seen in Figures 1 and 2.

The thought process regarding the geometry of PT deformation proceeded as follows:

1. The bending of the PT under weight-loading produces tensile stresses at the bottom of the PT that result in local creep elongation at the bottom of the PT. Essentially, the arc length of a line on the outside surface at the bottom of the PT (PT arc length) will increase with time.

2. Assuming that bending stress and fast neutron flux are constant with time in service and ignoring reductions in creep rate with neutron fluence, it is expected that the creep-induced elongation of the PT arc length will be constant with time in service.
3. However, the PT creep sag rate is seen to be decreasing with time in service. Is there a simple geometric argument to explain how the elongation rate of the PT arc length could be constant while the creep sag rate is decreasing with time in service?

Point 3, above, suggested the following relationship:

$$dy/dt = (dy/ds)\,(ds/dt) \quad (1)$$

Where dy/dt is the rate of creep sag, dy/ds is the rate of change in creep sag with arc length, and ds/dt is the rate of change in arc length. As indicated previously, ds/dt is assumed to be constant. If it could be shown that dy/ds reduces with time in service, with ds/dt, due to creep deformation, being constant, then dy/dt would also decrease with time in-service, as indicated in Figures 1 and 2. Note that y is the sag deflection of the bottom of the PT, i.e., the vertical distance of a point on the bottom of the deformed PT from the same point on a straight and horizontal PT. Figure 4 depicts the PT sag profile for F06 and illustrates the differentials dx, dy, and ds.

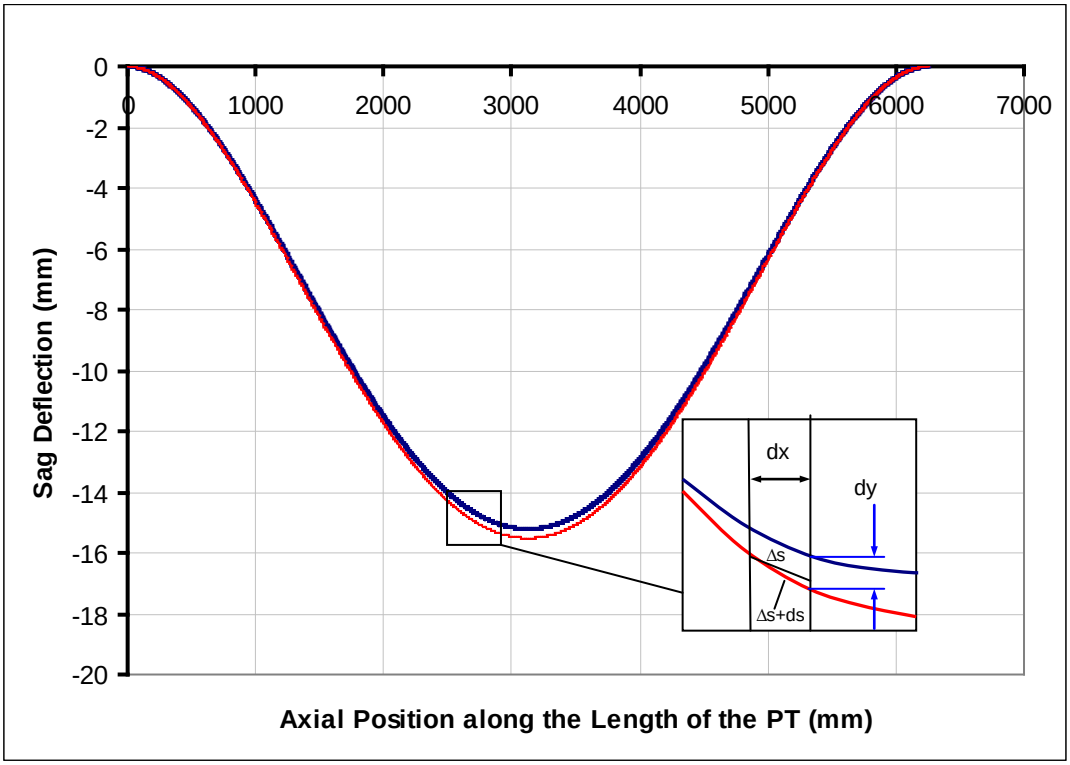

Figure 4 – PT Sag Profile for F06 with Illustrations for dx, dy, and ds

The blue line depicts the creep sag profile at 27 kEFPH and the red line represents the profile with an increment in sag of dy at a given position over a time step dt. Note that x is the axial coordinate. Over the interval dx, the length of the sag profile at 27 kEFPH is Δs. With creep deformation of the PT under bending stresses, the arc length of the sag profile from x to x+dx increases by the increment ds.which results in dy at x+dx, all over the time step dt.

In order to study the variation in dy/ds for PT F06 at different times in service, finite difference computations of the PT arc length at 0, 27, and 157 kEFPH were performed in EXCEL. The PT

sag profile used in the computation of the PT arc length was that for a fixed-fixed beam under uniform lateral loading:

$$y(x) = w\, x^2\, (L - x)^2/24\, EI \qquad (2)$$

Where y(x) is the sag deflection, w is the load per unit length of the beam, x is the distance along the length of the beam, L is the length of the beam, E is the beam elastic modulus, and I is the area moment of inertia of the cross-section of the beam.

For each of the three cases, a small increment in sag was applied to the sag profile and a numerical approximation for dy/ds was obtained.

A summary of the PT arc length computations is presented in Table 1. The 0 EFPH sag profile case represents the sag of the PT under static loading. The sag profiles for 27 and 157 kEFPH represent the measured creep sag profiles for PT F06. The sag and arc length increments, dy and ds, are presented with the computed values of dy/ds in Table 1.

Table 1 – Computation of dy/ds for PT F06 at Different Times

Time (kEFPH)	y (mm)	dy (mm)	S (mm)	ds (mm)	dy/ds (mm/mm)
0	1.65	1.93	6250.00106	0.003937	490.06
27	15.21	0.89	6250.09030	0.010936	81.83
157	35.08	0.72	6250.48011	0.019795	36.16

Note that S is the arc length for the entire PT, computed for the PT prior to the application of sag increment, dy, which applies to the centre of the channel.

Table 1 indicates that there is a rapid decrease in dy/ds with increasing PT sag. For a constant rate of PT arc length elongation, the PT sag rate would decrease with time.

Using dy/ds values from Table 1, dy/ds at 157 kEFPH was calculated to be (36.16 ÷ 81.83) or 44.2% of that at 27 kEFPH. From Equation 1, assuming a constant ds/dt over time, dy/dt at 157 kEFPH would also be 44.2% of that at 27 kEFPH. The 44.2 % value computed from Table 1 compares reasonably well with the 40% value obtained for F06 in Section 2. .

In an attempt to reduce the predicted 44.2% creep sag rate ratio to a value closer to 40%, it was postulated that in-service induced deformation of the CT could reduce bending stresses and, therefore, the FC creep sag rate. An investigation of the affects of CT deformation on bending stress is summarized in Sections 4 and 5.

4. In-Service CT Deformation – Curvature and Inner Diameter Profiles

An example of the deformation of the CT, resulting from CT curvature, due to creep sag, combined with local deformation of the CT cross-sections, is presented below. The example is for the CT of Fuel Channel F06 in PLGS, which was inspected in 2004 at 157 kEFPH.

From the inspection of F06, in 2004, PT sag and curvature measurements were obtained. The PT sag and curvature profiles are given in Figure 5, which was reproduced from [5]. The PT sag data of Figure 5 was used to generate a corresponding CT sag profile.

In addition, PT gauging data from the 2004 inspection were combined with PT-CT gap profiles to generate an estimated CT inner diameter profile, depicted in Figure 6, from Reference [6].

Although the PT-CT gap profile used to generate the CT inner diameter profile was examined and appeared to be reasonable, the gap profile was not subject to quality assurance verification.

Therefore, until the PT-CT gap data is verified, the CT inner diameter profile presented in Figure 6 should be treated as preliminary.

The CT profile of Figure 6 indicates that there are local areas of diametral expansion of the CT at the spacer locations. The expansions are in the vertical direction only, and induce ovality in the CT, such that at the spacer location, the vertical diameter of the CT exceeds the horizontal diameter. The spacers are designed to support the weight of the fuel channel, and in turn are supported by the CT. The local deformation of the CT at the spacer locations, depicted in Figure 6, results from the high contact stresses that develop in the CT from spacer contact loading. Both curvature due to sag and CT diametral expansion were thought to stiffen the CT.

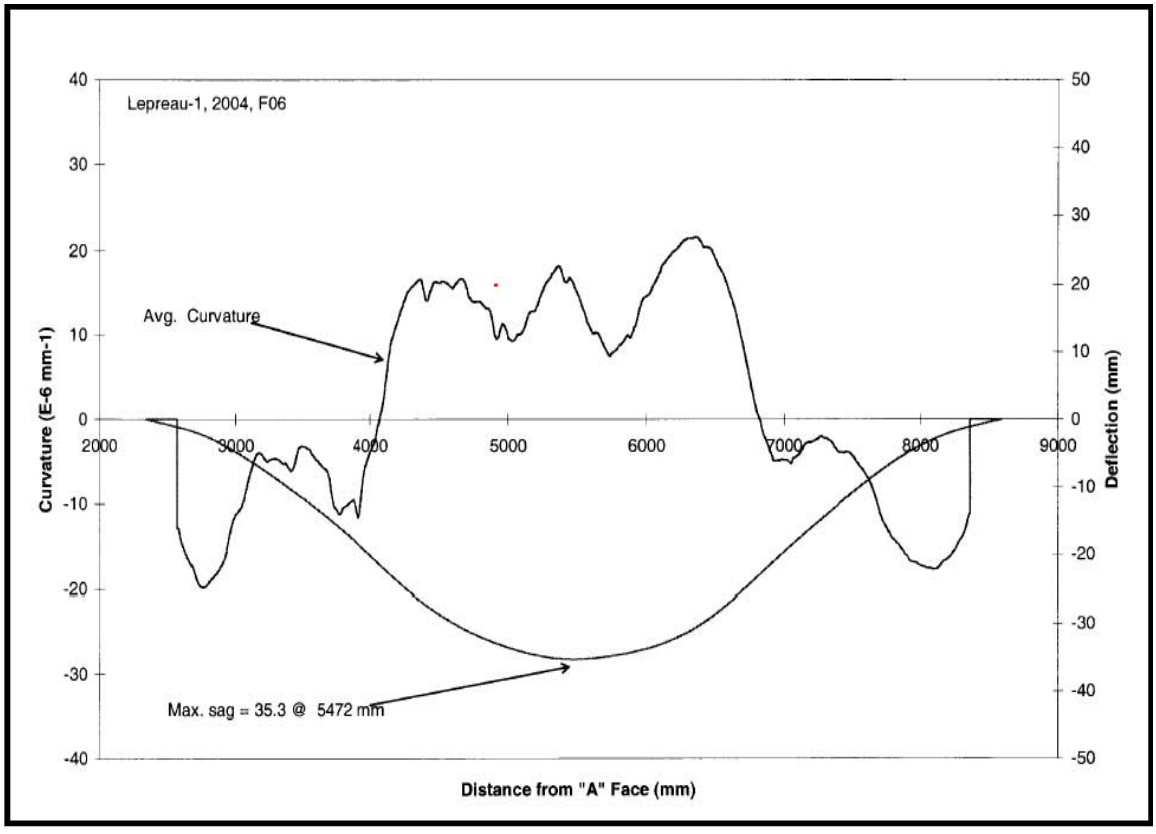

Figure 5 – PT Sag and Curvature for PLGS F06 at 157 kEFPH

Figure from 87-31100-PIP-003, was provided by T. Langlais, NB Power Nuclear. The A Face is the East inspection face for the reactor for the 2004 Fuel Channel Inspection. The PT sag profile measurements are nominal values. For assessments, measurement error of plus or minus 1 mm on sag measurements are customary. The peaks in PT curvature represent local minimum radia of curvature of the PT due to bending of the PT at spacer locations.

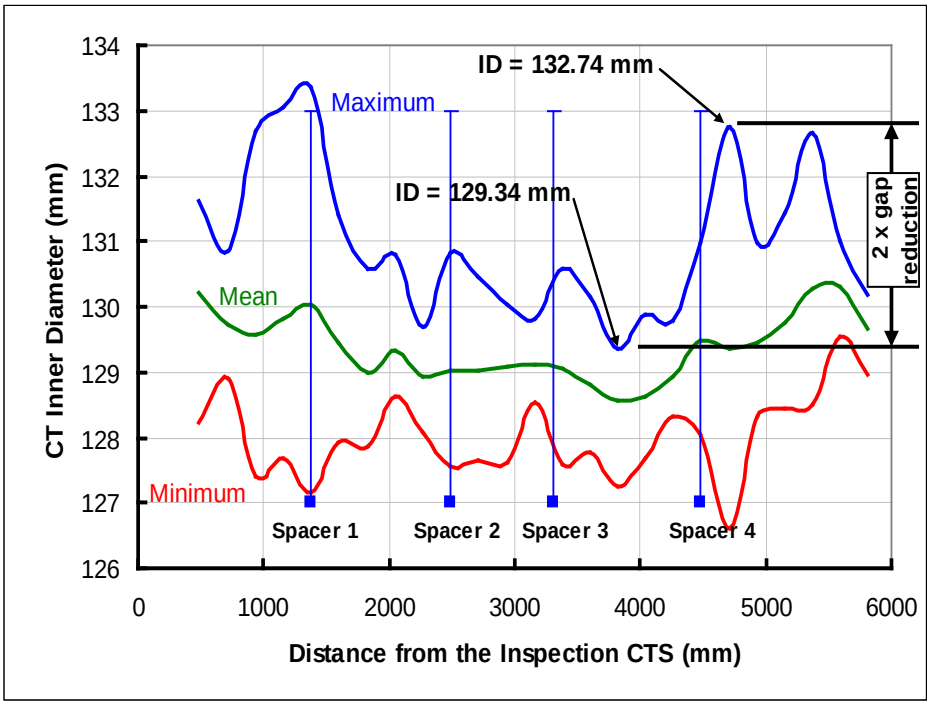

Figure 6 - Inner Diameter Profiles for the CT of F06 in PLGS at 157 kEFPH

CTS stands for Calandria Tube Sheet. The red line represents minimum diameter values at each section. Mean and maximum diameter values for each section are plotted in green and blue, respectively. The nominal inside diameter of the CT is 129 mm. At various sections of the CT, deformation has altered the section properties of the CT. The stress distribution at these sections deviates from that for a circular CT. The raw inspection data was provided by NB Power Nuclear staff.

5. Comparative Stress Analysis for a Pristine and a Deformed CT

When indications of non-linear creep sag of the PTs appeared, a physical explanation was sought for why the creep sag of the PT would decrease with time in-service, which led to the investigations summarized in this section.

In CDEPTH, the elements of the PT and CT models are modelled as straight beams, conventionally with a uniform cross-section. Intuitively, because the deformations of the PT and CT seem to be relatively small, the use of straight beam models for the PT and CT has continued in CDEPTH has not been questioned. However, in recent years, fairly significant PT and CT deformations have been detected. Early speculation was that the diametral deformation of the CT and curvature of the CT would increase its stiffness and would reduce the rate of creep sag with time in-service, explaining the trend seen in Figure 1.

Following that line of thought, a comparative stress analysis was performed for the pristine CT in F06 in PLGS and for the deformed CT at 157 kEFPH. . The pristine CT was assumed to be straight and cylindrical, as in the CT stress calculation for CDEPTH. The deformed CT was assigned local curvatures due to the creep sag and vertical and horizontal outer diameters based on the results of the inspection at 157 kEFPH, shown in Figures 5 and 6. For both cases, σ/M was calculated for sections of the CT at discrete axial positions along the length of the CT, where σ is the axial stress due to bending and M is the applied bending moment. For the pristine CT, σ/M was calculated using the flexure formula for straight beams. For the deformed CT,

σ/M was calculated using the following closed form solution for beams of constant curvature, from [7]:

$$\sigma = \frac{My}{Ae(R-y)} \tag{3}$$

Where y is the distance from the neutral axis for the given section, A is the cross-sectional area of the section of the CT, e is the eccentricity of the section (the distance between the neutral axis and the geometric centroid of the section), and R is the radius of curvature for the section. The results of the comparative stress analysis are presented in Figure 7.

In Figure 7, the ratio of the maximum **σ**/M value at a given section for the deformed CT to that for the same section in the pristine CT is plotted for various sections of the CT. In this case, the maximum **σ**/M ratio is plotted for the central 2 m length of the CT. As seen in the figure, the reduction in bending stress in the deformed CT, relative to the pristine CT, is not significant. Over the central 2 m segment of the deformed CT, the average is **σ**/M ratio is 0.984. One would expect a reduction of 1.6% in bending stress in the central segment of the deformed CT that would lead to a reduction in the CT creep sag rate, compared to that in the pristine CT.

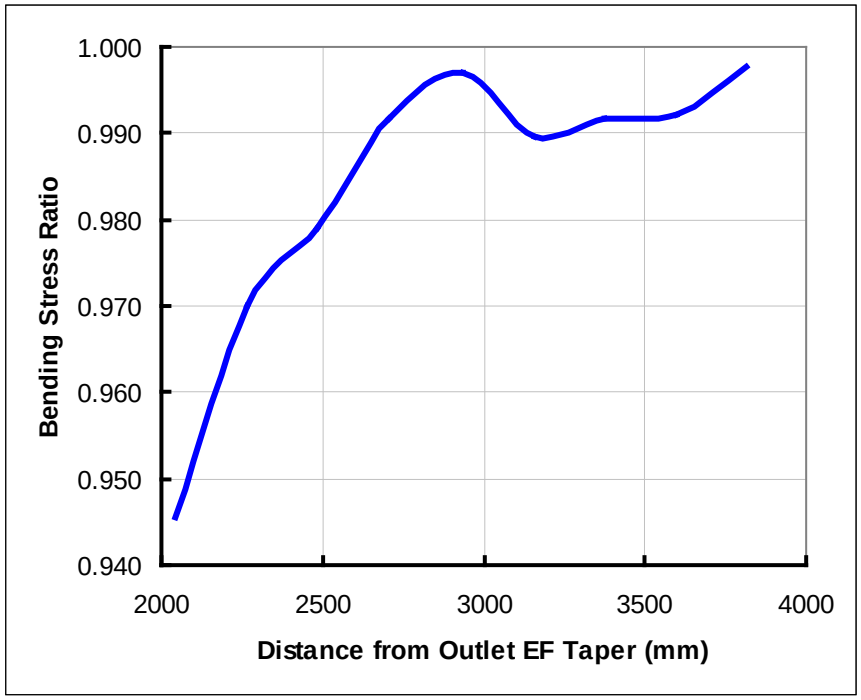

Figure 7 – Plot of Bending Stress Ratio for the Deformed and Pristine CT from F06 in PLGS versus Distance from the Outlet EF Taper

Note: EF stands for End Fitting. .

6. Discussion of Results

At this point, the results given in Sections 3 and 5 can be combined as follows:

Recalling that dy/dt = (dy/ds) (ds/dt), from Section 3, dy/ds for the PT at 157 kEFPH was found to be 44.2% of dy/ds at 27 kEFPH.

Also, from Section 5, it was predicted that the bending stress per unit bending moment in the CT would be reduced by 1.6% in the deformed PT compared to the pristine CT. Assuming no significant change in bending moments, this would result in a 1.6% reduction in ds/dt in the deformed CT at 157 kEFPH compared to that of the pristine CT. The bending stress at 157 kEFPH would then be 98.4% of that in the pristine CT. For the purposes of this paper, it is assumed that reductions in ds/dt for the CT would be similar to those for the PT.

Considering the influence of the reduction in dy/ds and in ds/dt for the PT over the interval from 27 kEFPH to 157 kEFPH, the PT creep sag rate at 157 kEFH can be expressed as a fraction of the creep sag rate at 27 kEFPH as follows:

$$dy/dt\ (157\ kEFPH) = (0.442)\ dy/ds \bullet (0.984)\ ds/dt\ (27\ kEFPH) = 0.435\ dy/dt\ (27\ kEFPH)$$

Therefore, it is predicted that the creep sag rate for the PT at 157 kEFPH would be 43.5 % of the creep sag rate at 27 kEFPH. In Section 2, the observed nominal creep sag rate for PT F06 at 157 kEFPH was determined to be 40.0% of the creep sag rate at 27 kEFPH. The predicted decrease in the rate of PT creep sag with time in service for F06, based on the geometry of PT deformation and (to as lesser degree) on the evolution of CT bending stress, matches the observed trend for PT F06.

7. Conclusions

1. PT sag measurements from the inspection of PLGS and G-2 indicate that PT and, therefore, CT creep sag are non-linear functions of time in service.
2. In the case of F06 in PLGS, the nominal PT creep sag rate at 157 kEFPH was found to be 40.0% of that at 27 kEFPH.
3. For a constant PT arc length elongation rate, PT sag profile geometry dictates that the PT sag rate will decrease with increasing sag. It was predicted that because of this geometric property, the creep sag rate for F06 at 157 kEFPH would be 44.2% of that at 27 kEFPH.
4. Based on a simple analysis of the geometry of PT deformation and CT bending stresses, it was predicted that the PT creep sag rate for F06 at 157 kEFPH would be 43.5% of that at 27 kEFPH, compared with the observed 40% value. Therefore, the non-linear trend for PT creep sag with time in service in Figures 1 and 2 can be explained on the basis of the geometry of PT deformation (with a small contribution from changes in CT bending stress).

8. Recommendations

Future predictions of FC creep sag should be conducted using non-linear models for creep sag with time in service. .

9. References

[1] S.S. Dua, W. Clendening, "Calandria Tube Sag and Contact with Mechanisms Workshop", Oakville, Ontario, Canada, February 19, 1990.

[2] A. Crandell,"Technical Basis of the Fuel Channel Ageing and Life Cycle Management Plan for Point Lepreau NGS", 87-31100-TD-004, Revision 0, June, 2005.

[3] P.J. Sedran, "Fuel Channel Ageing and Life Cycle Management Plan", Gentilly-2, 66-31100-TD-001, Revision 0. May 31, 2004.

[4] R.G. Sauve, N. Badie, G. Morandin, "Creep Response of Fuel Channels in CANDU Nuclear Reactors: Computer Code CDEPTH, Version 8.2", Kinectrics Report: 8745-001-RA-0001-R00, October, 2001.

[5] A. Lepage, T. Edwards, T. Krause, G. Longhurst, S. Donahue, D. Kalenchuk, K. Sonnenburg, T. Joulin, and A. Martin, "Fuel Channel Periodic Inspection: 2004, May – Final Report", Point Lepreau – 1, 87-31100-PIP-003, September, 2004.

[6] P.J. Sedran, B. Rankin, "The Use of OPEX (in the Form of Inspection Data) to Obtain Unanticipated Calandria Tube Ovality Measurements", 9th CNS International Conference on CANDU® Maintenance, Toronto, Ontario, Canada, December 4-6, 2011

[7] J.E.Shigley, "Mechanical Engineering Design", Third Edition, McGraw-Hill Book Company, Toronto, 1977.

10. Acknowledgements

Thanks are due to Bill Rankin, NB Power Nuclear, PLGS and to Michel Cantin, Hydro-Québec - Centrale Gentilly-2 for permission to use data from various inspections (Figure 1).

Attachment 5

A METHOD FOR PREDICTING CT-LIN CONTACT USING CANDU 6 INSPECTION RESULTS

Bill Rankin – NB Power Nuclear, Point Lepreau Generating Station
Paul J. Sedran – Canadian Power Utility Services (CPUS) Limited

ABSTRACT

In the Point Lepreau Generating Station (PLGS), the Liquid Injection Nozzle (LIN) was installed 120 mm below the Calandria Tube (CT) above it. Since the creep sag rate of the fuel channel exceeds that of the LIN, CT-LIN contact may be possible. CT-LIN contact is considered unacceptable since it will result in fretting damage to the CT.

Because of concerns about potential CT-LIN contact, various measurements of CT-LIN gap and CT and LIN elevations have been performed in different CANDU 6 reactors.

A method for predicting time-to-contact of the CT with the LIN, using inspection data, was developed by CPUS for PLGS in 2005. The method involves using updated CDEPTH fuel channel models to predict CT creep sag rates and using LIN creep sag rates derived from CT-LIN gap measurements. CT-LIN time-to-contact predictions using this method indicated no contact before 200 kEFPH, resulting in the decision to cancel further CT-LIN inspections in PLGS. The same assessment was undertaken for Gentilly-2 (G-2) but is awaiting further inspection results.

For CANDU 6 reactors without CT-LIN gap measurements, it is proposed that the LIN initial sag and sag rate deduced from measurements in Wolsong 1 and Wolsong 4 can be used to model the sag behaviour of the LIN.

CT-LIN contact predictions can then be performed for any CANDU 6 reactor using:

1. Updated CDEPTH models to predict CT sag versus time in-service
2. Sag measurements from Wolsong Units 1 and 4 to determine LIN sag versus time in-service, or if available, CT-LIN gap measurements.

The development of the above method is outlined in this paper. Examples of CT-LIN time-to-contact predictions are presented for PLGS and G-2.

Nomenclature

Elevation - vertical distance, measured as positive in the downward direction from the horizontal reference plane. Each fuel channel has its own horizontal reference plane which contains the centerline of the un-deformed Pressure Tube (PT).

Q21-L5 – the point on the bottom of the CT of Q21 that would contact the top of LIN 5
L5-Q21 – the point on the top of the LIN that would contact with Q21-L5

1. Introduction

In the Point Lepreau Generating Station (PLGS), the Liquid Injection Nozzle (LIN) was installed with a 120 mm gap relative to the Calandria Tube (CT) above it. Since the creep sag rate of the fuel channel exceeds that of the LIN, CT-LIN contact was possible.

CT-LIN contact is considered unacceptable since it would have resulted in fretting damage to the CT. Fuel channel creep sag, leading to CT-LIN contact is therefore considered to be a life-limiting factor for CANDU fuel channels. Various analyses related to CT-LIN contact for PLGS and G-2, performed in 2005 - 2007, have led to the development of a general method for predicting CT-LIN contact times, presented in this paper. The following provides a summary of the historical background for this paper.

In response to the CT-LIN contact issue for the CANDU 6, ultrasonic measurements of CT and LIN sag were performed in Wolsong Units 1 and 4 in 2000. Optical CT-LIN gap measurements were performed in G-2 in 2003 and 2006 and in 2004 in PLGS. The optical CT-LIN gap measurements were supplemented by Pressure Tube (PT) sag measurements for specific PTs. These inspections were designed to allow for the measurement of the in-service elevations at discrete points along the LIN, which were previously unknown.

In 2005, the 2004 CT-LIN gap measurement data for PLGS were used with standard CDEPTH fuel channel models to predict CT-LIN contact times. For each fuel channel, linear equations were used to represent the elevations the contact points at the bottom of the CT and at the top of the LIN versus time in-service. Contact was predicted by solving for the time at which the two elevations would be equal. It was predicted that CT-LIN contact could first occur at 188 kEFPH, which was unacceptable [1]. However, considerable conservatism was found in the standard fuel channel models.

In 2005, in response to the unacceptable time-to-contact predictions, a reassessment [2] of CT-LIN time-to-contact was performed for critical fuel channels in PLGS which involved:

1. the development and use of an updated CDEPTH fuel channel model to predict fuel channel sag
2. the use of inspection data to define an in-service elastic curve[1] for the LIN that was intended to be used to predict LIN creep sag rates.

It was predicted in References [2] and [3] that CT-LIN contact in PLGS would occur well after reactor shutdown at 185 kEFPH for refurbishment. On the basis of that assessment, no further work related to CT-LIN contact was performed for PLGS.

The same analysis was performed [4] for G-2, using data from the 2003 and 2006 inspections. Unfortunately, anomalies in the measurements prevented the use of the G-2 CT-LIN gap data in the same way that the PLGS data was used. Further inspections are planned for G-2

For the PLGS and G-2 assessments, it was expected that LIN creep sag rates would be obtained from the various inspection measurements, but this was not achieved. In the absence of empirical LIN creep sag rates for PLGS, two creep sag rate cases were used: (1) assuming no future sag of the LIN and (2) assuming a first-principles estimated sag rate, which was a less-than-satisfactory approach.

Note 1 – operating sag displacement curve from elastic sag deflections under dead weight loading plus creep sag deformation due to irradiation and thermal creep

At this point, the ultrasonic measurements of LIN sag performed by KEPRI in Wolsong Units 1 and 4 [5] proved to be invaluable. From those measurements, the initial sag and the rate of LIN creep sag were deduced. It is proposed that the initial sag and creep sag rate of the Wolsong LIN be used to predict the sag behaviour of the LIN for other CANDU 6 reactors.

In view of the PLGS and G-2 assessments and the Wolsong inspection data, the following general method is proposed for predicting CT-LIN contact for a given CANDU 6 fuel channel when no inspection results are available:

1. Use the updated fuel channel model to predict CT sag versus time in-service and set up a linear equation for the CT contact point elevation versus time in-service
2. Use the Wolsong LIN initial elastic curve and creep sag rates and set up an equation for the LIN contact point elevation versus time in-service.
3. Solve the system of equations to predict the time-to-contact

When reliable CT-LIN gap measurements are available, a reactor-specific equation for LIN elevation can be derived using the CT-LIN gap measurements.

Examples of CT-LIN time-to-contact predictions using this method are presented in this paper for PLGS and G-2.

To validate the proposed CT creep sag prediction method, CT creep sag rates were predicted for the Row Q CTs in G-2 using an alternative method and were compared with those of the proposed method.

In the CANDU 6 reactor CT-LIN contact will first occur between the Row Q channels and LIN #5. Analysis results are presented only for the Row Q fuel channels in this paper.

2.0 Input Data Used in the Assessment

This section provides an outline of the input data that was used to develop the proposed method.

2.1 PT Sag Measurements

PT sag measurements in PLGS, presented in Figure 1, were performed during fuel channel inspections in 1986, 1988, 1991, 1998, 1999, and 2004.

The sag measurements were used in the development of updated CDEPTH fuel channel models.

2.2 PT In-Service Dimensions

An example of diametral expansion and wall thinning with time in-service for the PLGS PTs is presented in Figure 2 for F06, which was inspected at 157 kEFPH.

In the standard CDEPTH fuel channel model, uniform design-basis PT dimensions are assumed. For F06, an incremental increase in PT stiffness would result from the observed deformation of the PT. These dimensional changes suggested that PT dimensions should be investigated as possible parameters to be updated in the CDEPTH fuel channel models

2.3 CT In-Service Dimensions

In the course of this work it was found that the stiffness of F06 at 157 kEFPH is significantly higher than that predicted with the standard CDEPTH model, which led to the hypothesis that CT ovalisation at the spacers might have stiffened the CT of F06.

For F06, CT inner diameter values at 72 angular locations were obtained along the length of the CT using data from the 2004 inspection of PLGS. Figure 3 presents a plot of CT maximum inner radius versus axial position for F06.

Figure 1 – Measured PT Sag versus EFPH for the PLGS PTs

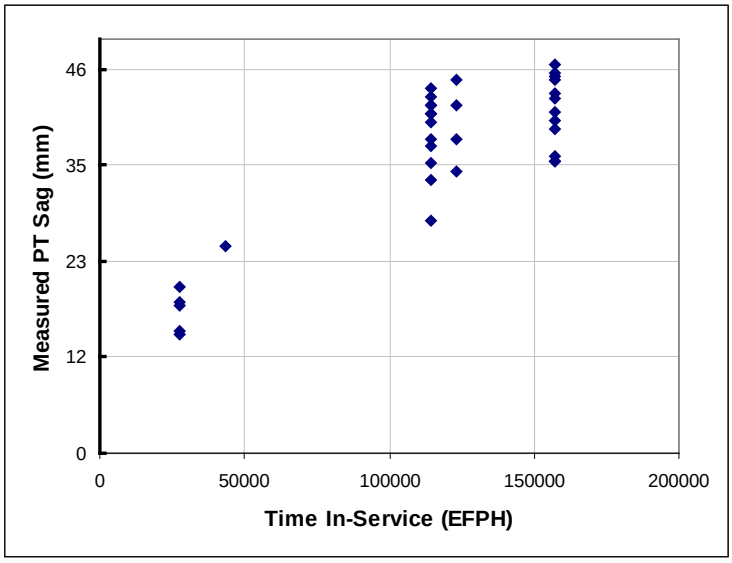

Although the CT-PT gap data used in Figure 3 appears reasonable, the inspection teams could not verify the accuracy of the data. The work proceeded keeping in mind that the CT-PT gaps required verification.

Figure 2 – In-Service PT Dimensions for F06 in PLGS

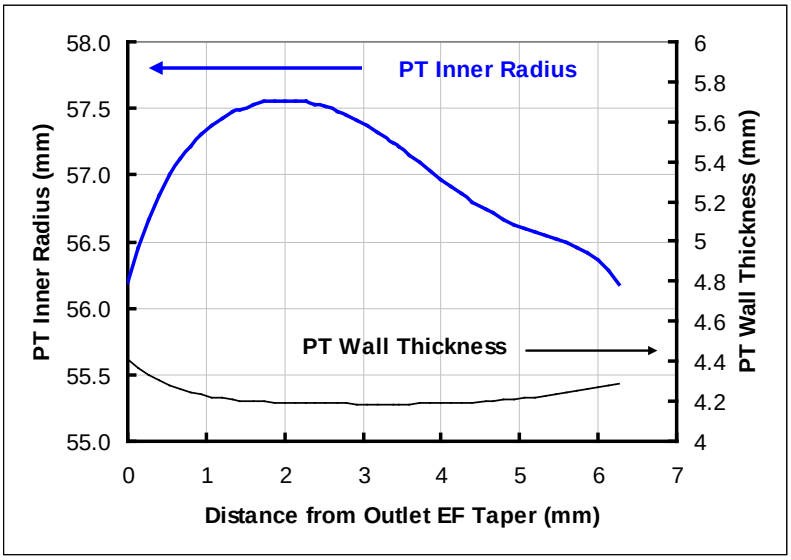

2.4 PT- CT Gap Measurements at 157,000 EFPH

PT-CT gap measurements from the 2004 fuel channel inspection were provided in Reference [6]. As an example, Figure 4 presents the gap data for F06 at 157 kEFPH. The data for specific channels was used to find the PT-CT gaps at L5-Q07 and L5-Q08.

Figure 3 – CT Maximum Inner Radius vs Axial Position for F06 Based on Preliminary CT- PT Gap Measurements

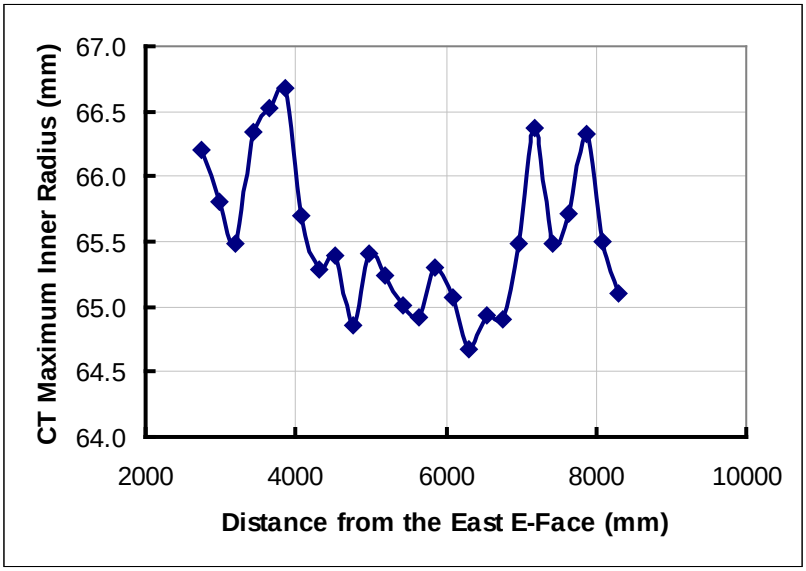

CT inner diameter at each axial position was measured as varying with angular position. The figure presents the maximum inner radius measured at each axial location.

Figure 4 – CT-PT Gap Measurements for F06 at 157 kEFPH

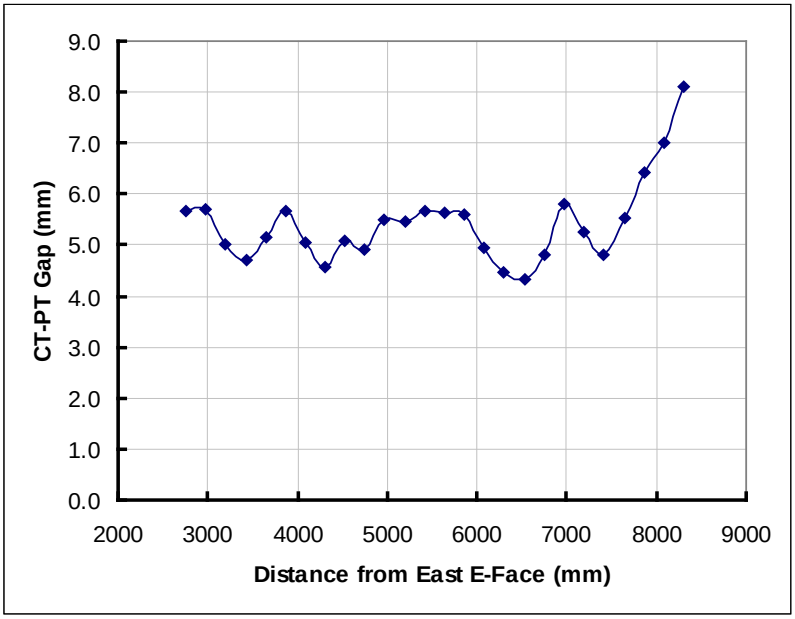

2.5 CT-LIN Optical Gap Measurements

Table 1 presents the 2004 optical gap measurement data [7] for the Row Q channels in PLGS. Note that the channels were fuelled during the gap measurements.

Table 1 – Optical Measurements of CT- LIN Gaps For Row Q in the 2004 Inspection

Fuel Channel	LIN	CT-LIN Gap (mm)
Q06	#5	10.1
Q07	#5	13.8
Q08	#5	14.2
Q09	#5	15.0

2.6 CT Spring-Back Measurements

During the 2004 inspection of the PLGS fuel channels, the following measurements were taken:

- with the channel fuelled (all 12 fuel bundles installed) the CT-LIN gap at F06-L2 was measured to be 16.2 mm
- with the channel defuelled the CT-LIN gap at F06-L2 was measured to be 20.7 mm

Therefore, the nominal elastic spring back deflection of the CT at F06-L2 was 4.5 mm.

2.7 LIN In-Service Sag Measurements from Wolsong 1 and 4

Reference 5 gives the ultrasonic inspections that were performed in Wolsong Units 1 and 4. The measurements in Table 2 proved to be very useful for determining the initial elastic curve and in-service elastic curve for the LIN.

Table 2 – Wolsong LIN Sag Measurements

Reactor	Inspection EFPH	LIN Sag (mm)
Wolsong 1	4512	4.9
Wolsong 4	126744	8.3

The LIN sag was measured with an ultrasonic probe in View Port #2. It was assumed that the probe was centred in the view port, 1.243 m from the pinned end of the LIN.

2.8 LIN Installation Data

LIN installation measurements and fuel channel dimensions were used to calculate the elevation of the support points of the LIN, presented in Table 3, which are required for the LIN elastic curve. Note that elevations for all points on the LIN are always relative to the horizontal datum through the centreline of the fuel channel.

Table 3 – Elevation of the PLGS LIN Support Points

LIN	Elevation (mm)
#5	120.24

2.9 Reactor Operating History

Until 1997, PLGS operated with a daily average power rating close to 100% (not including zero-power days). Starting at about 100 kEFPH, the reactor underwent gradual power derating. Figure 5 is a plot of lifetime daily averaged reactor power at various times in the operating history of PLGS. The specific EFPH values at which the daily lifetime averaged reactor power levels were calculated are listed on the figure.

The power derating of PLGS, seen in Figure 5, moderated PT flux and temperature conditions compared to design-basis PT operating conditions.

In the standard CDEPTH fuel channel models for PLGS, PT fast neutron flux values were assumed to be constant with time and were based on data compiled in 1993 when the average lifetime power for PLGS was 98.3 % Reactor Power. From Figure 5, a lifetime average daily power of 98.3 % would be applicable to PLGS up to 100 kEFPH but not later. Therefore, the fast neutron flux profiles in the standard CDEPTH models overestimate the actual fluxes experienced by the PLGS fuel channels after 100 kEFPH of operation.

Figure 5 – Lifetime Averaged Reactor Powers Computed at EFPH Values for the Various Inspections of PLGS

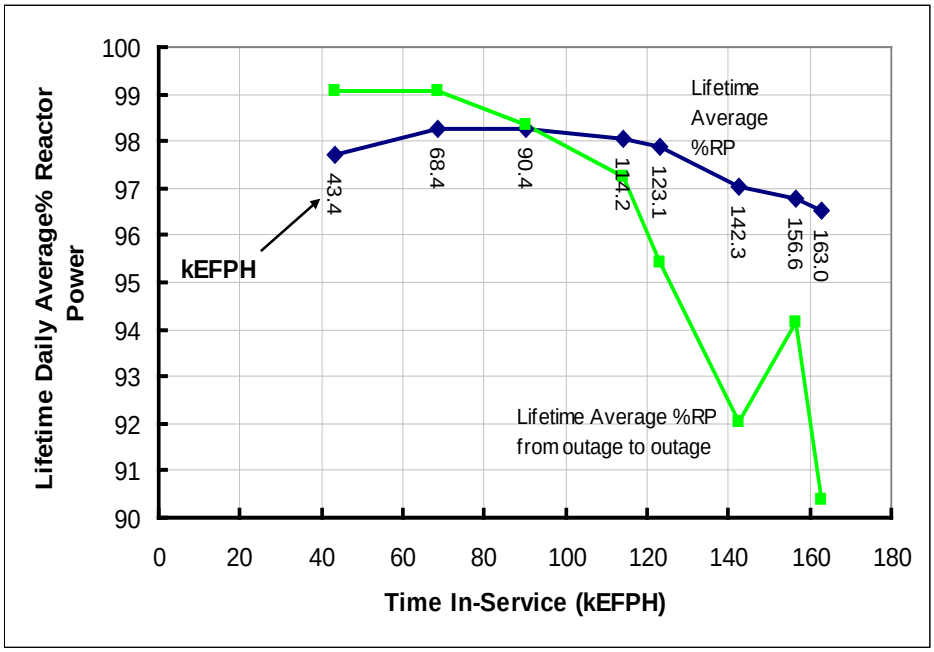

Each of the kEFPH values given represent times at which the reactor was shut down for inspections or SLAR outages.

3.0 Analytical Methods

3.1 CDEPTH 8.2

CDEPTH 8.2 is the code that was used to predict fuel channel sag deformation with time in-service for this paper. The equivalence of CDEPTH 8.2 and CDEPTH 9.0 for fuel channel sag predictions was documented in Reference [1].

3.2 ANSYS 9.0

ANSYS 9.0 was used to predict the initial elastic curve of the LIN.

3.3 Time-to-Contact Predictions

Time-to-contact predictions were generated for each potential contact point on LIN #2 and LIN #5 with the CTs in Row F and Q, respectively. The time-to-contact for each potential contact point was calculated by solving two linear equations for elevation versus time in-service. The first equation is for the contact point at the bottom of the CT and the second is contact point at the top of the LIN.

Figure 6 illustrates the process of calculating the CT-LIN time-to-contact, determined by the point of intersection of the CT and LIN elevations. In the figure, the elevation of the contact points on the CT and the LIN are plotted versus time in-service. The figure includes representations of the PLGS and Wolsong LIN elevation measurements and linear equations for the elevation of the contact points on the CT and the LIN.

Figure 6 – Illustration of the Process of Calculating CT-LIN Time-to-Contact

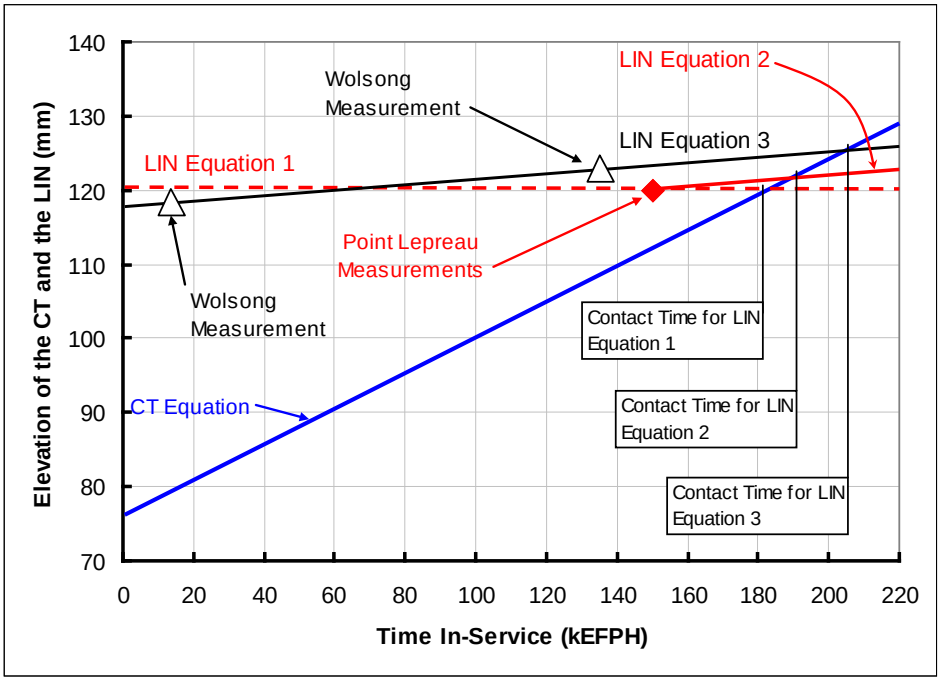

The elevation equation for the CT contact points was derived from CDEPTH 8.2 results with the updated model, described in Section 4.0.

As indicated in the figure, three different LIN elevation equations were derived. Equation 1 is based on LIN elevation measurements from PLGS, not crediting future sag of the LIN. Equation 2 is based on the same measurements but credits future creep sag of the LIN at an estimated rate. Equation 3 is based on Wolsong LIN elevation measurements that provided a linear equation for LIN elevation.

4.0 Updating of the CDEPTH fuel channel Models

In this paper the term, “updating” means the modification of input parameters in the standard CDEPTH fuel channel models to bring them up-to-date with recent developments, including calibration to measurements.

The standard CDEPTH fuel channel models were developed in the 1980s to predict the onset and spreading of CT-PT contact due to spacer movement. By necessity, high levels of conservatism were implemented in the standard models, as discussed in Sections 4.1 and 4.2.

4.1 Comparison of PT Sag Measurements and Predictions Using Standard CDEPTH Fuel Channel Models

For PLGS and Gentilly-2, it was found that predictions of PT sag using standard CDEPTH models overestimated recent in-service PT sag measurements. For example, Figure 7 shows the relationship between predicted PT sag and measured PT sag for PLGS. In the figure, M/P ratio (the ratio of Measured to Predicted sag) is plotted versus time in-service. A trend of decreasing M/P ratio with time in-service is indicated in Figure 7. For the 2004 inspection data, M/P ratio was found to range from 0.98 to 0.78.

Figure 7 – M/P Ratio for PT Sag Versus EFPH for the PLGS Pressure Tubes

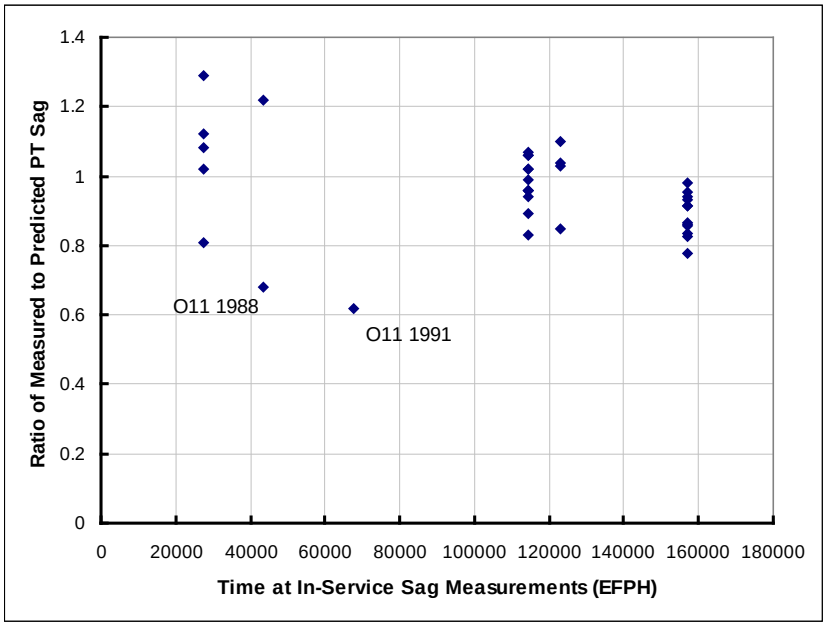

Note that the O11 measurements in 1988 and 1991 were investigated and discarded.

4.2 Measured Fuel Channel Spring-Back versus Spring Back Predicted with the Standard CDEPTH Model for F06

It was predicted, using the standard CDEPTH model for F06 that F06-L2 would spring back by 8.3 mm as a result of defuelling. The measured spring back at F06-L2 during the 2004 inspection was 4.5 mm.

4.3 Updates to the Standard CDEPTH Fuel Channel Model

The results presented in Sections 4.1 and 4.2 justified the modification of the standard CDEPTH fuel channel model for use in fuel channel sag predictions, in order to reduce the level of conservatism in the predictions of the model.

The following parameters in the model were investigated for potential modification:

1. PT In-Service Dimensions and CT End Bell Modelling
2. PT End Support Conditions
3. CT Ovality at Spacer Locations
4. The CT East End Support Condition

For Item 1, the PT in-service dimensions shown in Figure 2 were implemented in the CDEPTH model of the PT and the shape of the end bell was incorporated into the model of the CT for F06. For Item 2, the PT end point rotational degree of freedom was changed from free to fixed at both ends of the PT. For Item 3, the CT inner diameter profile of Figure 3 was incorporated into the CDEPTH model of the CT. For Item 4 the axial degree of freedom on the East end of the CT was changed from free to fixed.

The investigation of the CDEPTH modelling was carried out by successively introducing the above modifications to the standard CDEPTH model for F06 and executing four different models in CDEPTH to simulate the fuel channel spring back process for F06.

The models consisted of:

1. The standard model for F06
2. Modification 2 for F06 – Items 1 and 2, above
3. Modification 3 for F06 – Items 1, 2, and 3, above
4. Modification 4 for F06 – Items 1, 2, 3, and 4, above

The results of the spring back study are presented in Figure 8, in which spring back predictions for F06 are compared with the nominal measured spring back value. As shown, the standard model significantly over predicts the measured spring back value, indicating that the standard CDEPTH model for F06 is too flexible. With successive modifications to the model, increases in stiffness were realised but the measured spring back value was still over predicted using the Modification 4 model for F06.

Next, the effects of CT elastic modulus were studied. The study was conducted by executing the Modification 4 model for F06 in CDEPTH to predict spring back for various values of elastic modulus. A summary of the study is presented in Figure 9. The figure indicates that a doubling of the standard CT elastic modulus value would be required for the spring back prediction of the Modification 4 model to match the measured spring back value. At this point it is not known whether the actual elastic modulus of the CT in F06 could possibly be twice the standard value. Some associated information is provided in Section 5.0

As outlined in Section 2.9, the fuel channel fast neutron flux profiles in the standard CDEPTH models overestimate the actual flux to which the fuel channels were exposed. This suggested fast neutron flux as a parameter to be modified in updating the CDEPTH fuel channel models for PLGS.

Consequently, flux profiles for reduced power levels were generated for F06 and were incorporated into the updated CDEPTH model for F06 to simulate the derating of the reactor with time in-service. The updated model for F06, including the reduced flux profiles, was executed in CDEPTH 8.2 along with the standard model for F06. The results of the CDEPTH analyses for F06 are presented in Figure 10.

Two differences in the standard and updated models are apparent in Figure 10. First, the initial straight part of the sag deflection curve is lower for the updated model since its modifications provide a greater stiffness than the standard model. Second, starting at about 120 kEFPH, the reduced flux profiles in the updated model are manifested as a slight reduction in the slope of the CT sag curve for the updated fuel channel model.

Figure 8 – Predicted F06-L2 Spring Back Deflections from CDEPTH 8.2 Compared with Measurements

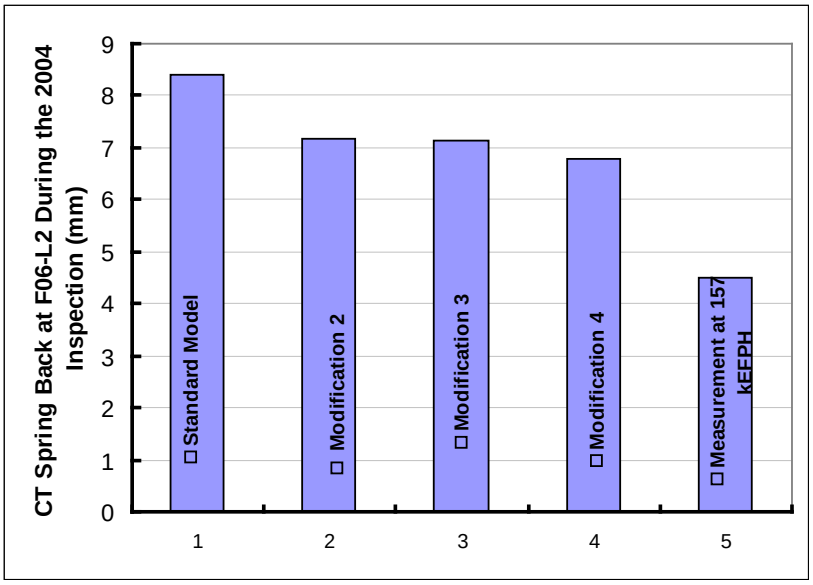

Figure 9 – F06 Spring Back Predictions with Modification 4 for Various Values of CT Elastic Modulus

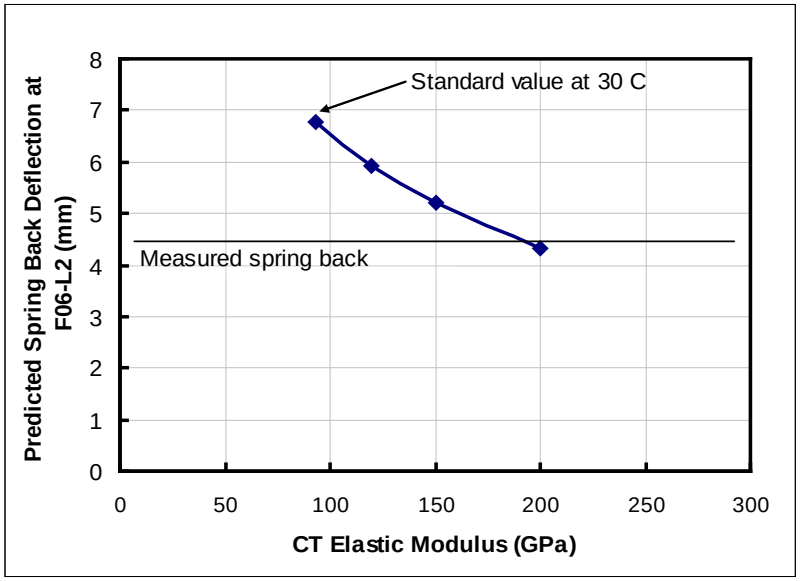

Figure 10 – Predicted CT Deflections for PLGS F06 Using Standard and Updated CDEPTH 8.2 Models

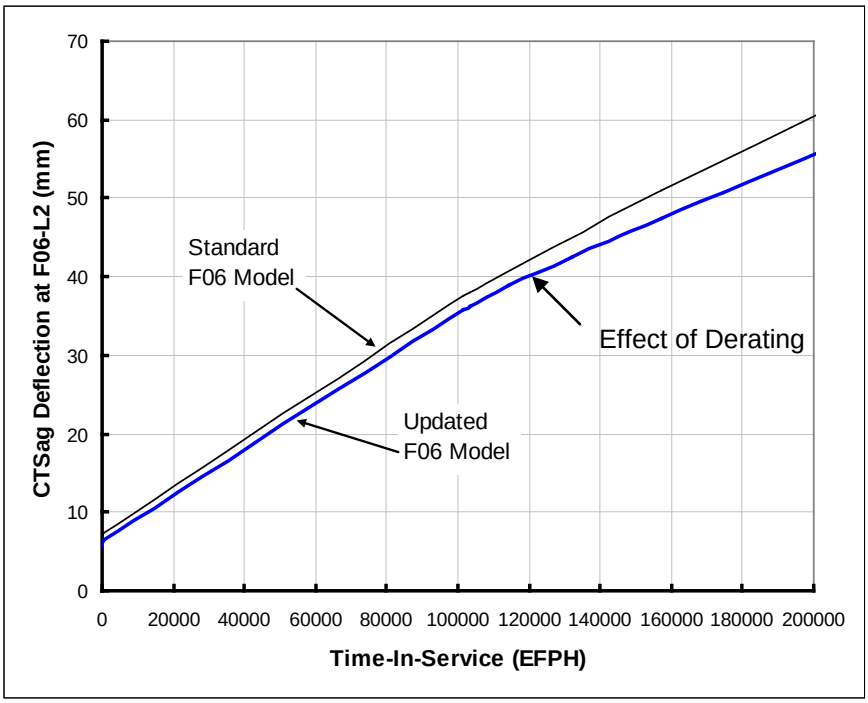

4.0 Predictions of CT Sag Using the Updated Fuel Channel Models

CT sag versus time in-service was predicted for the Row F and Row Q fuel channels in PLGS using the updated fuel channel models (Modification 4) with CDEPTH 8.2, including reduced flux profiles. Elevation versus time in-service values for the contact points on the CTs were extracted from the CDEPTH 8.2 outputs.

From CT elevation versus time in-service, linear equations for the elevations of the contact points on the CTs were derived. Table 4 presents a summary of the linear equations for the contact points on the CTs in Row Q.

Figure 11 provides a comparison of the CT creep sag rates for the standard and the updated CDEPTH models.

Table 4 - Parameter Values for the PLGS Row Q CT Elevation Equations

Contact Point	X_{CT} (m)	CT Sag Rate (mm/7k EFPH)	Intercept (mm)
Q02-L5	3.332	0.89	80.53
Q03-L5	2.903	1.26	82.52
Q04-L5	3.340	1.29	82.60
Q05-L5	2.898	1.42	82.27
Q06-L5	3.355	1.46	84.61
Q07-L5	2.899	1.67	82.11
Q08-L5	3.362	1.69	81.84
Q09-L5	2.903	1.62	82.41
Q10-L5	3.351	1.71	81.93
Q11-L5	2.902	1.75	79.91
Q12-L5	3.359	1.72	81.68
Q13-L5	2.899	1.71	81.15
Q14-L5	3.357	1.66	82.63
Q15-L5	2.903	1.71	81.21
Q16-L5	3.344	1.68	80.76
Q17-L5	2.901	1.60	83.38
Q18-L5	3.342	1.79	78.25
Q19-L5	2.899	1.33	83.75
Q20-L5	3.339	1.10	79.23
Q21-L5	2.905	1.09	77.65

X_{CT} is the distance from the outlet end fitting taper

Figure 11 – Comparison of Predicted Row Q CT Creep Sag Rates from Standard and Updated CDEPTH Fuel Channel Models for PLGS

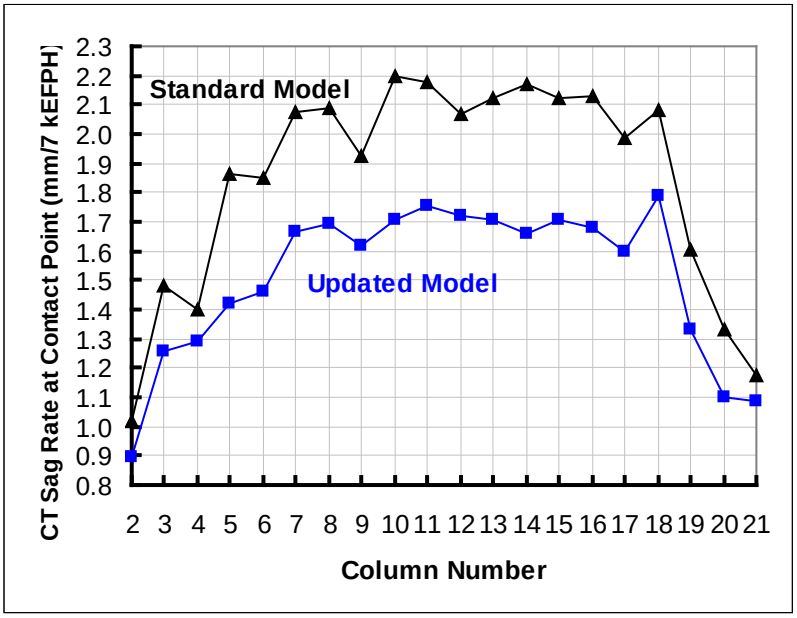

5.0 Use of In-Service PT Sag and CT-LIN Gap Measurements to Define the In-Service Elastic Curve of the LIN in PLGS

The in-service elastic curve of the LIN was determined in a three-step procedure:

1. The as-installed elevations of the support points of the LIN were found
2. The in-service elevations of the LIN were found at two axial locations where CT-LIN gaps were measured
3. Elastic curves were fitted through the support points and the two points with known elevations on the LIN for different end conditions at the pinned end of the LIN.

Although the LIN is pinned at the South end of the reactor, the actual support condition at that end is uncertain. Therefore, both fixed and pinned conditions were considered.

Accounting for as installed distances from the CT to the LIN, as-installed bow of the CTs, and as-installed sag of the CTs, the elevation of the LIN end points was determined to be 120.2 mm.

The in-service elevations of L5-Q07 and L5-Q08, were obtained as the sum of:

1. the measured sag of the PT (plus an adjustment for fuel weight effects)
2. the PT outer radius
3. the measured PT-CT gap
4. the CT wall thickness
5. the measured CT-LIN gap.

Table 5 provides the data used to calculate the elevations of LIN #5 and the results of the calculations

Table 5 – Measurements for Finding the Elevations of L5-Q07 and L5-Q08

Contact Point	PT Sag (mm) [1]	PT Outer Radius (mm)	PT-CT Gap (mm)[2]	CT-LIN Gap (mm)	CT Wall Thickness (mm)	LIN Elevation (mm)
L5-Q07	45.8	57.907	5.7	13.8	1.37	124.6
L5-Q08	46.6	57.168	5.3	14.2	1.37	124.9

Note 1: sag was measured with no fuel in the channel and was adjusted to account for the weight of the fuel and coolant under in-service conditions

Note 2: measured with no fuel in the pressure tube but with coolant and the inspection tool

Figure 12 illustrates the determination of the in-service elastic curves for LIN #5 from the support point elevations and the measurements at L5-Q07 and L5-Q08 for the two different end conditions at the pinned end of the LIN.

The elastic curve of the LIN from about 4500 mm to 7200 mm is practically independent of the South end support condition. For the rest of the LIN, the South end support condition has a small effect on the elastic curve.

For the PLGS assessment, it was not clear which LIN South end support condition should be used. It was subsequently decided that for the PLGS-specific assessment, a fixed support condition for the South end of the LIN would be assumed.

Figure 12 – Determination of the In-Service Elastic Curve for Lin #5 in PLGS at 157 kEFPH

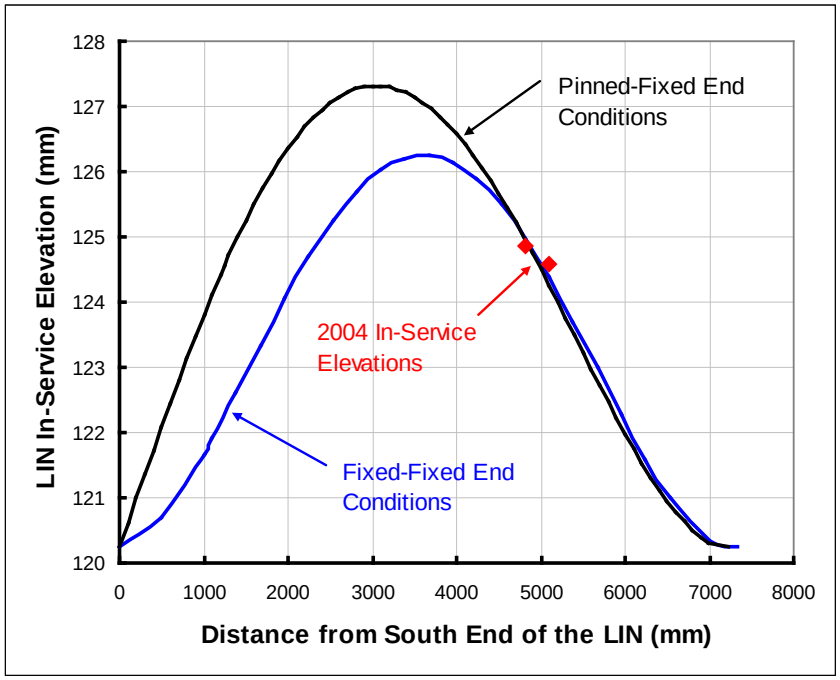

5.1 Evaluation of the In-Service Elastic Curve for LIN #5

From Figure 12, the maximum in-service sag of LIN #5 was determined to be 6 mm, whereas the initial sag of the LIN was predicted to be 14 mm [1]. A similar difficulty occurred in using the CDEPTH fuel channel model to predict spring back deflection, which will be discussed later. This inconsistency meant that the in-service measurements could not be combined with the predicted initial elastic curve to determine the rate of LIN creep sag, as planned for Reference [1].

Because of some discrepancies in the 2003 CT-LIN gap measurements for G-2, it was tentatively concluded that the method outlined in Section 5.0 tended to underestimate the elevation of the LIN in G-2, and by extension, in PLGS.

However, in the 2006 inspection of G-2, direct LIN sag measurements were obtained [8], from which an in-service elastic curve for LIN #5 in G-2 was produced. Figure 13 presents the in-service elastic curve and the four elevation measurements used to derive it.

Figure 13 – LIN #5 Elevation Measurements and Derived Elastic Curve for G-2 at 141.6 kEFPH

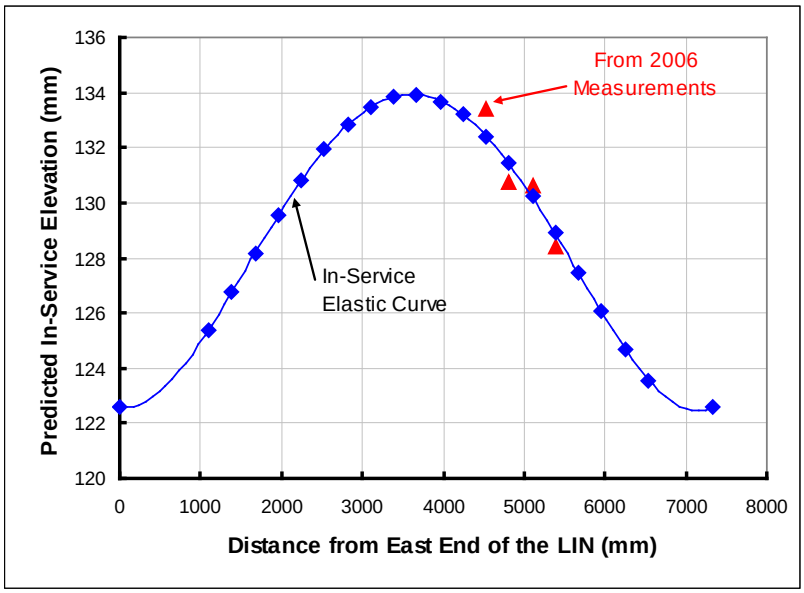

Comparing Figures 12 and 13, and in consideration of the Wolsong data presented in Section 7, the elevation of LIN #5 in Figure 12 is probably underestimated, which will lead to underestimations of the time-to-contact for PLGS.

Despite underestimating the actual sag of the LIN, the in-service LIN elevation of Figure 12 was used in the CT-LIN time-to-contact assessment for PLGS. The LIN elevation of Figure 12 was employed with the following assumptions: (1) that the LIN will not sag in the future, which is conservative, (2) that the LIN will sag at an estimated rate, derived in Section 6.

6.0 Estimation of the Creep Sag Rate for LIN #5

After the failure to deduce LIN creep sag rates from the inspection measurements, an estimated LIN creep sag rate was derived based on CRNL 4001, as follows.

Based on the ratio of bending stress and fast neutron flux for the LIN relative to Q12, the expected ratio of LIN/CT creep sag was calculated to be 0.20, assuming identical material properties. With a predicted creep sag rate of 1.51 mm/7 kEFPH for Q12, the creep sag rate of LIN #5 would be 0.303 mm/7kEFPH at the centre of the LIN.

7.0 Prediction of the Initial and In-Service Elastic Curves and LIN Creep Sag Rates from Inspections in Wolsong Units 1 and 4

Elastic curves for LIN #5 in Wolsong Unit 1 for fixed-fixed and pinned-fixed end conditions at 124.7 kEFPH were generated from the data in Table 2 of Section 2.7 and are plotted in Figure 14. Figure 14 shows that the end condition at the start of the LIN has a significant effect on the in-service elastic curve of the LIN. For time-to-contact to be conservatively under predicted, the magnitude of LIN in-service sag should be underestimated. Therefore, for the prediction of the in-service elastic curve, a pinned support condition was selected for the pinned end of the LIN.

Figure 14 – Determination of the In-Service Elastic Curve for LIN #5 In Wolsong Unit 1 at 126.7 kEFPH

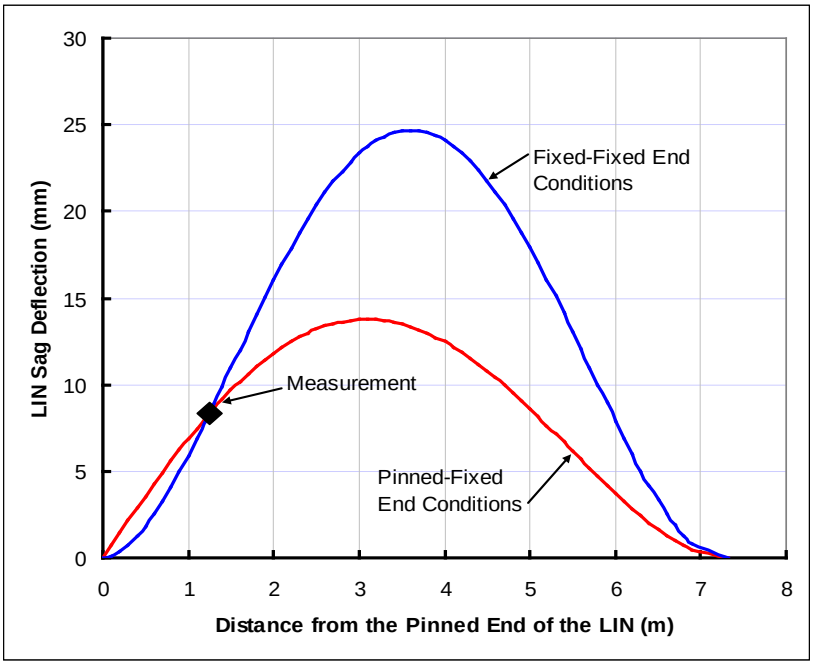

Next, the initial elastic curve of the LIN for Wolsong was determined from the LIN sag measurements, as illustrated in Figure 15.

Using the initial and in-service elastic curves in Figure 15, LIN creep sag rates were calculated and are presented in Figure 16. Figure 16 also includes a plot of the estimated LIN creep sag rates for PLGS from Section 6.0, for comparison.

Figure 15 – In-Service and Derived Initial Elastic Curve for LIN #5 in Wolsong

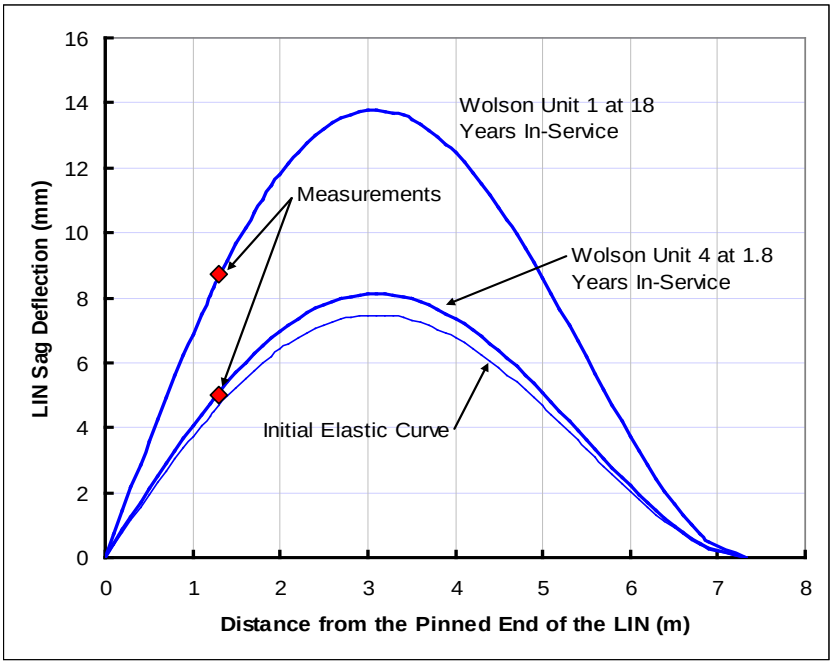

Figure 16- Creep Sag Rates for Wolsong LIN #5 and Estimated Creep Sag Rate for PLGS LIN #5

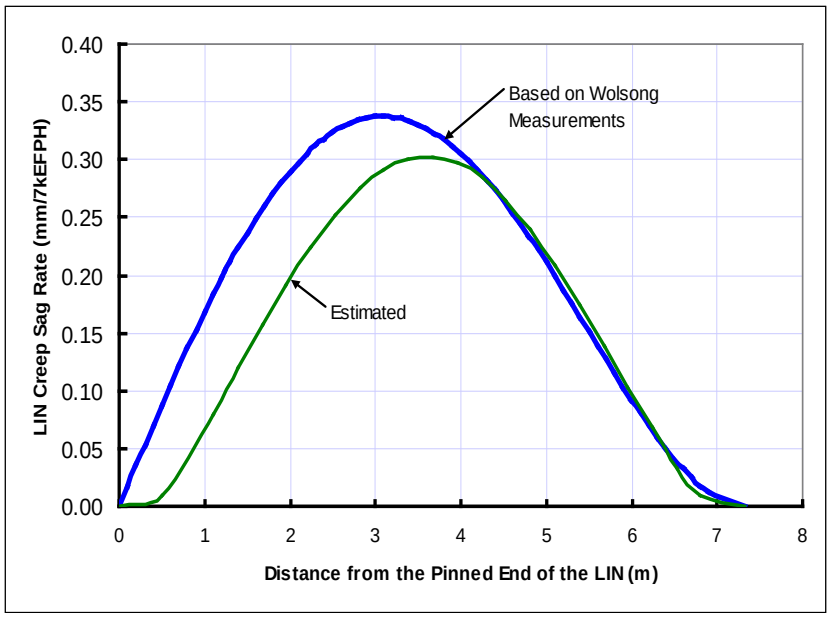

7.1 Comparson of LIN Elastic Curves Based on Wolsong Measurements and the 2006 LIN Sag Measurements for G-2

Figure 17 presents the predicted in-service sag at 141 kEFPH for LIN #5 from the Wolsong measurements for comparison with the 2006 LIN sag measurements at G-2. The sag profile for two different end support conditions are shown for the G-2 LIN. Figure 17 shows that the Wolsong and the 2006 G-2 LIN sag measurements produce similar LIN sag profiles provided that pinned-fixed end conditions are assumed for the LIN.

Figure 17 - Predicted Elastic Curves at 141.5 kEFPH For LIN #5 in Wolsong and G-2

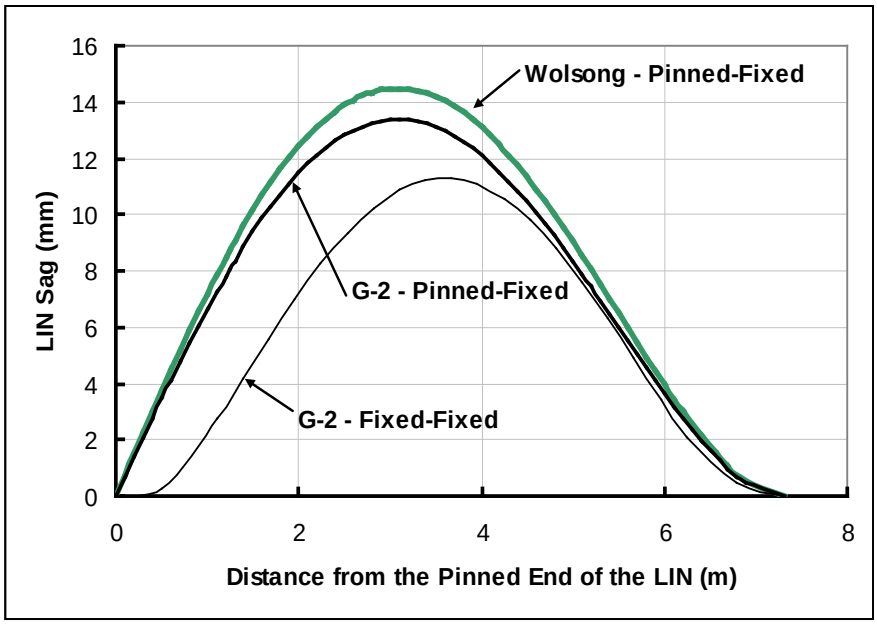

8.0 Predictions of CT-LIN Time-to-Contact for PLGS and Gentilly-2

Time-to-contact predictions for PLGS and G-2, using reactor-specific LIN elevation measurements are presented in Sections 8.1 and 8.2. Section 8.3 provides predictions for G-2 based on the use of Wolsong LIN creep sag properties. Section 8.4 presents an alternative treatment for predicting CT creep sag rates to validate the updated fuel channel models.

8.1 Predictions for PLGS Using Reactor-Specific LIN Elevation Measurements

Time-to-contact predictions for PLGS were performed using the CT elevation equations of Table 4 and the LIN elevations of Figure 12, assuming two different LIN sag rates: (1) zero creep sag beyond that at the 2004 inspection, and (2) creep sag at the estimated rate from Section 6.0. Figure 18 presents a summary of the time-to-contact analysis.

As shown in Figure 18, it was predicted that none of the channels in Row Q would be subject to CT-LIN contact by 185 kEFPH. For no future creep sag of the LIN, it is predicted that CT-LIN contact would first occur in Q06 at 206 kEFPH.

Figure 18 – Time-to-Contact Predictions for the PLGS Row Q Fuel Channels Using Updated Fuel Channel Models With Different LIN Creep Sag Rates

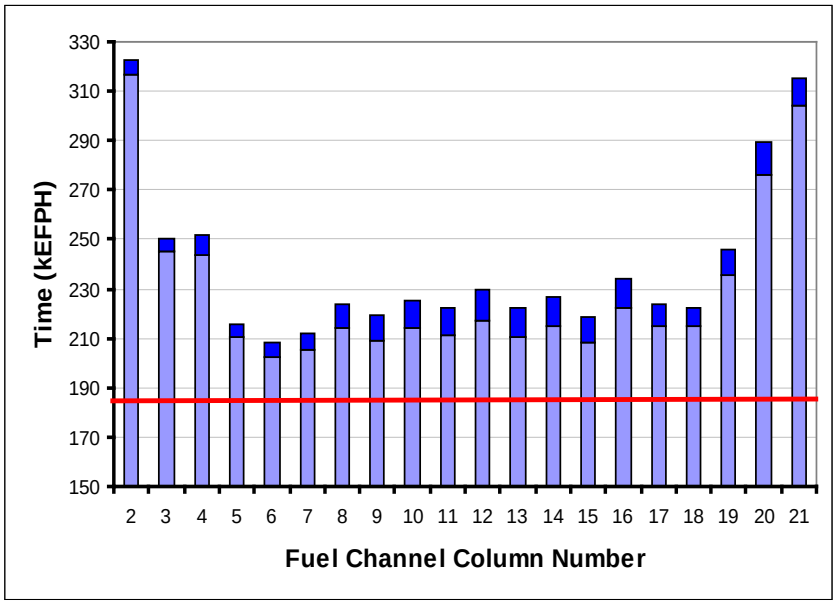

Note: the light bars represent time-to-contact for zero creep sag of the LIN beyond 157 kEFPH. The dark bars represent the increase in time-to-contact for creep sag of the LIN at the estimated rate. The total height of the light and dark bars represents the time-to-contact for creep sag of the LIN at the estimated rate. The horizontal line represents the planned time in-service for plant shutdown for retubing.

8.2 Predictions for Gentilly-2 Using Reactor-Specific LIN Elevation Measurements

The analysis of Section 8.1 was repeated for G-2 using reactor-specific CT and LIN elevation equations described in Sections 8.2.1 and 8.2.2. For this assessment it was assumed that G-2 will by shut down for retube at 196 kEFPH.

8.2.1 CT Elevation Equations for G-2

Table 6 [4] provides elevation equations for the contact points on the Row Q CTs in G-2, obtained from the predictions of the updated G-2 fuel channel models.

Table 6 - Parameter Values for the G-2 Row Q CT Elevation Equations

Contact Point	X_{CT} (m)	CT Sag Rate (mm/7 kEFPH)	Intercept (mm)
Q02-L5	3.319	0.77	123.52
Q03-L5	2.898	0.98	124.70
Q04-L5	3.330	1.50	126.05
Q05-L5	2.895	1.39	127.48
Q06-L5	3.330	1.44	128.89
Q07-L5	2.898	1.50	130.23
Q08-L5	3.337	1.36	131.42
Q09-L5	2.900	1.51	132.42
Q10-L5	3.338	1.57	133.19
Q11-L5	2.902	1.51	133.69
Q12-L5	3.340	1.51	133.91
Q13-L5	2.900	1.53	133.83
Q14-L5	3.345	1.51	133.47
Q15-L5	2.900	1.55	132.83
Q16-L5	3.343	1.46	131.95
Q17-L5	2.900	1.47	130.84
Q18-L5	3.334	1.48	129.57
Q19-L5	2.892	1.22	128.18
Q20-L5	3.324	0.98	126.75
Q21-L5	2.900	0.79	125.35

X_{CT} is the distance from the outlet end fitting taper

8.2.2 LIN #5 Elevation Equations

CT elevation equations for LIN #5 were derived based on Figure 13, assuming two different LIN sag rates: (1) zero future creep sag of the LIN (beyond that at the time of the 2006 inspection) and (2) creep sag of the LIN at the estimated rate from Section 6.0.
.

8.2.3 CT-LIN Time-to-Contact Predictions

The results of the CT-LIN time-to-contact analysis for G-2 are presented in Figure 19. As indicated in Figure 19, it was predicted that none of the Row Q CTs in G-2 will contact LIN #5 at 196 kEFPH. It was predicted that the earliest contact would occur in Q04 at 235 kEFPH, conservatively assuming no further creep sag of the LIN beyond 141.6 kEFPH.

Figure 19 - Time-to-Contact Predictions for the G-2 Row Q Fuel Channels Using Updated Fuel Channel Models With Different LIN Creep Sag Rates

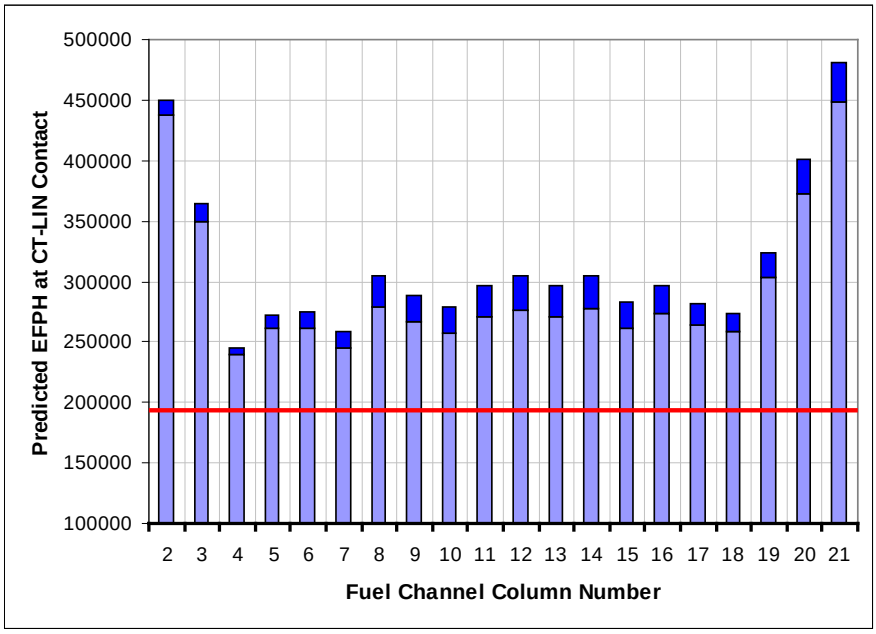

The notes to Figure 18 apply here,

8.3 Assessment for Gentilly-2 Using Wolsong LIN Elevation Data

The purpose of this analysis is to investigate the use of the Wolsong LIN elevation equations to predict CT-LIN contact in G-2. The CT elevation equations used in this analysis are the same as those given in Section 8.2.1.

8.3.1 LIN #5 Elevation Equations

For this analysis the intercepts for the LIN elevation equations were obtained from the initial elastic curve of Figure 15. The LIN creep sag rates given in Figure 16 were used to determine the slopes for the LIN elevation equations.

8.3.2 CT-LIN Time-to-Contact Predictions

Time-to-contact predictions for the Row Q fuel channels in G-2, using the creep sag properties of LIN #5 in Wolsong, are presented in Figure 20. Comparing Figures 19 and 20, there is a general improvement in the time-to-contact with the use of Wolsong LIN elevation measurements instead of the G-2 LIN elevation measurements. With the Wolsong LIN creep sag properties, Q04 is still the critical channel with contact predicted at 250 kEFPH, rather than at 235 kEFPH, with G-2-specific LIN elevation measurements.

Figure 20 – Time-to-Contact Predictions for the G-2 Row Q Fuel Channels Using Updated Fuel Channel Models With Wolsong LIN Creep Sag Rates

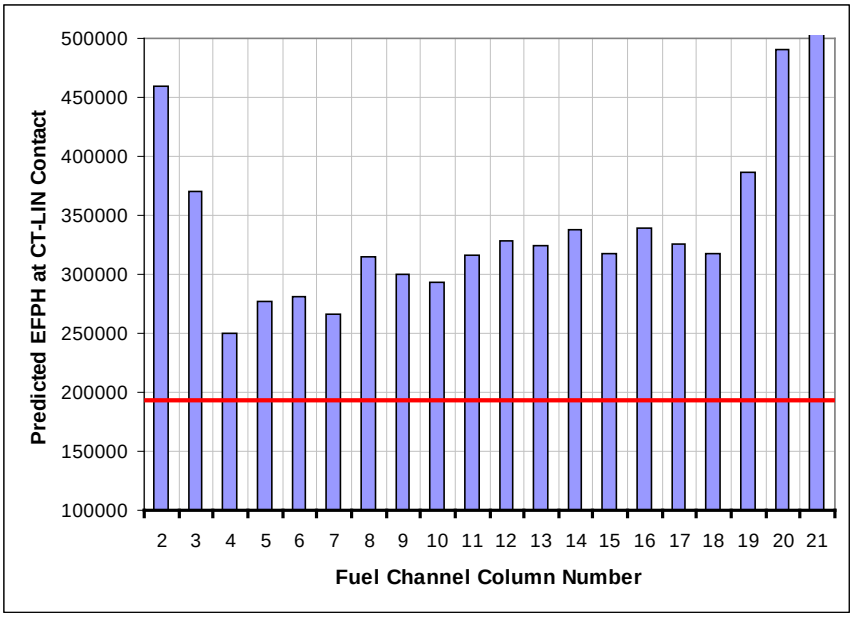

The notes to Figure 18 apply here,

9.0 Discussion of Results

9.1 LIN Creep Sag Behaviour

Under predictions of LIN elevation from the G-2 CT-LIN gap measurements and indications from Figure 12 for PLGS show that the method of combining PT sag measurements with CT-LIN gaps underestimates the sag of the LIN.

However, direct measurements of LIN sag, performed in G-2 and in Wolsong Units 1 and 4 have produced reasonable in-service elastic curves and creep sag rates for LIN #5. It is important to note that the LIN #5 sag rate from the Wolsong measurements matches the estimated LIN sag rate for G-2 and that the in-service elastic curve at 141.6 kEFPH for G-2 agrees well with that for Wolsong. The creep sag behaviour of the Wolsong LIN has therefore been confirmed by an alternative method.

9.2 CT Creep Sag Rate Predictions

To illustrate the level of conservatism in the updated fuel channel models, predicted and measured CT elevation values for Q06 at 141.6 kEFPH are compared in Figure 21. Q06 is a typical channel. Figure 21 indicates that there is still some conservatism in the updated fuel channel model.

Figure 21 – Comparison of Predicted CT Elevation vs Time In-Service with CT Elevation from PT Sag Measurements for Q06-L5

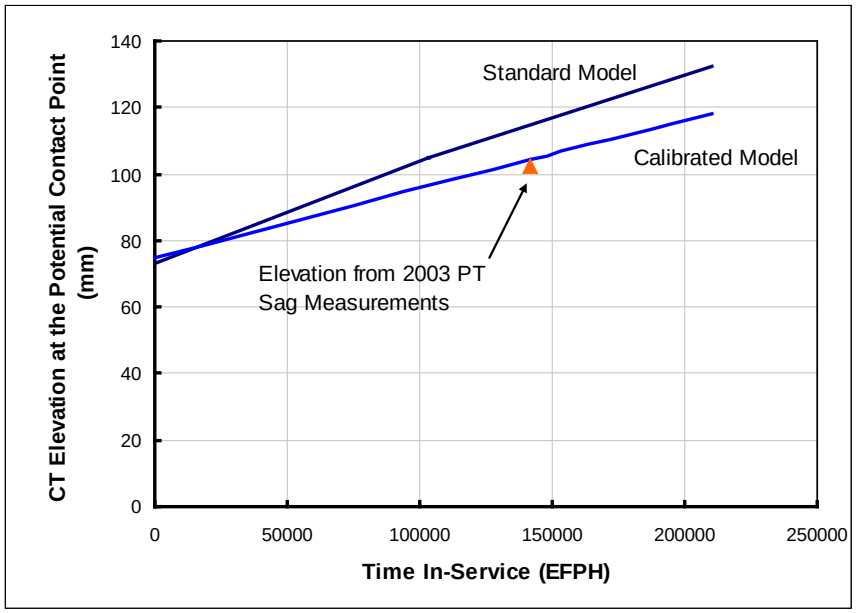

9.2.1 Alternative Treatment for CT Creep Sag Rate Predictions

The treatment of CT creep sag rate up to this point has been purely analytical. It would be beneficial to validate the CT creep sag rate predictions through the use of an alternative method. For this purpose the PT sag data was used in a statistically-based treatment, as follows.

Figure 22 is a plot of measured PT sag versus channel power for the Row Q in G-2. All the data points in the figure were measured at 141.6 kEFPH. The regression line and 95% upper prediction limit for PT sag versus channel power are plotted in the figure.

Figure 22 – Measured PT Sag for Row Q Channels in G-2 Vs Channel Power

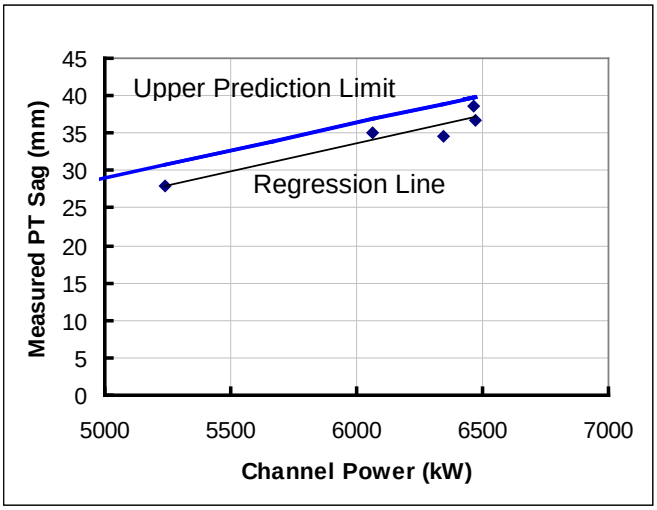

The upper prediction limit for PT sag vs channel power was used to predict PT sag for the Row Q channels at 141.6 kEFPH as depicted in Figure 23. Measured PT sag values are also plotted in Figure 22 for comparison with the predicted upper bound values.

Figure 23 – Predicted Upper Bound PT Sag for the Row Q Channels in G-2 at 141.6 kEFPH

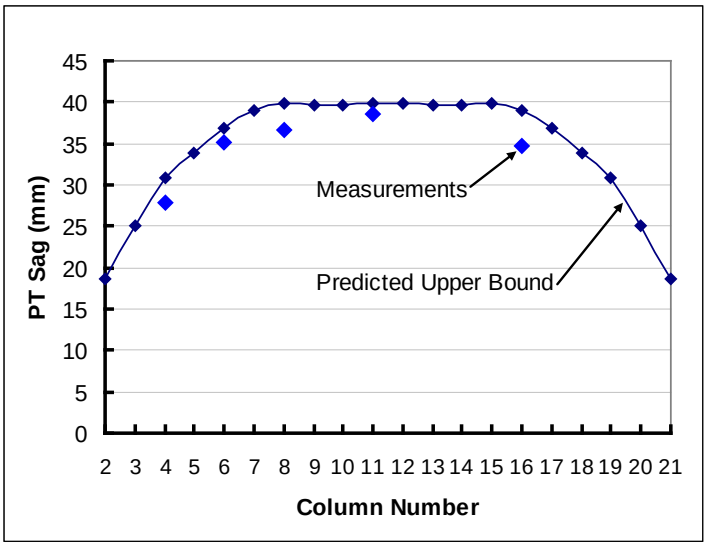

Next, PT sag versus time curves were fitted through each of the predicted upper bound PT sag values for the Row Q channels of the form:

$$Sag = a\ t^{b}$$

where a and b are constants and t is the time in-service.

The power function fit to PT sag versus time in-service was determined by trial and error using STATGRAPHICS 5.1, and is plotted in Figure 24.

Figure 24 – PT Sag Measurements in G-2 versus Time In-Service

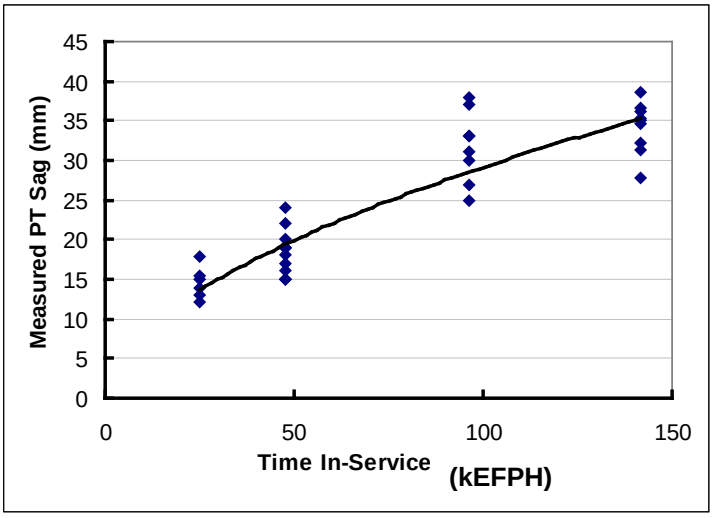

Finally, the PT sag versus time functions for the channels were differentiated with respect to time to generate CT creep sag rates for the Row Q channels in G-2, given in

Figure 25. Comparing Figures 11 and 25, it is seen that the alternative treatment of CT creep sag rate presented above predicts somewhat lower CT creep sag rates than those derived from the updated fuel channel models. Although conservatism was removed in the process of updating the fuel channel models, an amount still remains. This is partially because the CT elevation equations are linear with time in-service whereas in the alternative treatment, a non-linear trend for CT elevation vs time was employed.

Figure 25 – Predicted Upper Bound CT Creep Sag Rates for the G-2 Row Q Fuel Channels

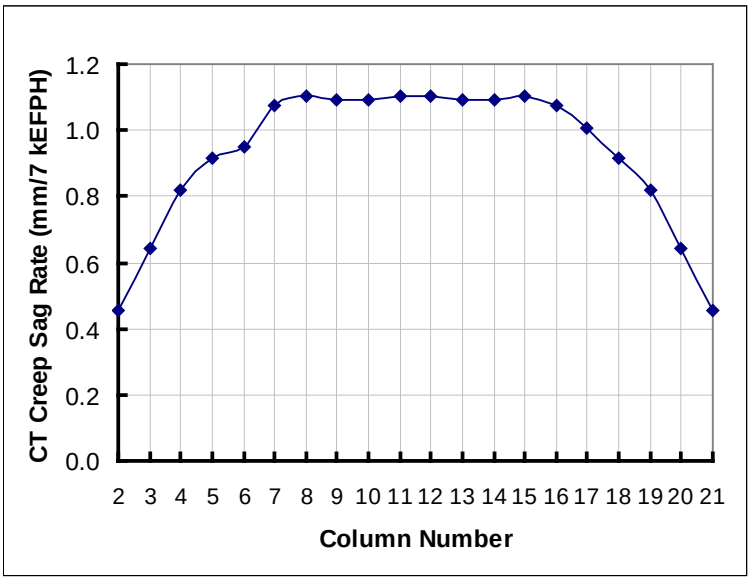

It is interesting that both the LIN and fuel channel structural models under predict the stiffness of the actual components relative to measurements. This observation points to the possible need to adjust elastic modulus values in the structural models.

10.0 Conclusions

1. The standard CDEPTH fuel channel models for PLGS and G-2 underestimate fuel channel stiffness and overestimate PT in-service sag, compared with measurements, resulting in under predictions of the time-to-CT-LIN contact.

2. The following details in the standard CDEPTH fuel channel models contribute to over predictions of PT sag: (1) free rotational degrees of freedom on the ends of the PT, (2) a free axial degree of freedom on the East end of the CT, (3) the use of PT flux profiles based on time-averaged reactor power levels compiled for 1993. With updates to these modelling details, the CT in-service sag predictions closely match CT sag values based on PT sag measurements.

3. The Wolsong LIN sag measurements currently provide the best estimate of LIN creep sag behaviour for use in CT-LIN time-to-contact predictions for CANDU 6.

4. Based on the results in Figures 18 and 19, it is concluded that CT-LIN contact could not have occurred in PLGS by 185 kEFPH and will not occur in G-2 by 196 kEFPH.

11.0 References

1. P.J. Sedran, CPUS Limited, *Scoping Analysis for the Prediction of Onset Times for CT-LIN Contact in PLGS*, 0028-REPT-ENG-001 Rev. 01, August 2, 2005.

2. P.J. Sedran, CPUS Limited*, CT-LIN Time-to-Contact Predictions for PLGS using Updated FC Models*, CPUS Technical Report 0040 REPT ENG 0003 00, September 30, 2005.

3. P.J. Sedran, CPUS Limited*, Update to Time-to-Contact Predictions for CT-LIN Contact in PLGS using Calibrated Fuel Channel Models*, CPUS Technical Report 0065 REPT ENG 0005 00, October 30, 2007.

4. P.J. Sedran, CPUS Limited, *Prediction of Onset Times for CT-LIN Contact in Gentilly-2*, CPUS Technical Report 0078 REPT ENG 0001 00, October 15, 2007.

5. T.R. Kim, S.M. Sohn, J.S. Lee, Korea Electric Power Research Institute, *Ultrasonic Devise to Measure Gap Between Calandria Tube and LISS Nozzle*, 7th International CANDU Maintenance Conference, Toronto, November 20 – 22, 2005.

6. W. Mayo, *Fuel Channel Periodic Inspection: 2004, May, Final Report*, AECL Report 87-31100-PIP-003, January, 2005.

7. T. Campbell, *AECL Inspection Report Calandria Tube to LISS Nozzle Gap Measurement*, 87-31230-INR-001 Revision 1, January 2005.

8. D. Kalenchuk, AECL, *Inspection Report Calandria Tube to LISS Nozzle Gap Measurement Gentilly-2,* 66-31230-INR-002, Revision 1D1, to be issued.

12.0 Acknowledgments

Trevor Langlais, John Slade, and Ray Baker of NB Power Nuclear, and Philippe Charest and Luc Pedneault of Hydro-Québec contributed to this work.

Attachment 6

A CHALLENGE TO A TRADITIONAL ASSUMPTION IN PRESSURE TUBE (PT) LEAK-BEFORE BREAK ASSESSMENTS

P.J. Sedran[1] and B.Rankin[2]

[1]RESD Inc.

[2]Point Lepreau Nuclear Generating Station

ABSTRACT

PT Leak-Before-Break (LBB) analysis involves the modelling of complex phenomena, such as:

1. Leakage and dispersal of vapour and water into the Annulus Gas System (AGS),
2. Axial growth of the leaking crack by Delayed Hydride Cracking (DHC),
3. Crack stability, determined by the crack length and Critical Crack Length (CCL)
4. The shutdown, cooldown, and depressurisation of the reactor in response to dew point and beetle alarms.

To account for significant variability in the models, a number of conservative assumptions, now engrained in CSA N285.8, have been built into the deterministic and probabilistic LBB analysis methods. Recently, the utilities have commented on the need to reduce the level of conservatism in the probabilistic LBB assessments. A prominent conservative assumption is that crack penetration of a DHC-susceptible PT will occur with the reactor at power.

With the reactor at power, crack penetration is expected to occur by tensile overload of the ligament due to pressure. Prior to crack penetration, DHC would not be active with the reactor at power but only during reactor shutdown /start up or cooldown/heatup cycles, thereby advancing the crack front and reducing the thickness of the remaining ligament until the ligament fails under pressure.

This crack behaviour was exemplified in B2N06, which first started leaking at zero power hot conditions following a reactor poison-out.

The intent of this paper, in response to comments by the utilities, is to promote a reduction in the conservatism in deterministic and probabilistic LBB assessment methodologies by challenging the assumption of crack penetration while the reactor is at power. It is shown that crack penetration is more likely during a reactor transient cycle. With this approach, LBB would be more achievable. A standard deterministic LBB analysis and modified analyses for crack penetration during reactor cooldown are presented in this paper for comparison.

1. INTRODUCTION

Out of necessity, the deterministic LBB analysis method in CSA N285.8-15 and the probabilistic methods of References [1] and [2], contain various conservative assumptions, which contribute to conservatism in the results of the various LBB analyses.

Over the past several years, probabilistic LBB assessments have been generated for the Bruce Power and OPG reactors. Although the predicted probabilities of PT rupture in the various assessments have met the acceptability criteria in CSA N285.8-15, the predicted PT rupture frequencies significantly overestimate the actual rupture frequencies as estimated from reactor operating history.

In May 2015, at the COG Fuel Channel Seminar, G. Shek provided an example of how the probabilistic LBB analysis generated PT frequencies that were at odds with operating experience. Following the presentation, OPG commented that, at this stage in the development of the LBB analysis, it was important that the excessive conservatism in the LBB analysis be removed. Essentially, the OPG comments constituted a request to the industry to revisit the assumptions in the current LBB analysis methods, which led to this paper.

For this paper, an assumption of particular interest in the LBB analysis is that the postulated crack always penetrates the PT with the reactor at power.

The validity of that assumption is discussed in this paper as well as the likelihood that crack penetration would occur during a shutdown or cooldown. In addition, a conventional deterministic LBB analysis for crack penetration at power is compared with an equivalent LBB analysis in which crack penetration occurs during a reactor cooldown.

2. THE CURRENT LBB ANALYSIS METHODS

Currently, there are three LBB analysis methodologies for CANDU PTs:

1. Deterministic LBB Analysis
2. Level 1 Probabilistic LBB Analysis
3. Level 2 Probabilistic LBB Analysis

The requirements first imposed by the Fitness-for-Service Guidelines [3] and continued by CSA N285.8 are that PT LBB must be demonstrated for a reactor when the hydrogen equivalent concentration in any PT reaches the terminal solid solubility limit for the dissolution of hydrogen in the PT material, the Tterminal Solid Solubility Limit TSSD at any sustained hot reactor condition.

Under current reactor operating procedures, Zero Power Hot (ZPH) represents the lowest-temperature sustained hot condition at which the PTs will operate. The attainment of TSSD at ZPH conditions is what first initiates the need for an LBB analysis.

In formulating the deterministic LBB methodology for Reference [3] it was decided that the LBB analysis would always assume crack penetration while the reactor is operating at

power. This was a greatly simplifying assumption that was highly conservative because in all the LBB analyses performed to date, TSSD was only attained at the inlet ends of the PTs but not at the outlets.

An example of a deterministic LBB analysis is provided in Figure 1 [4]. The analysis summarized in Figure 1 is for PT L12 in the Point Lepreau Nuclear Generating Station (PLGS) for the conditions present at the time of reactor shutdown for refurbishment on April 1st, 2008. It is assumed that the reactor is operating at 96% reactor power when the crack penetrates the PT. The crack in the PT is postulated at the axial location with the highest temperature at 96% reactor power, 315.7 °C. In the top half of Figure 1, PHTS pressure and temperature are plotted versus time from the start of leakage. The pressure/temperature plots show how the operator would control the reactor during the Sequence of Events (SOE). In the bottom half of Figure 1, crack length and CCL, calculated at each time step in the SOE, are plotted versus time from the start of leakage.

For this paper, the main point in Figure 1 is that penetration of the PT wall at t = 0 h and subsequent crack growth by DHC are assumed to take place with the reactor at 96% reactor power.

At the time, there was no attempt to justify or to provide a rationale for postulating that the crack would penetrate the PT wall and grow by DHC with the reactor at 96% reactor power. It was a convenient assumption which was known to be conservative and was repeated in every LBB analysis.

An evaluation of the LBB analysis of Figure 1 is provided in Section 2.1.

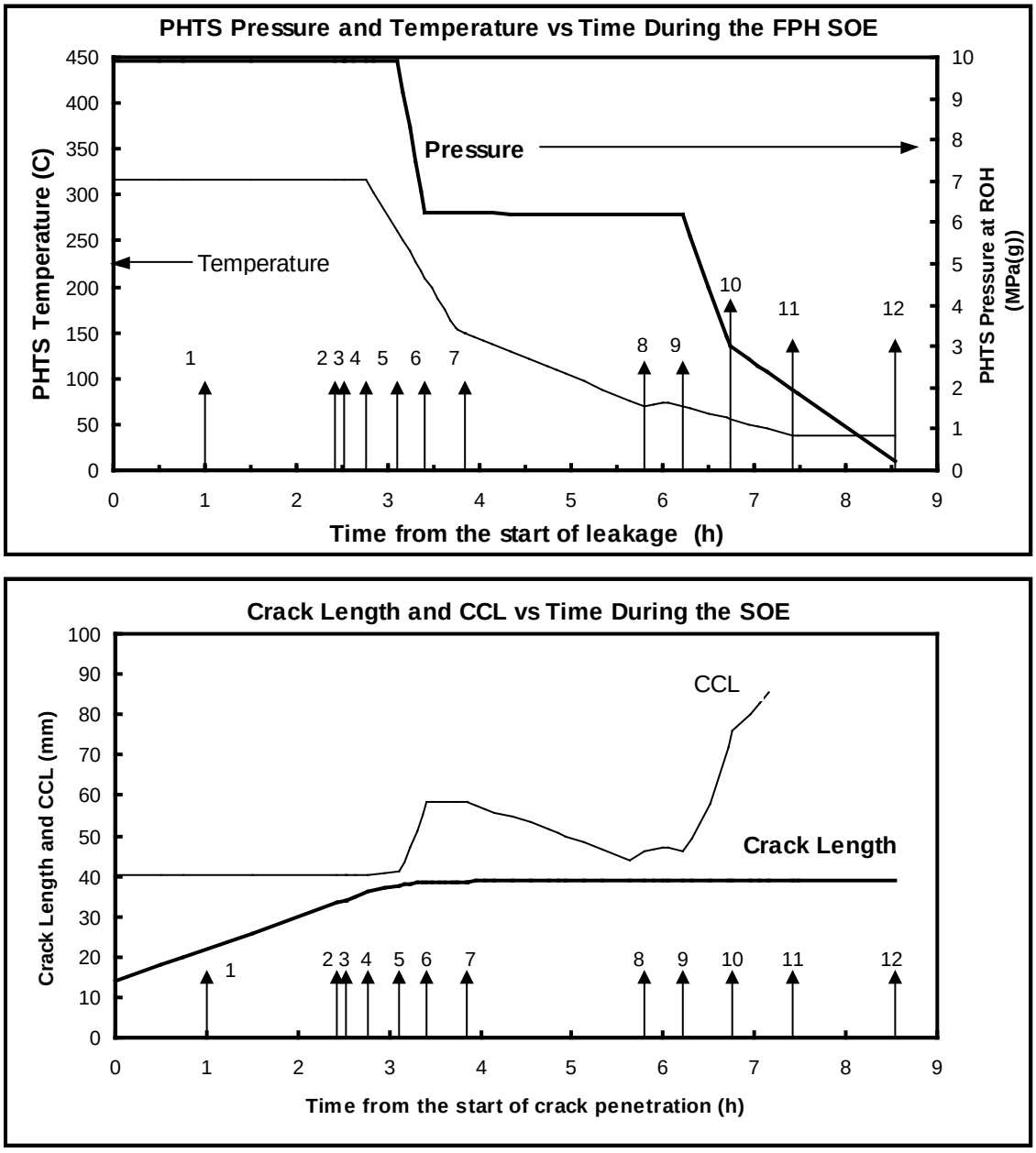

Figure 1. Summary of a Standard Deterministic LBB Analysis for PLGS L12

At t=0 h the reactor is at 96% of Full Power. The postulated flaw in L12 is a 14.1 mm through-wall crack. The leak rate is zero at this time. A description of the SOE is as follows: 1 – The first AGS indications are received. 2 – The entire AGS string is filled. 3 - Dew point and beetle alarms are triggered. 4 – Leak is confirmed and reactor shutdown starts. 5 – Cooldown and depressurization of the PHTS starts. 6 – PHTS pressure reaches 6.23 MPa(g) and is held constant. 7 – Cooldown rate is switched from 2.75 to 0.67 °C/minute. 8– At 70 °C SD cooling pumps are started. 9 – PHTS pumps are shut down and cooldown of the PHTS starts at a rate of 0.45 °C/minute. Depressurization of the PHTS starts at a rate of 6.06 MPa/h. 10 – Cooldown continues and the rate of pressure reduction switches to 1.56 MPa/h. 11 – PHTS temperature stabilizes. 12 – PHTS is cold, depressurized.

2.1 Analysis of the Current LBB Methodology

For L12, the hydrogen equivalent concentration is a major determinant of its susceptibility to DHC. As, a starting point, the hydrogen equivalent and TSSD concentrations at the postulated crack in L12 were calculated for the conditions of the LBB analysis of Figure 1. A summary of the calculations for 96 % reactor power and the Zero Power Hot (ZPH) condition is provided in Table 1.

Table 1 – Hydrogen Equivalent Concentration in PT L12 for the LBB Analysis

PT	Condition	Hi (ppm)	T (°C)	Tav (°C)	Date	Time (HH)	D (ppm)	Heq (ppm)	TSSD (ppm)
L12	96% RP	6.0	315.7	313.5	2008-04-01	193,248	78.6	45.4	71.1
L12	ZPH	6.0	260	313.5	2008-04-01	193,248	78.6	45.4	34.1

Hi is the initial hydrogen concentration and Heq is the current hydrogen equivalent concentration.

At an operating temperature of 315.7 °C, the bulk Heq concentration of 45.4 ppm is below TSSD at the postulated crack. No bulk hydrides would be present at the crack. However, at the ZPH condition, for a temperature of 260 °C, the bulk Heq concentration exceeds TSSD. This means that hydrides would be present at the postulated crack during operation at ZPH, which can last for several hours. With bulk hydrides present during sustained operation at ZPH, DHC would be possible. In this situation, CSA N285.8 calls for an LBB analysis to be performed.

CSA N285.8 provides a criterion for when the LBB analysis must be performed but does not specify the details of the analysis. For example, for the L12 LBB analysis, the DHC models might predict crack growth at ZPH conditions but not at 96% RP. Therefore, it would be reasonable to postulate through-wall cracking leading to an LBB scenario at ZPH conditions but the postulation of through-wall cracking at 96% RP is inconsistent with DHC theory. This is because on heating to 315.7 °C, the bulk hydrides would dissolve completely, preventing the possibility of DHC.

In addition, for the reactor to operate at 96% RP, the postulated crack would have been heated from room temperature to 315.7 °C. It was demonstrated experimentally that DHC is not possible at temperatures above 200 °C if the specimen were heated to temperature [5], a rationale for which was provided in Reference [6].

In summary, the assumption that through-wall cracking would occur in L12 after heating to the 96% RP condition, leading to the LBB scenario of Figure 1, now a standard assumption in deterministic and probabilistic LBB analyses, is excessively conservative.

3. PROPOSED MODIFICATION TO THE CURRENT LBB ANALYSIS METHOD

Since crack penetration by DHC at power has been ruled out, the following alternative scenario for crack penetration is proposed:

The prerequisite for crack penetration is a large, part-through wall crack that can grow by DHC. The growth of the crack occurs primarily during a reactor cooldown with a small

amount of growth during reactor heatup. As the crack tip advances radially into the PT with each cooldown, the ligament at the surface of the PT becomes progressively thinner. At this point, there two possibilities:

1. During a cooldown the ligament is thinned to the point that it can sustain pressure during the next heatup but when the reactor starts to operate at power, the resultant pressure causes the ligament to rupture – Case 1
2. During a cooldown, the crack penetrates the wall of the PT by DHC or the ligament ruptures under pressure – Case 2.

In both cases, the PT pressure boundary would be breached, creating a leak path into the AGS, which would initiate two distinct SOEs. In the first case, the SOE would essentially be identical to that depicted in Figure 1. In the second case, crack penetration would occur during a temperature reduction, either during reactor shutdown or cooldown.

The probabilities of PT rupture in Cases 1 and 2 are substantially different. At t=0 h, the crack growth rate for Case 1 is higher than for Case 2, while CCL is lower for Case 1 than for Case 2.

3.1 Preliminaries for the LBB Analysis for Case 2

The LBB analysis of Figure 1 stands for Case 1. In order to make a direct comparison of the LBB analyses for Cases 1 and 2, various input parameter values for the Case 2 LBB analysis were made identical to those for the Case 1 LBB analysis, as indicated in Section 3.3.1

3.1.1 Common Parameter Values for Case 1 and Case 2 LBB Analyses

Common values were used for the following parameters:

Crack Length at Penetration = 14.15 mm

PT Inner Radius = 56.152 mm

PT Wall Thickness = 4.076 mm

Time to First Dew Point Indication = 1 h

Water Volume to Fill AGS String and Reach Beetle Well = 80 kg

3.1.2 Conditions at t = 0 h

The first step in the LBB analysis is to establish when the crack would first penetrate the PT wall during the shutdown or cooldown. For Case 2, the postulated crack has a crack length of 14.1 mm, for consistency with the LBB analysis of Case 1.

To establish the time of crack penetration from the start of the shutdown, the following steps were performed:

1. Estimate the minimum thickness of the ligament that could withstand 10.67 MPa, the pressure at the crack at 96% RP
2. Predict the time at which DHC would initiate at the during the temperature reduction

3. Calculate the time required for the crack to penetrate the ligament by DHC and determine the temperature and pressure at the time of crack penetration, which is t = 0 h for the LBB analysis

Each of these steps is summarized in Sections 3.1.2.1 – 3.1.2.3.

3.1.2.1 Estimation of Ligament Thickness

The minimum ligament thickness was estimated by calculating the thickness of ligament that would be entirely plastic due to the stress field at the crack tip. In the calculation, the crack depth was increased until the crack depth plus the radius of the plastic zone coincided with the PT wall thickness. In reality, a fully plastic ligament likely would fail by creep during operation at 96% RP, so this approach would underestimate the minimum ligament thickness that would remain intact at 96% RP, which is conservative for this assessment. With an underestimated ligament thickness, the time required for the crack to grow through the ligament would be underestimated, which means that the temperature and crack growth rate at t = 0 h would be overestimated, which is conservative for the LBB analysis.

3.1.2.2 Prediction of the Start Time for DHC

For a bulk hydrogen equivalent concentration of 45.3 ppm, the flaw-tip hydrogen equivalent concentration was calculated to be 73.5 ppm. During the reactor shutdown/cooldown, TSSP at the flaw tip would be reached at a temperature of 258 °C such that hydride precipitation would start at this time. At 260 °C, the reactor would be held at the ZPH condition, so crack-tip hydride growth would occur just after the start of the cooldown from the ZPH condition.

3.1.2.3 Prediction of the Time at Crack Penetration

At 96% RP, at a temperature of 315.7 °C, TSSD is 71.1 ppm, so all the hydrogen in the bulk is in solution. However, with crack-tip hydrogen enhancement, the flaw-tip hydrogen equivalent concentration is predicted to be 73.5 ppm so that ratcheting flaw-tip hydrides would be present. During the cooldown from the ZPH condition, crack-tip hydride ratcheting would start at 258 °C, as indicated above. At this stage, the task is to determine how long it would take for the crack tip to penetrate the ligament by DHC or to thin the ligament to the point that it would rupture.

There are two complications involved in this assessment. The first is that as the pressure is reduced, an incubation time effect would be introduced into the DHC process. The second complication is that during the cooldown from 258 °C, there would be an undercooling effect such that DHC would start at a temperature below that at which flaw-tip hydrides would start precipitating. For the purpose of this paper, the most conservative assumption would be that the ratcheting crack-tip hydrides would fracture shortly after crack-tip hydride precipitation starts at 258 °C and that the ligament would rupture. Under this assumption, leakage into the AGS would start shortly after the crack reaches a temperature of 258 °C, which represents t = 0 h for the LBB analysis.

For this assessment, it is, therefore, assumed that crack penetration would occur during the cooldown, at a temperature of 258 °C, noting that for the cooldown, it is assumed that there is no temperature difference from the ROH to any point along the PT.

4. MODIFIED LBB ANALYSIS

In the standard LBB analysis of Figure 1, AGS indications were received with the reactor at power, so emergency shutdown/cooldown procedures were assumed in the LBB analysis. In the modified LBB analysis, a standard shutdown/cooldown was assumed because the operator would not receive any AGS indications until after starting the cooldown of the reactor.

Figure 2 depicts the typical reactor shutdown/cooldown for PLGS that was used in the modified LBB analysis. Starting at 260 °C, the temperature at the ROH is the same as that at the crack. The pressure at the flaw during the cooldown was calculated as the sum of the pressure at the ROH plus the pressure drop from the crack to the ROH, predicted as a function of temperature from thermal hydraulic computations for L12 at different operating conditions.

The modified LBB analysis basically consists calculating crack length and CCL at various time steps after the start of leakage from the PT, as outlined in CSA N285.8.

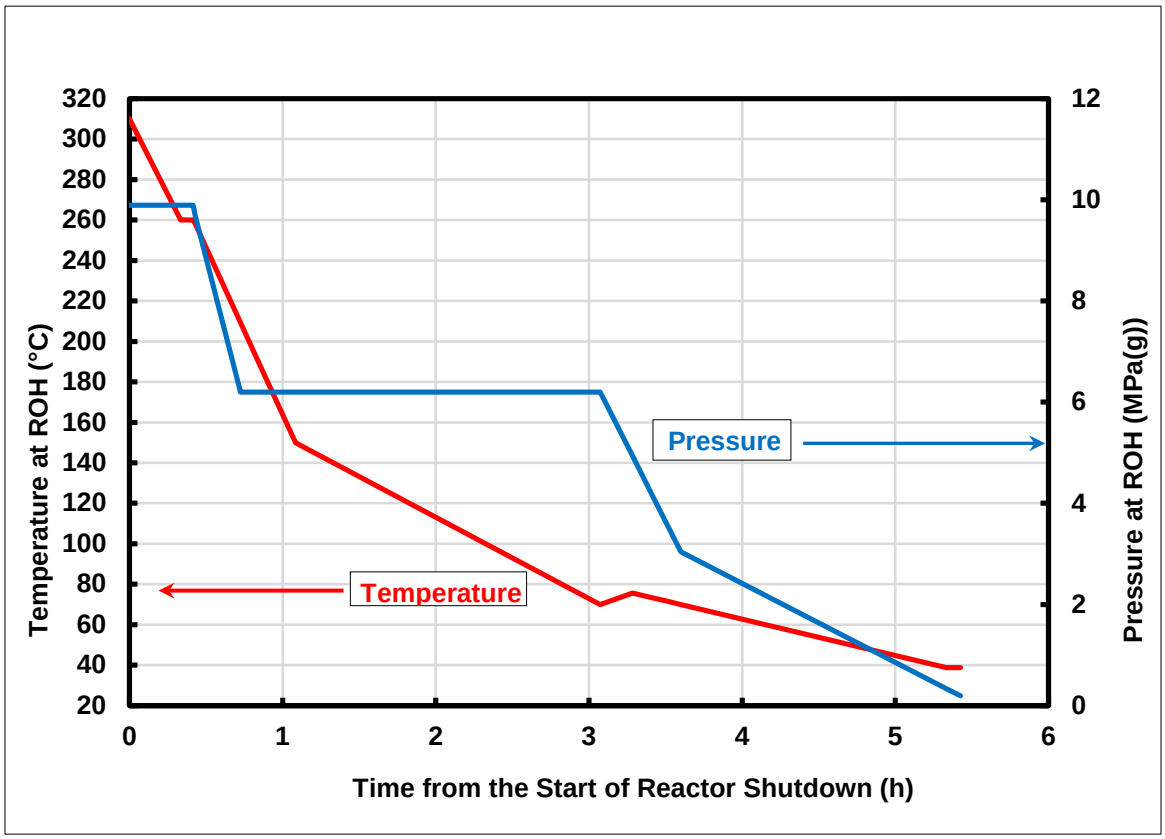

Figure 2. Typical Normal Shutdown and Cooldown for PLGS

A detailed description of the input data and the various calculation methods employed in the standard LBB analysis for L12 can be found in Reference [4]. The various calculations in the modified LBB analysis use the same input data and calculation methods. A brief description of the various input parameters in the modified LBB analysis is provided in the sections that follow.

4.1 Crack Length at Penetration (from Reference 4)

The crack length at penetration was determined by postulating a growing crack and finding its aspect ratio and limiting size based on plastic collapse criteria, as follows.

In [7], the mean axial length of a crack at penetration in the axial–radial plane of the pressure tube (L_p) is given as a function of the length of the flaw from which the crack had initiated (L_0):

$$L_p = 10.92 + 0.82\ L_0 \qquad (1)$$

Based on the known flaws in the PLGS PTs, 4.152 mm was established as a bounding length for debris frets. For an initiating length of 4.152 mm, the mean length at penetration would be 14.325 mm. At penetration, the mean aspect ratio of DHC cracks that could grow from the initiating flaw was found to be 2c/a = (14.325 mm)/(4 mm) = 3.58. On this basis, it is assumed that the bounding postulated flaw would have an aspect ratio of 3.58, on approach to penetration.

As the crack starts to approach the PT outer surface, the ligament at the crack tip would yield, eventually becoming fully plastic. Failure of the ligament would subsequently occur by tensile overload, creating a through-wall crack and a leak path from the PT.

Based on the above, the postulated flaw for L12 was derived as the largest flaw with an aspect ratio of 3.58 with a ligament just at the rupture limit.

The hoop stress required for plastic collapse was calculated using the expression:

$$\sigma_{h'} = \sigma_f \left\{(1- a/w)/(1 - a/(wM))\right\} \qquad (2)$$

where a is the flaw depth, w is the pressure tube wall thickness, σ_f is the flow stress, and M is the bulging factor , from CSA N285.8:

$$M = [(1+1.255(c^2/r_m w))-(0.0135(c^4/r_m^2 w))]^{0.5} \qquad (3)$$

where r_m is the mean radius of the pressure tube and 2c is the flaw length.

Setting $\sigma_{h'}$ equal to the applied hoop stress, $\sigma_h = PR_i/w$ as the condition for plastic collapse, gives

$$PR_i/w = \sigma_f \left\{(1- a/w)/(1 - a/(wM))\right\} \qquad (4)$$

The flaw depth for plastic collapse was found from this expression, since w is a function of a and all the other parameter values are known. A summary of the plastic collapse analyses of the postulated flaws in K12 and in L12 is presented in the Table below.

Table 2 - Summary of Plastic Collapse Analyses for Postulated Flaws in L12

PT	T (°C)	P (MPa)	R_i (mm)	w (mm)	σ_h (MPa)	σ_f (MPa)	M	σ_h' (MPa)	σ_h'/σ_h	a (mm)	2c (mm)
L12	315.71	10.70	56.152	4.076	158.1	717	1.12	158.0	1.0	3.952	14.150

From the table it is concluded that should a flaw penetrate L12, the maximum flaw length at penetration would be 14.150 mm.

4.2 Leak Rate

Leak rate was calculated using Equations D.12-1 and D12-3 from CSA N285.8 for a 20 mm long through-wall crack and was adjusted using a factor of 0.697 to account for the shorter crack length at penetration

4.3 DHC Axial Growth Rate

The DHC axial growth rate for the postulated crack was calculated at discrete time steps in the SOE using Equation D.10-13 in CSA N285.8-05. For temperatures of 100 °C or less, a growth rate of 0.003 mm/h was used as per CSA N285.8-05.

4.4 Critical Crack Length

CCL for the postulated crack was calculated at discrete time steps in the SOE using Equation D.13-9 in CSA N285.8-05.

4.5 Modified LBB Analysis Results and Discussion of Results

Figure 3, similar to Figure 1 presents a summary of the modified LBB analysis. As indicated in the figure, crack penetration occurs at t = 0 h, just after the start of the reactor cooldown. A noteworthy result of the analysis is that the crack growth during the SOE is predicted to be minimal, which is due to the moderate temperature at which axial crack growth starts and the low temperature for the rest of the SOE.

In Figure 3, the plot of CCL versus time for the start of leakage displays the expected changes in CCL with changes in pressure and temperature.

For the standard LBB analysis, dew point response predictions are based on modelling of AGS operation with the reactor at power. For this paper, the response of the AGS to a leak during reactor cooldown was not available. Therefore, there are no actual predictions of dew point alarm times for the analysis of Figure 3. All that can be said is that the AGS testing performed at ZPH conditions in Pickering, Darlington, and Wolsong Unit 1 and the B2N06 PT rupture event indicate that there would be positive indications of moisture in the AGS during the SOE depicted in Figure 3.

As for the beetle alarm, in Figure 1, a beetle alarm is predicted at t = 2.5 h. For the modified LBB analysis of Figure 3, the predicted leak rate over the SOE would be inadequate to trigger a beetle alarm. In this case, dew point readings would be the primary indicators of a leak from the PT. A secondary indicator could be the suppression of channel outlet temperatures in channels with water-filled annuli, which may be detected by the operator.

A second noteworthy result from Figure 3 is that the CCL value throughout the SOE is significantly greater than the corresponding crack length.

Comparing Figure 1 with Figure 3, it is seen that in the standard deterministic LBB analysis, the minimum difference between CCL and crack length is 4 mm, compared with 29 mm for the modified deterministic LBB analysis. Therefore, for crack penetration during a cooldown, the margins against PT rupture are significantly greater than those for crack penetration with the reactor at power.

The implication from comparing Figures 1 and 3 is that the probability of PT rupture assuming crack penetration at power for all simulations is greater than the probability of PT rupture, accounting for crack penetration at power and during the cooldown.

In comparing Figures 1 and 3, a significant consideration is the relative frequency of Case 1crack penetration with the reactor at power and Case 2 crack penetration during a shutdown/cooldown of the reactor. For Case 1 to take place, a crack would need to propagate to a specific limiting size, stop growing and the ligament would then have to rupture with the reactor at power. For Case 2, the flaw would have to grow by DHC on a number of cooldown and heatup cycles and penetrate the PT wall during any cooldown. Intuitively, Case 2 has a higher probability of occurrence than Case 1 because it is not very likely that a crack would be exactly at the limiting size when the reactor starts to operate at power.

Operating experience with leaking PTs provides support for the statement that crack penetration at power should be expected to be less frequent than crack penetration at other conditions. In 23 incidents of PT leakage, in Ontario Hydro reactors, the leaks were all discovered with the reactor in a shutdown condition, which supports the position that crack penetration at power is not a very probable event.

5. CONCLUSIONS

1. In the event of a large crack that threatens to penetrate the PT wall, it is more likely that the crack will penetrate the PT during a reactor cooldown than during operation at power.
2. Should the crack penetrate the PT wall during the cooldown instead of during operation at power, the deterministic margin against PT rupture would be significantly greater.
3. If crack penetration in a probabilistic LBB analysis were modelled by random selection from the two possible scenarios, there would be a significant decrease in the predicted probability of PT rupture, compared to that predicted with the current probabilistic LBB analysis method that always assumes crack penetration at power.

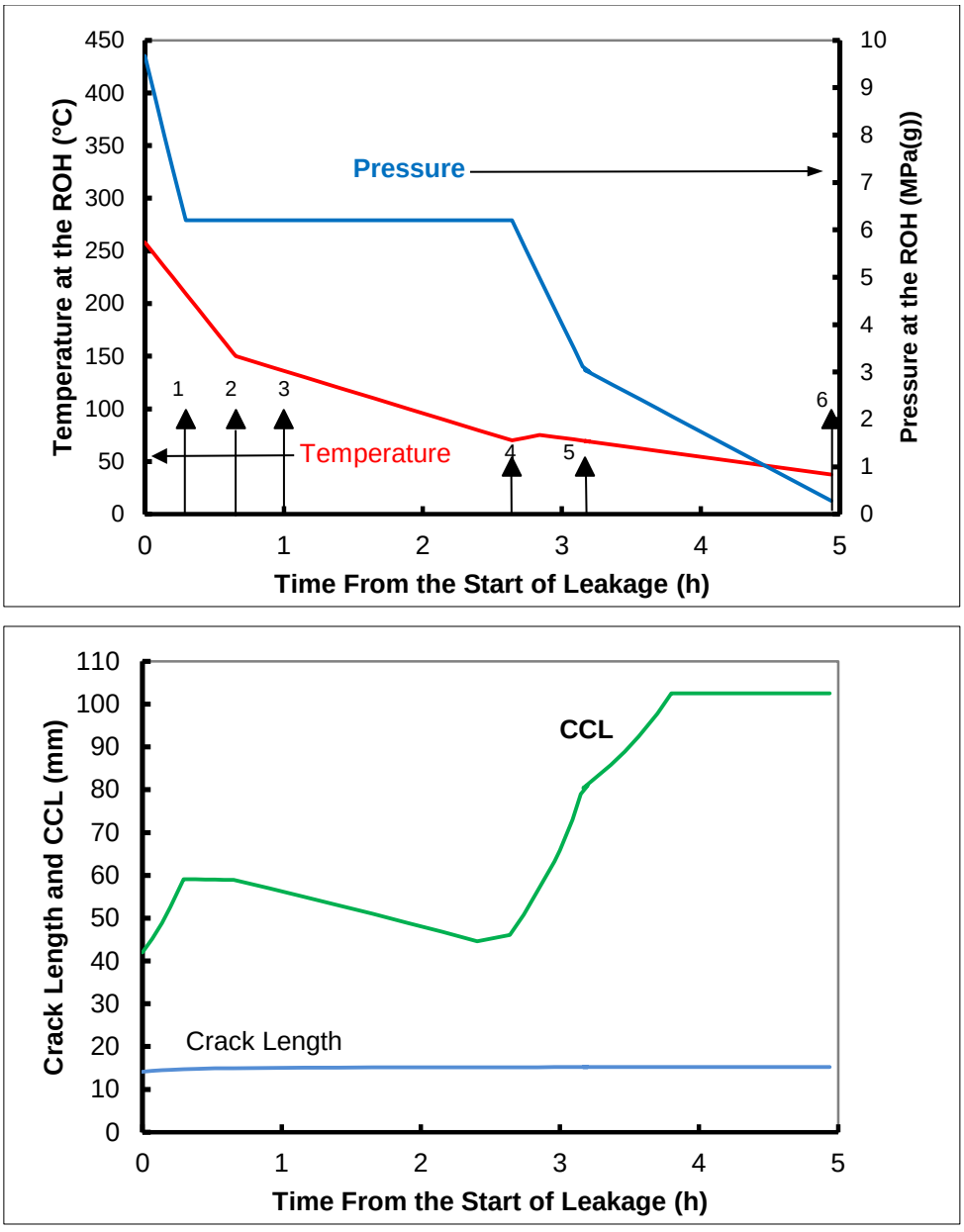

Figure 3. Summary of a Modified Deterministic LBB Analysis for PLGS L12

Crack penetrates the wall at t = 0 h during reactor shutdown. 1. Hold pressure at 6.2 MPa. 2. Change cooldown rate. 3. First Dew Point Indications of Moisture. 4. Shutdown Cooling Pumps are Started. 5. PHTS Pumps are Shut Down and Depressurisation rate is reduced. 6. Reactor is Cold, Depressurized.

6. RECOMENDATIONS

- For the deterministic LBB analysis, the assumption that crack penetration occurs with the reactor at power is highly conservative but it is recommended that it be continued.

- For probabilistic LBB analyses, it is recommended that the probabilistic code be modified to include a module to simulate crack penetration. With this modification, a small number of simulations would have crack penetration at power and the majority of simulations would feature crack penetration during reactor shutdown/cooldown or heatup/startup.

7. REFERENCES

[1] D. Scarth, M. Kozluk, D. Graham, W. Reinhardt, “Technical Basis for Level 1 Probabilistic Leak-Before-Break Evaluation of Zr-2.5Nb Pressure Tubes”, COG Report No. COG-JP-4363-V285, June 2013.

[2] D.H.B. Mok, “Technical Basis for Level 2 Probabilistic Leak-Before-Break Evaluation of Zr-2.5Nb Pressure Tubes”, COG Report No. COG-JP-4363-V147, June 2013.

[3] "Fitness-for-Service Guidelines for Zirconium Alloy Pressure Tubes in Operating CANDU Reactors," COG Report No. COG-91-66, May 1991.

[4] P.J. Sedran, “Point Lepreau GS Deterministic Leak-Before-Break Assessment”, Report No. 87-31100-220-016 (Revision 2), 2003, February.

[5] Ambler, J.F.R., “Effect of Direction of Approach to Temperature on the Delayed Hydrogen Cracking Behavior of Cold-Worked Zr-2.5Nb”, *Zirconium in the Nuclear Industry: Sixth International Symposium*, ASTM STP 824, D.G. Franklin and R.B. Adamson, eds., ASTM, pp. 653-674, 1984.

[6] Developments in Delayed Hydride Cracking in Zirconium Alloys, M.P. Puls, Fuel Channels and Material Engineering, AECL-SP, May 2004.

[7] “Penetration and Stability of Axial Part-Through DHC Cracks in Zr-2.5Nb Pressure Tubes”, N-REP-#1110-10000, A.C. Wallace, SES NOSS, OPG, February, 2000.